ClassNK Technical Journal

No.7 2023（I）

Special Feature: Activities for Safe Operation of Container Ships

ClassNK Technical Journal　No.7　2023（I）

— CONTENTS —

Prefatory Note

Introduction to the Special Feature on

"Activities for Safe Operation of Container Ships"

Corporate Officer, Director of Research Institute, ClassNK
Yukihito FUJINAMI

I would like to take this opportunity to welcome all our readers to this Special Feature of ClassNK Technical Journal No. 7 on "Activities for Safe Operation of Container Ships."

We publish the ClassNK Technical Journal to contribute to technical progress in the maritime industry by making the technological activities and research results of the Society available to all those concerned. In our previous ClassNK Technical Journal No. 6, we focused on the concepts of risk assessment and risk-based design in the maritime field, and reported on related trends and recent research and development results.

In recent years, a large number of container ships have been built accompanying increasing global demand for container freight. At the same time, it can be said that container ships have shown the greatest changes among all ship types in the current century, including remarkable increases in the size of container ships due to the effects of reduced-speed operation to meet environmental regulations. For these container ships, the Society conducted a comprehensive revision of Part C of the ClassNK Rules for the Survey and Construction of Steel Ships in 2022, which has made it possible to carry out safer and more rational structural design and evaluation than in the past. We have also issued three sets of Guidelines for container ships in the current fiscal year 2023, and are expanding our support services in response to the needs of container ship operation.

For ClassNK Technical Journal No. 7, we have assembled a Special Feature entitled " Activities for Safe Operation of Container Ships," which presents an overview of the structural rules and above-mentioned Guidelines for container ships. This issue also includes a diverse range of other articles and papers on various research and development achievements, the technical activities of Class NK, trends in the International Maritime Organization (IMO) and other relevant topics.

Based on the needs of society and the industry, we will continue to make diligent efforts in research and development which contribute to ensuring the safety of human life and property at sea, protecting the marine environment and creating innovations that lead society in order to contribute to the further development of the maritime industry.

We sincerely request the continuing understanding and support of all those concerned in the future, as in the past.

Revisions of "Guidelines for Container Stowage and Securing Arrangements (Edition 3.0)" and Future Outlook

Fuminori YANAGIMOTO*

1. INTRODUCTION

Because cargoes loaded on container carriers are stowed not only in the holds but also on the deck, the container securing technology called lashing is necessary. Since the number of containers loaded on a vessel must be as large as possible to improve the economy of container carrier operation, container stacks exceeding 10 tiers are no longer rare. In addition to the self-weight of the containers, the loads caused by the rolling, pitching and heaving motions of a container carrier also act on these container stacks. Thus, as part of the container stacking and lashing method, it is necessary to calculate the strength of container stowage and securing arrangements so as to ensure that excess loads are not generated in the containers and lashing devices. Each classification society, including ClassNK (hereinafter, the Society), provides procedures for these calculations for the strength of securing arrangements in the form of rules or guidelines.

After the Society issued the first edition of "Guidelines for Container Stowage and Securing Arrangements" (hereinafter, Guidelines) in 2009, the second edition was released in 2014. However, the motion evaluation equations of a ship and procedures for calculating securing strength were unchanged from the first edition. Because upscaling of container carriers also continued in the meantime, and 24 000 TEU class Ultra Large Container Ships (ULCS) have now appeared, the applicability of the semiempirical motion evaluation equations adopted at the time of the 2009 Guidelines was a concern. Moreover, since the need to consider the nonlinear behavior of container stacks accompanying the introduction of fully automatic twist locks in recent years had also been pointed out, a revision of the Guidelines was carried out to contribute to achieving more rational container stowage by incorporating the results of Comprehensive Revision of Part C of the Society's Rules for the Survey and Construction of Steel Ships, which was carried out until 2022, and the results of research in the Society's Research Institute.

2. OVERVIEW AND COMPOSITION OF GUIDELINES AND MAIN POINTS OF REVISIONS

2.1 Overview and Composition of Guidelines

Table 1 shows the composition of the Guidelines by chapter. The composition of the Guidelines are unchanged from the second edition. Chapter 1 to Chapter 3 describe general items such as the overview of container stowage. Chapter 4 explains the basic concepts of the procedures for strength evaluation of container stowage and securing arrangements. Chapters 5 and 6 specify the design loads and strength evaluation methods used in strength evaluations of stowage and securing arrangements. The revisions this time targets mainly at Chapters 5 and 6. Chapters 7 and 8 are chapters that were newly established when the second edition of the Guidelines was released in 2014, and specify the class notations corresponding to the ship's lashing calculation program (so-called lashing computer) and the character of classification corresponding to IMO CSS Code Annex 14.

Table 1 Chapter composition of Guidelines

Chapter 1	OVERVIEW OF CONTAINER STOWAGE AND SECURING ARRANGEMENTS
Chapter 2	STRENGTH OF CONTAINERS AND SECURING DEVICES
Chapter 3	PRECAUTIONS FOR HULL STRENGTH RELATED TO STOWAGE AND SECURING ARRANGEMENTS
Chapter 4	STRENGTH EVALUATION METHODS FOR STOWAGE AND SECURING ARRANGEMENTS
Chapter 5	DESIGN LOADS FOR STRENGTH EVALUATION OF CONTAINER STOWAGE AND SECURING ARRANGEMENTS
Chapter 6	STRENGTH EVALUATION OF CONTAINER STOWAGE AND SECURING ARRANGEMENTS
Chapter 7	LASHING CALCULATION PROGRAM
Chapter 8	SAFE DESIGN FOR CONTAINER LASHING

* Research Institute, ClassNK

2.2 Main Points of Revisions

Although various revisions were made in the third edition of Guidelines, the main revisions concerned the following three points. (The relevant chapters are shown in parentheses.)

i） Review of motion and load equations (Chapter 5)

ii） Updating of route correction factors (Chapter 5)

iii） Revision of methods of strength evaluation of stowage and securing arrangements (Chapter 6)

In addition to these revisions, the Society also plans to provide calculation tools and web applications corresponding to the content of the Guidelines to improve the convenience of the Guidelines and facilitate their use by a greater number of users. The provision of these digital tools is also described in the following chapter, together with the details of the respective revisions mentioned above.

3. OVERVIEW OF MAIN REVISIONS

3.1 Review of Motion and Load Formulae

In strength evaluations of container stowage and securing arrangements, the Guidelines consider the case of longitudinal waves (head seas and following seas) and the case of transverse waves (beam seas). In the former case (head/following seas), strength calculations of securing arrangements consider the loads acting on container stacks as a result of heave acceleration, the angular component of the acceleration of gravity due to the pitch angle and pitch angular acceleration, and in the latter case (beam seas), calculations consider the loads acting on container stacks as a result of the angular component of the acceleration of gravity due to the roll angle, roll angular acceleration and heave acceleration. In addition, the pressure due to wind loads acting on containers which are exposed to wind is also given. Fig. 1 shows a schematic diagram of the loads in a beam sea.

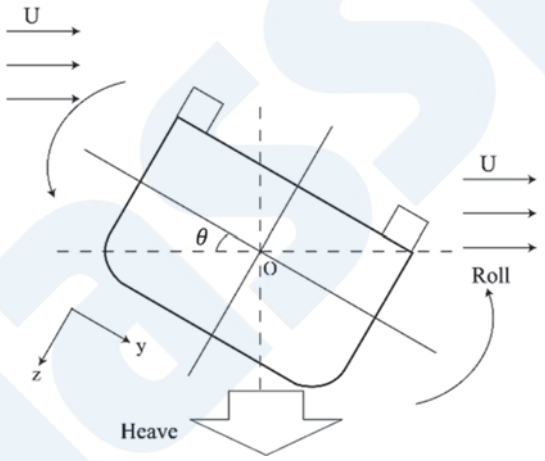

Fig. 1 Schematic diagram of loads in beam sea

Because ship hull motion and acceleration had been given as semiempirical formulae in the Guidelines until now, there were questions about their applicability to the ULCS of recent years. Therefore, in this revision, a decision was made to use equations that are physically meaningful and related to evaluations of structural strength, based on the results of the Comprehensive Revision of Part C of the Rules for the Survey and Construction of Steel Ships carried out from 2017 to 2022. A flowchart of the derivation of the motion and load equations in the Comprehensive Revision of Part C is shown in Fig. 2. The motion and load evaluation equations in the Rules and these Guidelines are obtained from the value of a simplified formula for the hull motion and acceleration for a unit wave amplitude, and applying nonlinearity effects and operational effects as coefficients to the maximum motion displacement and acceleration of the hull found by using the maximum wave height occurring once in 25 years obtained from a long-term forecast using direct load analysis (DLA) and wave scatter diagram for the North Atlantic Ocean. For the details of this flow, see paper No. 3 in this edition of ClassNK Technical Journal (Japanese ed.) [1].

The “operational effect” considered in the flowchart in Fig. 2 is obtained by an evaluation of the sea states that the ship actually encounters using AIS data and hindcast data. Although the details may be found at Miratsu *et al*. (2022) [2], the

operational effect factor is derived by comparing the long-term prediction values found from the wave scatter diagram provided in IACS Rec. 34, and the long-term prediction values obtained from the wave scatter diagram for the actually-encountered sea states. A similar technique is also used in the review of the route correction factors described in the following.

In addition to the review of the load equations, this revision of the Guidelines also eliminated the previous provision setting the minimum value of 20° for the roll angle. Where this provision is concerned, conventionally, the roll angle had been set at a minimum of 20°to adequately secure an adequate safety margin, as the roll angle is the controlling factor in evaluations of container securing strength. However, it was deemed possible to eliminate this provision from the current revision, considering the facts that a quantitative evaluation of the sea states encountered by container carriers is possible by using AIS data and hindcast, it is now possible to construct physically meaningful motion equations in the above-mentioned Comprehensive Revision of Part C, and based on the results of an analysis of the measured data from actual ships to date, a roll angle of 20° is considered to be an unrealistic requirement, except in the case of parametric rolling. On the other hand, similar to the Comprehensive Revision of Part C, calculations for container securing strength are performed on the assumption that a certain roll angle occurs by applying a lower limit value of the metacentric height *GM* for calculation of the roll angle. Because the lower limit value of *GM* is given as a function of the ship's breadth *B*, and not as a constant value, it takes a form that can respond to the upscaling of ships.

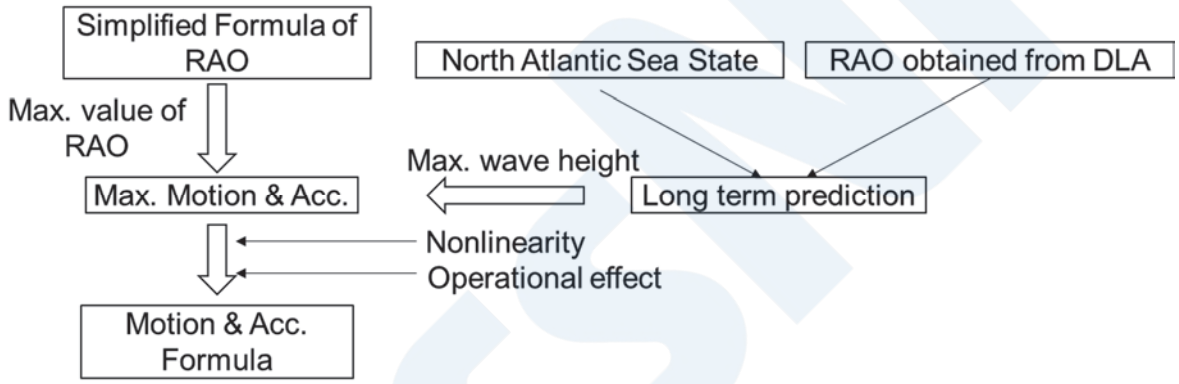

Fig. 2 Flowchart of the motion and load equation

Table 2 shows a comparison of the roll angles before and after the revision of the Guidelines. GM was set to 1.5 m for all ship sizes. Since the roll angle is influenced by various parameters such as C_w and *KG* in addition to *GM*, the author wishes to note that the calculations in Table 2 are only examples. For ship sizes of 8 000 TEU class or larger, the roll angle had been decided based on the limitation of a minimum roll angle of 20° in the second edition, but the roll angle has now decreased by about 2 to 5° because this limitation is no longer applied in the third edition of the Guidelines. Similarly, the roll angle for feeder container carriers (A, B) has also decreased by about 5°. From the influence evaluation in structural strength evaluations, it is considered that the roll angle evaluation equations obtained in the Comprehensive Revision of Part C do not conflict with the data for actual ships. Thus, it can be said that excessive safety factors for load evaluation equations could be eliminated as a result of this revision.

Table 2 Comparison of roll angles (*GM* = 1.5 m)

No.		A	B	C	D	E
Size(TEU)		2.5k	3k	8k	14k	24k
Roll angle (deg.)	2nd ed.	26	25.6	20	20	20
	3rd ed.	20.6	20.4	17.7	16.8	14.9

It is thought that many of the container stack collapse accidents of recent years were caused by parametric rolling due to the occurrence of large roll angles even in head or following seas. In addition to the fact that parametric rolling is an extremely

strong nonlinear phenomenon, the maximum rolling angle also changes depending on the order of the waves that a ship encounters, even in sea states with the same significant wave height and mean wave period. For this reason, it is difficult to obtain the maximum response by the method used in the above-mentioned Comprehensive Revision of Part C. Therefore, in addition to assuming appropriate seamanship to avoid parametric rolling, techniques that support evasive navigation to avoid parametric rolling, such as the use of polar charts, etc., are also provided separately.

3.2 Updating of Route Correction Factors

The loads used in evaluations of hull structural strength are generally obtained assuming that the ship navigates for 25 years in the North Atlantic Ocean (IACS Rec.34), which is the sea area with the most severe sea states. The loads obtained in the Comprehensive Revision of Part C described in section 4.1 are also the same. This practice is adopted because the sea areas where ships will actually be used during their life, including vessels sold as used ships, are unknown. On the other hand, if the routes in short-term navigation are known in advance, there are no safety-related problems for securing strength evaluations using the motions and accelerations assumed in the sea states the ship will encounter when passing through those waters.

Therefore, in calculations of the strength of container stowage and securing arrangements, it is possible to use the loads obtained assuming the waters to be navigated which were determined in advance. Although Fig. 3 shows the significant wave height values for each sea area, it can be understood that there are large differences depending on the sea areas. The reduction factor for the load calculation formula for the sea area to be navigated described in Fig. 4.1 is called the route correction factor.

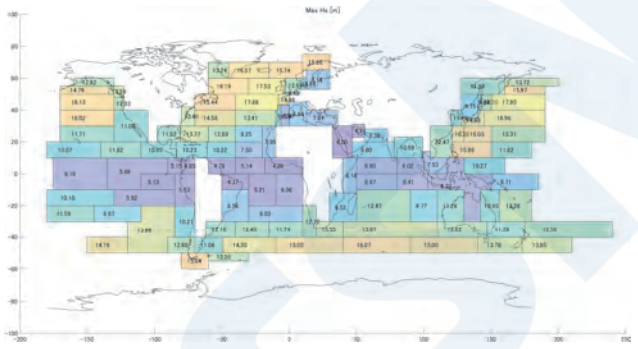

Fig. 3　Maximum significant wave heights of each sea area

While route correction factors were also provided in the Guidelines before revision, they were limited to the main routes and could not be used for any arbitrary route. As an additional problem, those factors were obtained empirically, and no technique for considering the ship sizes of individual ships was provided. Therefore, this revision provides a general technique for obtaining route correction factors, and the Society also plans to provide a web application for evaluating the route correction factors of arbitrary routes.

The sea states that occur on each route also differ depending on the season. Figs. 4, 5 and 6 show the significant wave height contours through the full year and in the summer and winter seasons, respectively, based on data acquired from the IOWAGA wave hindcasting database for the period from 1994 to 2018. Through the full year, high significant wave heights can be seen worldwide except around the equator. However, the significant wave height decreases during the summer and winter seasons, even in sea areas where high significant wave heights were seen through the year as whole. In calculating the route correction factors, this revision of the Guidelines provides a technique that makes it possible to obtain different factors not only for the route which a ship is navigating, but also for the season when it navigates that route.

One method for obtaining route correction factors, for example, is calculation using a ratio of the significant wave height. However, these Guidelines recommend making long-term predictions using the RAO (Response Amplitude Operator: response for a regular wave of a unit amplitude) of the individual ship after obtaining the target route and the seasonal wave scatter diagram for the encountered sea states. Although the RAO can also be obtained by a direct load analysis (DLA), a complicated procedure is required. Therefore, this revision uses the simplified formula proposed by Matsui *et al.* [3], which was also adopted in the Comprehensive Revision of Part C. The standard practice is to find the route correction factors by using this RAO as the numerator, and as the denominator, using the product obtained by multiplying the values of long-term predictions based on the wave scatter diagram for the North Atlantic Ocean for the full year by the operational influence factor [2]. This method was

adopted because a systematic evaluation carried out by the Research Institute showed that use of evaluations using wave height ratios resulted in excessively conservative results. As an additional reason, more accurate route correction factors can be found by long-term predictions using the RAO of the individual ship because the synchronous period will differ depending on the actual ship, etc.

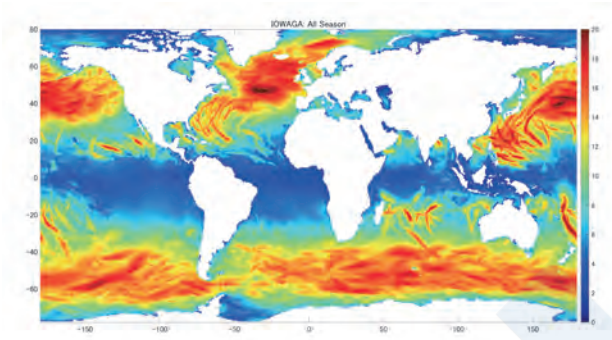

Fig. 4　Map of significant wave heights (full year)

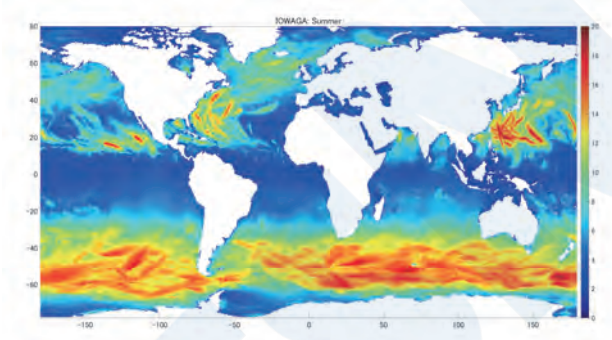

Fig. 5　Map of significant wave heights (summer)

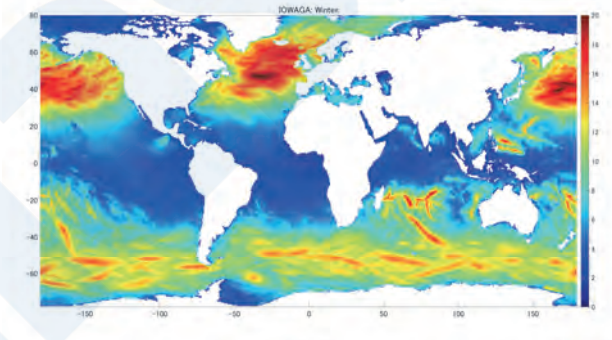

Fig. 6　Map of significant wave heights (winter)

As examples of the wave scatter diagrams used in making long-term predictions, in addition to the diagram for the North Atlantic Ocean given by IACS Rec. 34, the statistical wave database called Global Wave Statistics (GWS) is frequently used. However, since GWS uses sea-state information observed visually from ships during navigation, the influence of the ship operational effect (storm avoidance during bad weather) is implicitly included. Therefore, wave hindcast databases prepared with wave models are used as the natural sea states. The databases of this type are the above-mentioned IOWAGA database created by IFREMER (English name: French Research Institute for Exploitation of the Sea) in France, and ERA5, which was created by ECMWF (European Centre for Medium-Range Weather Forecasts). For more information regarding this type of wave model, please refer to paper No. 6 in this edition of ClassNK Technical Journal (Japanese ed.) [4].

Wave scatter diagrams of encountered sea states are prepared by obtaining the sea states encountered by container carriers by combining container carrier voyage data using AIS data with the natural sea-state data. In this process, appropriate statistical

processing is important, since the AIS data only exist for limited periods. Although several statistical processing methods are available, Fig. 7 shows the result of using a generalized Pareto distribution as one example.

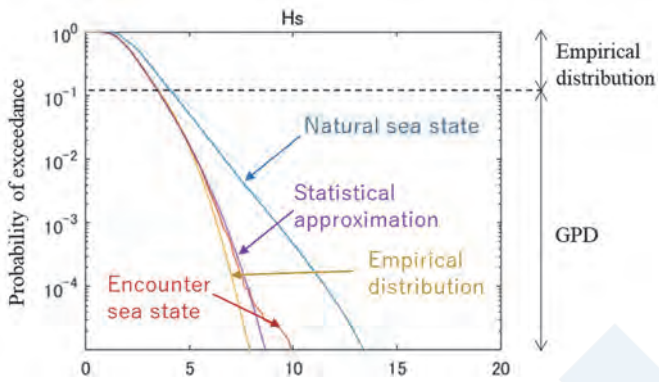

Fig. 7　Statistical processing of encountered sea states

Even on the same route, when seasonal factors are considered, a load decrease of about 30%, for example, can be expected for a feeder container carrier operating in the spring season on an Asian coastal route, in comparison with the load for the full year on the same route. In the case of a mega container carrier exceeding 10 000 TEU operating on an Asia-Europe route, load reductions of approximately 10% in spring and 20% in summer can be expected.

As a result of the updating of the route correction factors described above, it is now possible to set the optimum design loads for the strength of container stowage and securing arrangements for the sea areas where individual ships will operate based on the sea states in each season. We also plan to provide an application that enables easy calculation of route correction factors corresponding to the navigation route and season.

3.3　Revision of Methods of Strength Evaluation of Stowage and Securing Arrangements

Container stacks are generally subject to various types of deformation, namely, racking, floating of the corner castings, compression and shearing, as illustrated in Fig. 8. It is necessary to determine the container securing method, the weight of the containers to be stowed and the container stacking sequence so as not to exceed the allowable loads that occur during these types of deformation. (The Safe Working Load is generally used as the allowable value.) In cases where lashing rods are connected, as shown in Fig. 9, attention must also be paid to the allowable load of the lashing rods because tensile loads are generated in the lashing rods when racking deformation occurs in a container stack. If lashing is not performed, the forces that act on the various parts of the container lashing system can be obtained by regarding the container stack as a single beam. However, when lashing is performed, it is necessary to find the elongation of the lashing rods in order to evaluate the forces they are expected to absorb. At this time, if the container lashing system is linear, the racking displacement vector U can be found by solving the equilibrium equation for racking force shown in Eq. (1). Here, K is the racking stiffness tensor and $F_{racking}$ is the racking external force vector.

$$KU = F_{racking} \qquad (1)$$

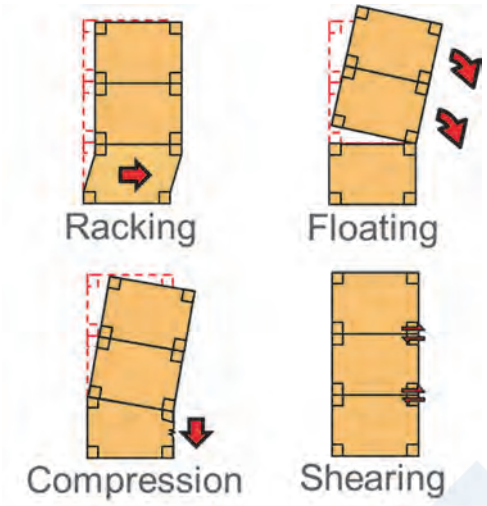

Fig. 8 Deformation behaviors of container stacks

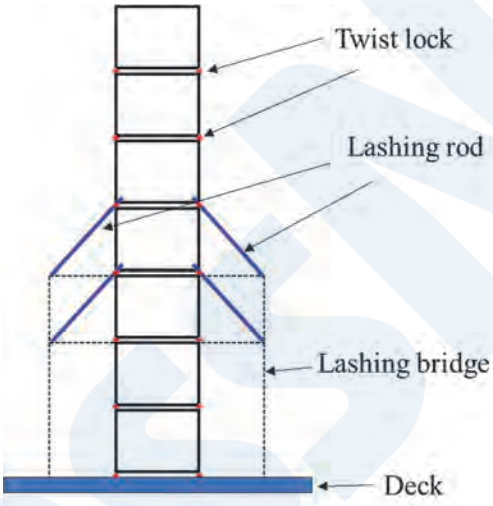

Fig. 9 Example of lashed container stack

For example, considering the case in Fig. 10, K in Eq. (1) comprises the racking stiffness $K_{container}$ of a container and the horizontal stiffness K_{rod} of lashing rods at the position where the lashing rods are connected (corresponding to displacement U_2) and lower positions. In linear problems, the amount of displacement can be obtained easily by solving Eq. (1), but this cannot be applied without modification to nonlinear problems. In calculating the strength of container stowing and securing arrangements considering nonlinearity, the forces acting on each part of the container lashing system can be evaluated directly by using finite element analysis, as in Ghesmi and Brindley (2021) [5] and Li *et al*. (2021) [6]. However, in using the finite element method as an evaluation technique for the Guidelines, there were problems in terms of the time and trouble required in modeling and convergence in nonlinear problems. Therefore, in the Guidelines, an equilibrium equation for nonlinear racking forces was created by expanding Eq. (1) to Eq. (2), where F_{rod_NL} is the nonlinear component of the lashing rod tensile force.

$$KU = F_{racking} - F_{rod\_NL} \qquad (2)$$

The nonlinearity of a container lashing system originates from the clearance that exists between the twist lock and the corner casting, as illustrated in Fig. 11. When a corner casting floats, a clearance exists until it comes into contact with the twist lock, so it so free floating (separation) can occur in the meantime. This means the lashing rod connected to the upper corner casting can elongate in this case. The tension (nonlinear tensile force) of the lashing rod caused by this free floating of the corner casting corresponds to F_{rod_NL} in Eq. (2).

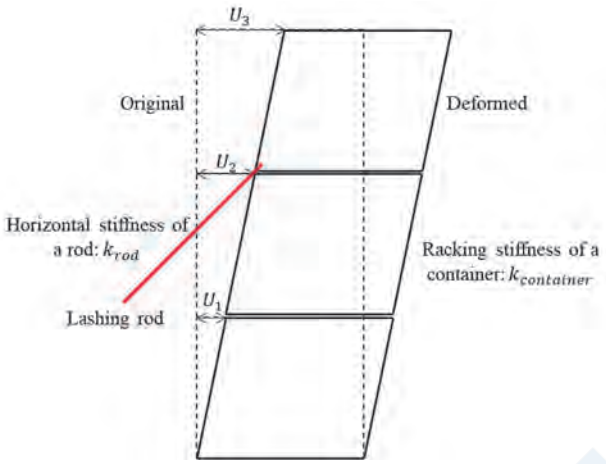

Fig. 10　Schematic diagram of lashed container stack

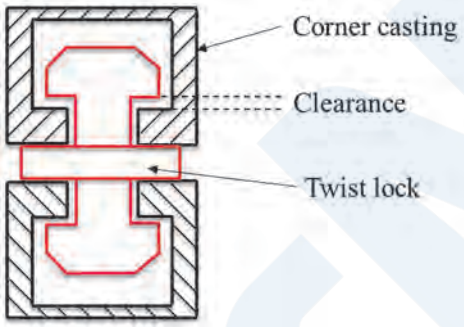

Fig. 11　Corner casting and twist lock

Although the nonlinear tensile force of a lashing rod is determined by the amount of floating of the twist lock, the amount of floating cannot be obtained without determining the tensile force of the twist lock, which is obtained as the result of Eq. (2). Accordingly, it is necessary to solve Eq. (2) by iterative calculation. This time, we developed an algorithm for obtaining the opening/closing and amount of floating of the twist locks by the bisection method, in order from the twist locks that exist at higher positions, for all twist locks positioned below the lashing rod connection, and verified its validity by comparison with the result of a nonlinear finite element analysis.

By considering nonlinearity, as described above, it is possible to evaluate the deformation behavior of container stacks in a more realistic form. The contribution of nonlinearity is particularly large in external lashing, as the lashing rods are connected to corner castings on the side where tension occurs, so the amount of vertical floating of the twist locks is reflected directly in elongation of the lashing rods. In internal lashing, on the other hand, only the increase in horizontal displacement accompanying rigid body rotation of the containers due to twist lock floating contributes to lashing rod tension, so the container stack deformation suppression effect of nonlinearity is small in comparison with external lashing.

In addition to introducing the above-mentioned nonlinearity, the new Guidelines also consider the stiffness of the lashing bridge, and the allowable loads for corner castings were also reviewed, reflecting recent trends.

4.　RESULTS OF TRIAL CALCULATION

Assuming a mega container carrier of 14 000TEU class, a trial calculation was carried out considering the revisions described up to this point, and the results were compared with the results of an evaluation according to the second edition of the Guidelines. Here, the object was a 10-tier container stack with two external lashings, and wind loads were not considered. However, in the calculation according to the third edition, the stiffness of the lashing bridges was considered.

In addition, calculations were performed using the equations provided in the respective Guidelines for the roll angle, roll angular acceleration and heave acceleration. Figs. 12 and 13 show the evaluation results, targeting the compressive load on

corner castings, which tends to be particularly severe. Figs. 12 and 13 show the cases of a container stack with a low center of gravity and a high center of gravity, respectively.

In the results in both Fig. 12 and Fig. 13, the usage factor (ratio of acting force to the allowable value) decreased in comparison with the former Guidelines. In particular, in the third edition calculation results for the container stack with a high center of gravity, the lashing rods work more because separation of the twist locks occurs, and the usage factor decreases greatly in comparison with the calculation results for the second edition. In the low center of gravity case, the load reduction and the review of allowable values resulted in a difference in the calculation results because separation did not occur. Although the same values were used for the stiffness of the lashing rods in the calculations according to the second edition and third edition, it should be noted that the stiffness of the lashing bridge is considered in calculations according to the third edition. Since this leads to a decrease in the stiffness of the lashing rods, care is necessary.

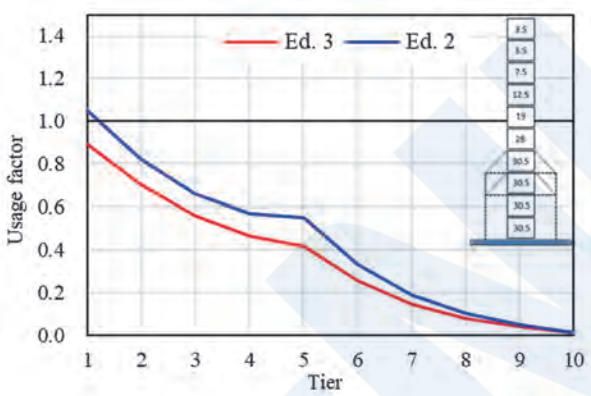

Fig. 12 Evaluation results of compressive load of corner castings (low center of gravity container stack)

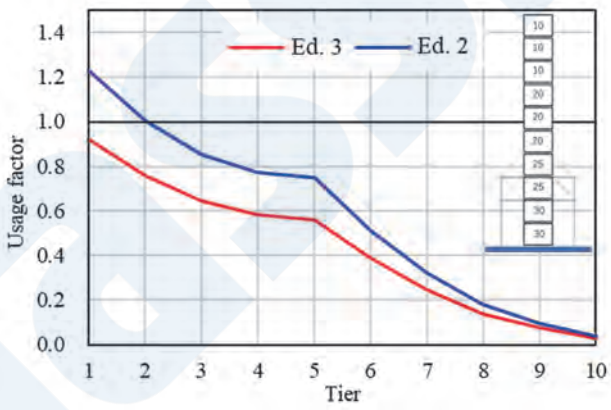

Fig. 13 Evaluation results of compressive load of corner castings (high center of gravity container stack)

5. SUMMARY AND FUTURE OUTLOOK

As explained up to this point, greater optimization and more realistic evaluations of the strength of container stowage and securing arrangements could be realized by incorporating the results of the Comprehensive Revision of Part C and the results of research by the Research Institute in the third edition of the Guidelines. In addition, the Society also plans to provide an application for calculation of route correction factors and calculation tools for use in strength evaluations of container stowage and securing arrangements to the related companies. Those with an interest in these items may contact the Research Institute.

On the other hand, in this revision work, we discovered several items which will require continuing study in the future. The first is integration with digital twin technology. In particular, by utilizing sea-state forecasting technologies, it is expected to become possible to conduct strength evaluations of container stowage and securing arrangements using the sea states which individual ships actually encounter during voyages. However, because the accuracy of sea-state forecasts decreases at dates further into the future, it will be necessary to verify the accuracy of forecast values and obtain a quantitative understanding of

the limits of the technology. Because the devices used in container lashing (securing devices, lashing bridges, etc.) are exposed to sea winds, a certain amount of wear and tear is assumed. Since safer container shipping will be possible if we can grasp these conditions quantitatively and in real time, we plan to conduct continuing research on use of digital twin technology.

REFERENCES

1) Shinomoto et al.: Development of Closed Formula of Wave Load Based Upon Long-Term Prediction – Heave Acceleration and Pitch Angle –, ClassNK Technical Journal, No. 3, pp. 113-125, 2021.
2) Miratsu et al.: Evaluation of ship operational effect based on long-term encountered sea states using wave hindcast combined with storm avoidance model, Marine Structures, Vol. 86, 103293, 2022
3) Matsui et al.: Simplified estimation formula for frequency response function of roll motion of ship in waves, Ocean Engineering, Vol. 276, 1141187, 2023
4) Fujimoto et al.: Estimation and Use of Wave Information for Ship Monitoring, ClassNK Technical Journal, No. 6 pp. 79-92, 2022.
5) Ghesmi and Brindley: A nonlinear finite element method to assess loads on container stacks, Ocean Engineering, Vol. 235, 109430, 2021
6) Li et al.: Experimental and numerical investigation on dynamic response of a four-tier container stack and lashing system subject to rolling and pitching, Applied Ocean Research, Vol. 109, 102553, 2021

Introduction of "Guidelines on Preventive Measures against Parametric Rolling"

Katsutoshi TAKEDA*, Masanori AKAGI*, Kinya ISHIBASHI*

1. INTRODUCTION

In response to a series of stack collapse accidents that are thought to have been caused by parametric rolling in large container carriers and other vessels [1)-4)], parametric rolling has attracted considerable attention in recent years, and preventive measures have also become an urgent issue.

In 2020, the International Maritime Organization (IMO) released Interim Guidelines on the Second Generation Intact Stability Criteria – MSC.1/Circ.1627 (hereinafter, SGISc), which specify assessment criteria for dynamic stability failure modes including parametric rolling. In addition, SGISc has made recommendations on a method for simulating parametric rolling and appropriate operational guidance for avoiding parametric rolling. [5)] At the same time, related industries are also implementing a variety of practical measures for avoiding parametric rolling by utilizing wave radar or weather services, reducing excessive roll by installing anti-roll tanks, and others.

Based on this background, ClassNK (hereinafter, the Society) issued "Guidelines on Preventive Measures against Parametric Rolling" (hereinafter, Guidelines; see Fig. 1) in February 2023 to encourage wide adoption of avoidance and preventive measures against parametric rolling [6)].

2. OVERVIEW OF GUIDELINES

The Society affixes the class notation to the classification characters of ships with effective measures against parametric rolling. The intentions of this Guidelines are to identify ships that take parametric rolling measures, improve the added value of ships and encourage adoption of parametric rolling measures. The Guidelines specifies the types of parametric rolling measures which the Society deems effective, and the class notation affixed to the ship's classification characters (Table 1), together with the necessary documentation, surveys and functional requirements to be applied.

Although the mechanism of parametric rolling has been known from an early date and research has also progressed rapidly in recent years, in the future, it will be important to encourage an adequate recognition of parametric rolling and wide adoption of effective measures against this phenomenon. Therefore, the Appendices of the Guidelines describe useful content for the captain, the crew and other related parties, such as the mechanism of parametric rolling and basic precautions for avoidance.

The Appendices also present an outline of the procedure for calculating the response of parametric rolling and methods for preparing polar charts showing the dangerous area where parametric rolling may occur. When it comes to preparing polar charts, the Appendices also explain the detailed procedure, which is based on the theory proposed by Umeda *et al*. [7) 8)]. This method is an extension of Grim's effective wave theory [9) 10)], which has been adopted in the Level 2-C2 criterion of SGISc, and enables us to estimate the roll response in short-crested irregular waves. Use of this method makes it possible to prepare polar charts in a relatively short time for all required sea states and loading conditions.

Table 1 Class notations affixed to ship's classification characters

Types of preventive measures	Abbreviation
(1) Compliance with SGISc (Second Generation Intact Stability Criteria)	PRPM (Design)
(2) Installation of devices and systems for prevention and reduction of parametric rolling, such as anti-roll tanks, etc.	PRPM (Device)
(3) Operational measures to avoid parametric rolling, such as polar charts, etc.	PRPM (Operation)

PRPM: Parametric Roll Preventive Measure

* Research Institute, ClassNK

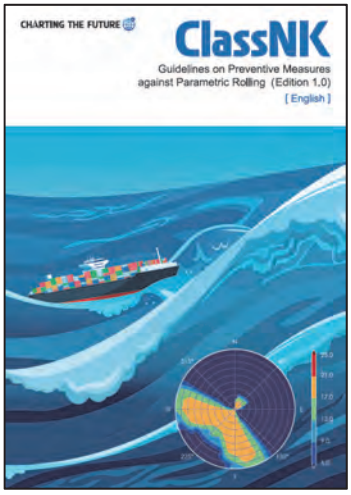

Fig. 1　Guidelines on preventive measures against parametric rolling [6)]

3.　PARAMETRIC ROLLING

3.1　Mechanism

Although parametric rolling is a type of resonance phenomenon, the mechanism is different from that of ordinary synchronous rolling. Synchronous rolling is a resonance phenomenon that occurs when the ship's natural roll period coincides with the wave encounter period, and its amplitude is increased due to forced oscillation of waves.

While parametric rolling is also a resonance phenomenon caused by waves, it is not caused by forced oscillation of waves. Rather, resonance occurs due to periodical changes in the righting moment of the ship when navigating in head seas, following seas or quartering seas. Parametric rolling occurs easily in ships with a slender hull form with large flairs around the bow and stern, such as container carriers and pure car carriers.

This section presents a simple explanation of the mechanism by which the roll of a ship is amplified by parametric rolling. As shown in Fig. 2, when a ship navigating in head seas or following seas enters the trough of a wave in the phase where it returns from a heeled condition to the upright position (Fig. 2 (1)), the waterplane area increases and the metacentric height *GM* becomes higher. When this happens, the righting moment also increases, causing the ship to roll at a large angular velocity in comparison with the ordinary rolling. Conversely, if the ship also enters the crest of a wave while rolling from the upright position to the opposite side (Fig. 2 (2)), the waterplane area decreases, reducing the ship's righting moment, causing the ship to roll to the opposite side with a larger angle than in the ordinary rolling. As this cycle is repeated, the amplitude of rolling increases, causing heavy rolling.

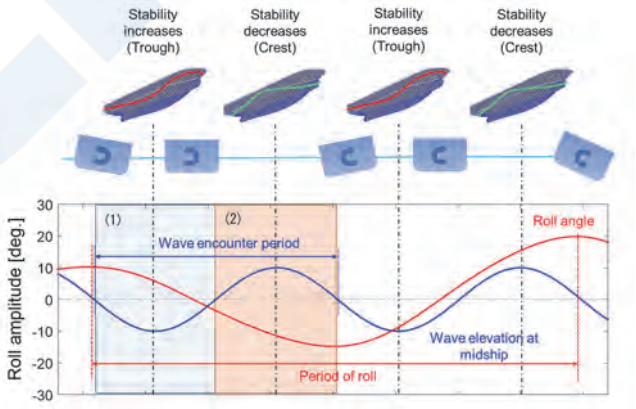

Fig. 2　Development of parametric rolling

As shown in Fig. 2, the ship encounters two crests and two troughs in one roll period. As is well known, one of the conditions

causing parametric rolling is that the wave encounter period T_E is approximately half of the ship's natural roll period T_R ($T_R \fallingdotseq 2T_E$). Theoretically, parametric rolling may occur under conditions that satisfy $T_R : T_E \fallingdotseq 2 : n$ ($n = 1,2,3 \ldots$), but only the condition $n = 1$ should be generally considered.

Another condition is that the amplifying effect due to changes in the righting moment exceeds the reducing effect of damping forces. This can be expressed as shown in Eq. (1). This theory is the basis for the Level 1 criterion of SGISc [10].

$$\frac{GM_{max} - GM_{min}}{2\overline{GM}} > \frac{4\alpha}{\omega_0} \qquad (1)$$

GM_{max}: Maximum (at trough) value of *GM* (m)
GM_{min}: Minimum (at crest) value of *GM* (m)
$\overline{GM}(= (GM_{max} + GM_{min})/2)$: Mean *GM* (m)
α: Linear roll damping coefficient
$\omega_0(= 2\pi/T_R)$: Natural roll circular frequency (rad/s)

From the Eq. (1), it can be said that parametric rolling occurs more easily as *GM* becomes smaller and its variation becomes larger. Generally, the variation of *GM* increases as the wave height becomes larger. At the same wave height, *GM* has the largest variation when the wavelength is equal to the ship length. In other words, when a ship encounters swells with a high wave height and a long wavelength equivalent to the length of the ship, there is an increased risk of parametric rolling.

3.2 Key Points for Avoiding Parametric Rolling

As mentioned previously, parametric rolling is a unique phenomenon that occurs suddenly when navigating in a head sea, following sea or quartering sea in sea states with large swells. If a ship encounters sea states conditions that can cause parametric rolling, heavy roll may occur in a short time. Then it would be almost impossible to take any action. For this reason, advance preparation, bearing in mind the possibility of parametric rolling, is essential. Early action should be taken to avoid dangerous areas with a high possibility of parametric rolling, and appropriate operation, i.e., immediate changes in the ship speed and course, must be made when advance signs of parametric rolling are detected. Therefore, the following describes the precautions and preparations which are considered important for avoiding parametric rolling.

(1) Natural roll period of the ship

Because parametric rolling is a phenomenon in which the periodic change of a ship's righting moment and the natural roll period are related, it is extremely important to determine the ship's natural roll period. The natural roll period T_R can be obtained theoretically by the following Eq. (2).

$$T_R = \frac{2\pi K}{\sqrt{gGM}} \qquad (2)$$

where, g is acceleration of gravity and K is the roll radius of gyration considering the effect of added mass. The Guidelines provide the simplified equation shown as Eq. (3), in which *K* is set empirically to $K \fallingdotseq 0.4B$ (B: breadth of the ship).

$$T_R \approx \frac{0.8B}{\sqrt{GM}} \qquad (3)$$

In estimation of the natural roll period from roll monitoring data rather than by the simplified equation, the use of data is effective after considering the applicable range and reliability of the estimation. However, it is important to remember that the roll periods observed during navigation change constantly due to the effects of waves and wind force, and are not necessarily identical with the actual natural roll period. In addition, it is considered necessary to collect measured data for a long period of time in order to estimate the natural roll period from roll monitoring data with high reliability.

The International Code on Intact Stability, 2008 (2008 IS Code) [11], which is cited in materials on ship stability and loading manuals, defines the following Eq. (4). Many onboard stability computers and loading computers output the natural roll period

based on Eq. (4). However, because these are based on actual data acquired with relatively small vessels such as passenger ships, cargo ships and fishing boats until 1980s, there have been warnings to the effect that they should not be applied to general merchant ships built in recent years [12]. Thus, the natural roll periods based on the 2008 IS Code should not be used as reference.

$$T_R = \frac{2 \times C \times B}{\sqrt{GM}}$$

$$C = 0.373 + 0.023\left(\frac{B}{d}\right) - 0.043\left(\frac{L_{wl}}{100}\right) \quad (4)$$

where, d is draft and L_{wl} is the length of water line of a ship.

(2) Direction and encounter period of swells

As conditions for parametric rolling, there is generally a high probability of parametric rolling when a ship encounters large swells with a length equal to or longer than the ship length within a range of approximately 60° to the right or left of the bow or stern, and the wave encounter period is also close to half of the ship's natural roll period. When wave radar is installed on the ship and can directly measure the wavelength, direction, period and wave height of swells, those measured values are used, but a rough estimate of the wavelength is also possible by a method using the chart in Fig. 3 [14]. In the example in Fig. 3, when a ship encounters swells with a wave encounter period of 25 s and a quarter direction of 30° from the stern side (quartering sea) while navigating at a speed of 20 knots, the chart shows that the actual wave period is approximately 9 s. The wavelength of the swell can be found in a simple manner by multiplying 1.56 by the square of the wave period, and is estimated at 126m in the example in Fig. 3.

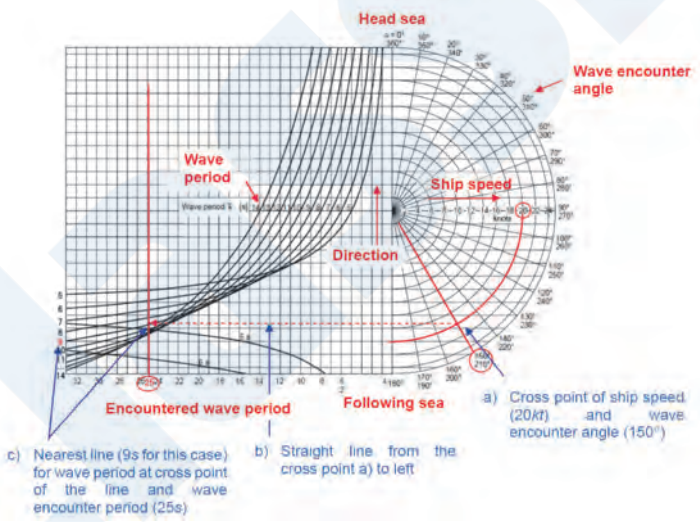

Fig. 3 Determination of the wave period (Source: Notice from Japanese Gov. (MLIT) [14] based on MSC.1/Circ.1228 [13])

(3) Ship's vulnerability to parametric rolling and operational guidance

SGISc (Second Generation Intact Stability Criteria) issued by the IMO specifies three evaluation levels (Level 1 to Level 3) respectively for dynamic stability failure modes, such as the dead ship condition, surf-riding, pure loss of stability and parametric rolling. When it comes to vulnerability to parametric rolling, Level 2-C2, which applies Grim's effective wave theory, is a practical method in terms of both evaluation accuracy and difficulty.

Although SGISs is not a mandatory code (as of July 2023), it is expected to attract attention in the future as part of measures against parametric rolling. Furthermore, when a ship does not comply with the vulnerability criteria, SGISc specifies application of operational guidance such as polar charts. When polar charts are provided for a ship, a good understanding of their content and method of use is important.

4. PREPARATION OF POLAR CHARTS

4.1 Overview of Polar Charts

The above-mentioned polar chart is one of the effective tools for avoiding parametric rolling, and it can visually represent the estimated roll angle or frequency of occurrence of rolling exceeding a certain threshold value for various loading and sea state conditions. For example, the polar chart in Fig. 4 shows the estimated maximum roll angles in a range of wave encounter angles and ship speeds, which are shown in the radius vector direction. Here, "head sea" and "following sea" are defined as 0° and 180°, respectively, and the ship's heading is fixed at 0°. The dangerous area where parametric rolling can occur is shown in an easily-understood form by a contour display of the estimated maximum roll angles.

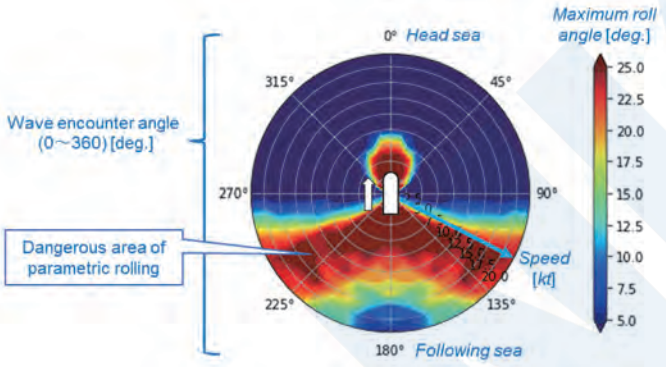

Fig. 4 Example of chart of estimated parametric rolling angles

4.2 Calculation of Parametric Roll Response

The governing equation with one degree of freedom (1-DOF) for obtaining the response values of parametric rolling can be expressed by Eq. (5).

$$\ddot{\phi} + 2\alpha\dot{\phi} + \gamma\dot{\phi}^3 + \omega_0^2 f(\phi, t) = 0 \qquad (5)$$

where, ϕ is the roll angle, α and γ are linear and cubic damping coefficients, respectively, and $f(\phi, t)$ is a nonlinear righting moment term and includes variation components of *GM* and righting arm *GZ*. Basically, the response of parametric rolling is determined by carrying out a numerical simulation based on the following conditions.

- As the wavelength λ, assume a sine wave having a length equal to the length between perpendiculars L_{PP} of the ship.
- Consider the variation of righting moment due to movement of waves.
- Assume a 5° heel condition of the ship as the initial condition.
- Carry out the calculation of the simulation for a sufficient time.
- Adopt the converged value of the roll angle amplitude in the calculation time domain as the response value. If the calculation does not converge, increase the number of calculation steps as necessary.

4.3 Polar Chart Preparation Procedure

Several methods for preparing polar charts are available. However, in the Guidelines, a preparation procedure based on the method proposed by Umeda *et al.* [7) 8)] is described. This method makes it possible to prepare polar charts that consider the response in quartering seas even in calculations using a simulation code with one degree of freedom. Fig. 5 shows a procedure for preparing the polar chart.

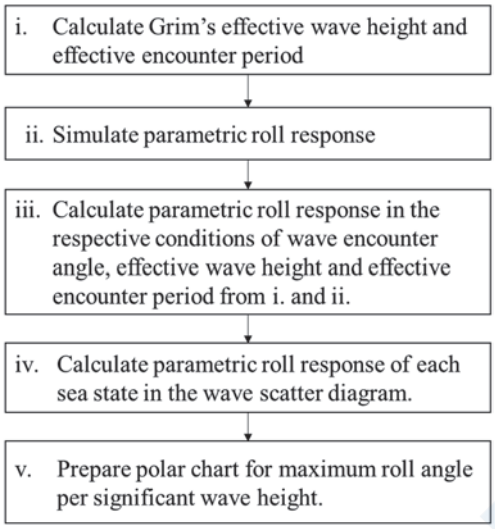

Fig. 5　Polar chart preparation procedure

First, using Eqs. (6) and (7), Grim's effective wave height H_{eff} can be obtained for each sea state, as defined by combinations of the significant wave height H_S and zero-crossing mean wave period T_Z in the wave scatter diagram, and each wave encounter angle. Although IACS Rec. 34 was revised in 2022 [15], the Guidelines refer to the Pierson-Moskowitz (P-M) type wave spectrum (Eq. (8)) and wave scatter diagram in the 2001 edition of IACS Rec. 34 [16], as well as SGISc. IACS Rec. 34 corresponds to sea states in the North Atlantic Ocean, and it is possible to use a different wave spectrum when preparing polar charts for designated sea areas or routes.

$$H_{eff} = 4.0043\sqrt{\int_{-\pi/2}^{\pi/2}\int_{-\infty}^{\infty} S\eta_{eff}(\omega, L_{PP}, \alpha)\, d\omega d\alpha} \quad (6)$$

$$S\eta_{eff}(\omega, L_{PP}, \alpha) = \left[\frac{\frac{\omega^2}{g} L_{PP}\cos\chi \sin\left(\frac{\omega^2}{2g} L_{PP}\cos\chi\right)}{\pi^2 - \left(\frac{\omega^2}{2g} L_{PP}\cos\chi\right)^2}\right]^2 S(\omega, \alpha) \quad (7)$$

$$S(\omega, \alpha) = \frac{H_S^2}{4\pi}\left(\frac{2\pi}{T_Z}\right)^4 \omega^{-5} \exp\left[-\frac{1}{\pi}\left(\frac{2\pi}{T_Z}\right)^4 \omega^{-4}\right] k\cos^2\alpha \quad (8)$$

$$k = 1/\int_{-\pi/2}^{\pi/2} \cos^2\alpha\, d\alpha$$

where, $S\eta_{eff}$ is the spectrum of the effective wave, ω is the circular frequency and χ is the wave encounter angle.

Next, from the effective wave spectrum, the ship speed U and the wave encounter angle, the effective circular encounter frequency $\bar{\omega}_e$ and effective encounter frequency $\bar{T}_e$ can be obtained using Eq. (9). As mentioned previously, in this paper, head seas and following seas are defined as 0° and 180°, respectively, but it should be noted that the definitions of the wave directions and the sign in the equations in the references [7) 8)] are different from those in this paper. Here, although the effective encounter period does not depend on the significant wave height, it is necessary to calculate parametric roll response for each encounter angle, ship speed and zero-crossing mean wave period.

$$\bar{\omega}_e = \sqrt{\frac{\int_{-\frac{\pi}{2}}^{\frac{\pi}{2}}\int_{-\infty}^{\infty}\left(\omega + \frac{\omega^2}{g} U\cos\chi\right)^2 S\eta_{eff}\, d\omega d\alpha}{\int_{-\frac{\pi}{2}}^{\frac{\pi}{2}}\int_{-\infty}^{\infty} S\eta_{eff}\, d\omega d\alpha}} \quad (9)$$

$$\bar{T}_e = \frac{2\pi}{\bar{\omega}_e}$$

If the effective wave height and the effective encounter period can be calculated, the estimated maximum roll angle for each sea state in the wave scatter diagram can be found by combining those results with parametric roll response. In the Guidelines procedure, the estimated roll angle of polar chart shows the maximum roll angle for a certain significant wave height, and not the results for each zero-crossing mean wave period.

4.4 Examples of Polar Charts

Fig. 6 shows examples of polar charts prepared by the procedure in the Guidelines. Here, we used the ship size and principal particulars [17] of the ClassNK's original 14 000 TEU container carrier (Table 2).

Table 2 Principal particulars of the ClassNK's original container carrier used in trial calculation [17]

Length (L_{pp})	352.0m
Breadth	50.0m
Draft	15.0m
C_b	0.676
Bilge keel (length)	From S.S.3.95 to S.S.6.0
Bilge keel (width)	0.4m

The natural roll period is a value which was obtained by a simple estimation from $0.77B/\sqrt{GM}$. Fig. 6 shows that when *GM* = 1.5 m ($T_R = 31.4s$), parametric rolling will occur under a following sea even in a sea state with a relatively small significant wave height. Especially in the case of quartering seas, the area where heavy roll occur shows almost no dependence on the ship speed. When *GM* becomes large and the natural roll period is 25 s or less, parametric rolling tends to occur even in a head sea. Furthermore, parametric rolling hardly occurs when *GM* is 4.5 m and the natural roll period is approximately 18 s. In large container carriers with small *GM*s, it is necessary to pay attention to the range from following seas to quartering seas. Thus, by preparing polar charts, the area where parametric rolling occurs at various *GM*s can be found in advance.

Fig. 6 shows examples of polar charts for significant wave heights which were prepared by the procedure in the Guidelines. That is, the figure shows the maximum roll angles at all zero-crossing mean wave periods for various significant wave heights. On the other hand, Fig. 7 shows polar charts for a condition of *GM* = 1.5 m for zero-crossing mean wave periods of 6.5 s, 8.5 s, 10.5 s and 12.5 s. Because the parametric rolling is related to the natural roll period of a ship and the wave encounter period, the area of parametric rolling can be narrowed as shown in Fig. 7 if the zero-crossing mean wave period can be identified. In actual operation, it is also possible to show polar charts reflecting the real sea state on a ship by linking with wave radar or weather routing, which is expected to be used for more practical operation support.

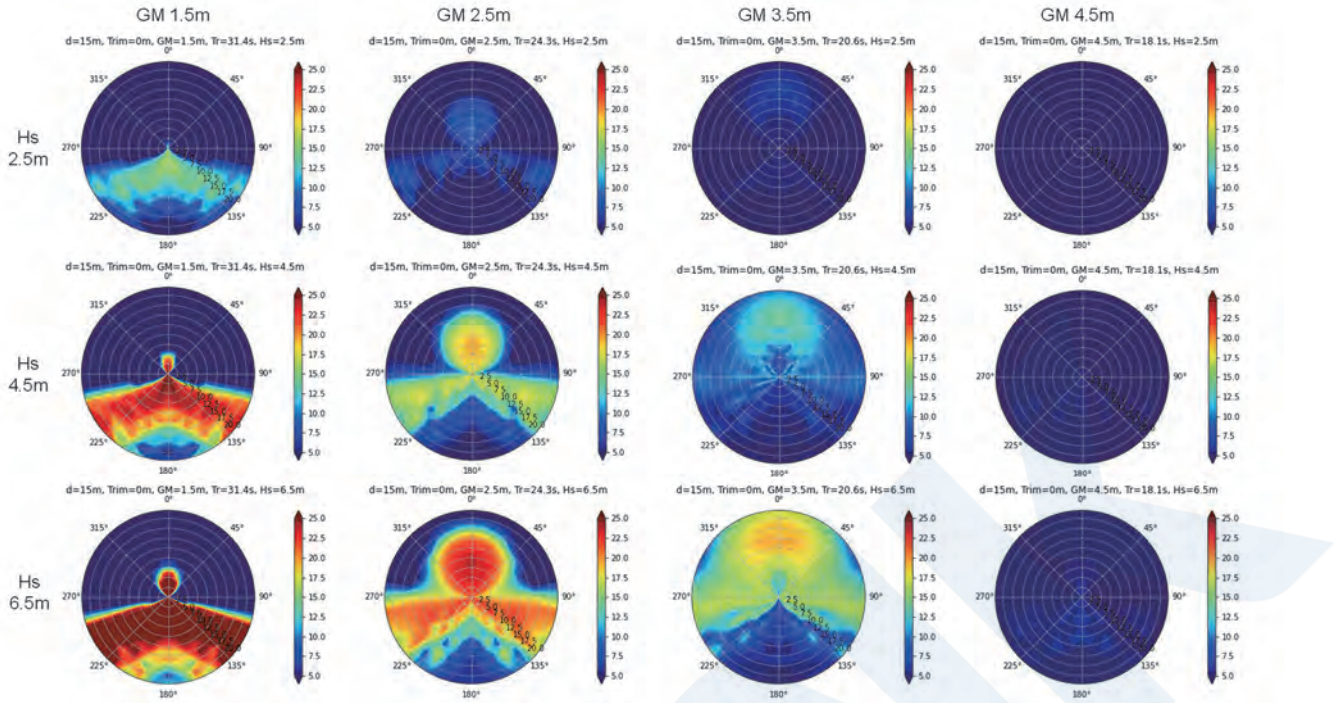

Fig. 6　Examples of polar charts for various *GM*s and significant wave heights
(*GM*: 1.5 m, 2.5 m, 3.5 m, 4.5 m / Significant wave height H_S: 2.5 m, 4.5 m, 6.5 m)

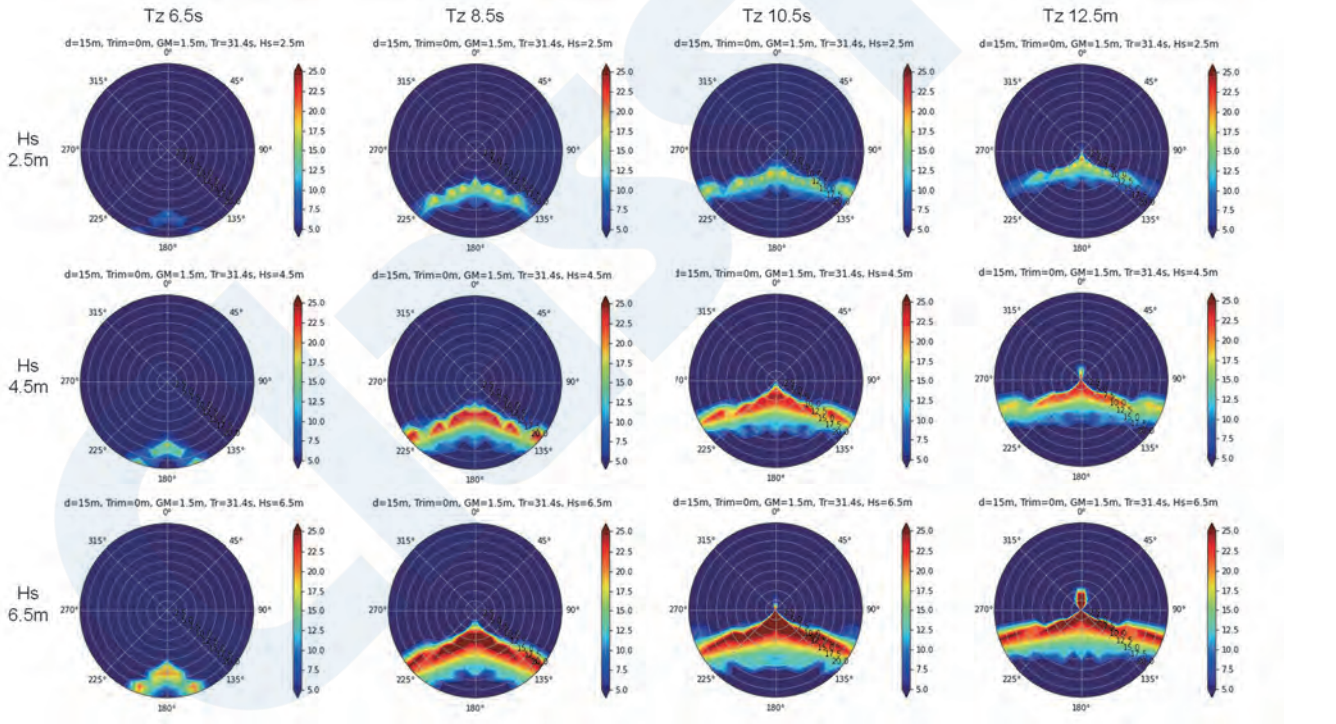

Fig. 7　Examples of polar charts for various significant wave heights and zero-crossing mean wave periods for GM = 1.5 m
(Zero-crossing mean wave period T_Z : 6.5 s, 8.5 s, 10.5s, 12.5 s / Significant wave height H_S : 2.5 m, 4.5 m, 6.5 m)

5.　CONCLUSION

In response to a heightened recognition of the need for preventive measures against parametric rolling, the Society issued Guidelines, and has announced the related requirements and the class notations to be affixed to ship classification characters,

and also presented a basic commentary on avoidance of parametric rolling. A method that expands the Level 2-2C criterion of SGISc to short-crested irregular waves was adopted, and a practical procedure for preparing polar charts was described. This method enables us to prepare polar charts for various assumed sea states and loading conditions in a relatively short time, without a long-term simulation for irregular wave conditions.

If ships are equipped with wave radar and have access to a weather service, polar charts corresponding to the actual encountered sea states can be displayed on board and it is expected to be utilized for more practical support for ship operation, for example, weather routing considering parametric rolling. Although not described in this paper, anti-roll tanks have also attracted attention as one of the measures against parametric rolling, and installation on ships have also increased in recent years.

The Society will continue to grapple with measures against parametric rolling in the future through various activities such as research and development of various measures, including anti-roll tanks, establishment of the related evaluation criteria, and technical support for preparation of polar charts.

ACKNOWLEDGEMENT

We wish to express our profound thanks to Professor Emeritus Naoya Umeda of the Graduate School of Osaka University for his generous advice and cooperation in the issuance of the Guidelines.

REFERENCES

1) MAIB: Report on the investigation of the loss of cargo containers overboard from P&O Nedlloyd Genoa North Atlantic Ocean on 27 January 2006, 2006
2) DMAIB: SVENDBORG MAERSK Heavy weather damage on 14 February 2014, 2014
3) MAIB: Report on the investigation into the loss of 137 containers from the container ship CMA CGM G.Washington in the North Pacific Ocean on 20 January 2018, 2020
4) DMAIB: MAERSK ESSEN – Marine accident report on loss of cargo on 16 January 2021, 2022
5) IMO: Interim Guidelines on the Second Generation Intact Stability Criteria. MSC.1/Circ.1627, 2020
6) Nippon Kaiji Kyokai (ClassNK): Guidelines on Preventive Measures Against Parametric Rolling, 2023.
7) Naoya Umeda and Yasuyuki Yamakoshi: Assessment of the Probability of Ship Capsizing due to Pure Loss of Stability in Quartering Sea, Spring Conference of the Society of Naval Architects of Japan, 1991 (in Japanese).
8) Naoya Umeda, et al.: Some Remarks on Simplified Operational Guidance for Parametric Rolling, JASNAOE Annual Autumn Meeting Vol.35, 437-440, 2022
9) O. Grim, 1961, Beitrag zu dem Problem der Sicherheit des Schiffes in Seegang, Schiff Hafen, 6, pp. 490-497 (in German).
10) IMO: Development of Explanatory Notes to the Interim Guidelines on the Second Generation Intact Stability Criteria, Annex Appendix 3, SDC 8/5/Add.2, 2021
11) IMO: The International Code on Intact Stability (2008 IS Code). MSC.267(85), 2008
12) Olger René Koop, et al.; Parametric Roll Excited by Low Wave Heights: a New Method to Avoid Critical Sea States Based on 2D Spectra., Stability and Safety of Ships and Ocean Vehicles, 2021
13) IMO: Revised Guidance to the master for avoiding dangerous situations in adverse weather and sea conditions. MSC.1/Circ.1228, 2007
14) Japanese Gov. Maritime Bureau, Ministry of Land, Infrastructure, Transport and Tourism (MLIT): Ship operation in following seas (warning notice), 2010 (in Japanese).
15) IACS: Rec.34 Rev2 Standard Wave Data, 2022
16) IACS: Rec.34 Rev.1 Corr1 Standard Wave Data, 2001
17) Kei Sugimoto, et al.: Non Linear Effect on Wave-Induced Loads for Hull Structural Design -Bulk Carrier, Container Carrier, Vehicles Carrier-, Conference on Ocean, Offshore and Arctic Engineering (OMAE), 2020

Guidelines for Additional Fire-fighting Measures for Container Carriers

Rule Development Department, Rule Development and ICT Division, ClassNK
Material and Equipment Department, Plan Approval and Technical Solution Division, ClassNK

1. INTRODUCTION

Requirements related to fire safety systems are specified in the SOLAS Convention, the ClassNK Rules, etc. The requirements are suitable for the features of machinery spaces, accommodation spaces, cargo spaces, etc. In many cases, the requirements for cargo spaces were originally established to apply to ships carrying conventional cargo such as general dry cargo. However, as a result of recent innovative technologies, ships may transport cargo with characteristics and properties different from those in the past. Although the SOLAS Convention and other international regulations are amended as necessary to ensure that their requirements are appropriate for the cargo transport mode , these revisions sometimes fail to keep up with actual social changes.

Even though the conventions applicable to container carriers have been amended in response to the increasing size of these ships, not a few serious fire accidents have occurred in recent years. The International Maritime Organization (IMO) is reviewing the conventions for further safety.

In the IMO, a draft of a new work plan with the aim of developing new requirements for fire safety measures on container carriers was approved in the 103th session of the Maritime Safety Committee (MSC103) held in May 2021. As per this plan, the discussions are to be completed by 2025, coming into force in January 2028. At the 8th session of the IMO's Sub-Committee on Ship Systems and Equipment (SSE8) held in February 2022 and the 9th session (SSE9) held in February 2023, some proposals to install video thermal monitoring systems and fixed water monitor systems were submitted to respond to fires on weather deck cargo spaces.

On the other hand, there have also been movements among some ship owners and ship management companies which operate mega container carriers. They intend to proceed with a voluntary response in advance of the discussions in the IMO. For supporting such ship owners and companies, Nippon Kaiji Kyokai (ClassNK, hereinafter, the Society) decide to release "Guidelines for Additional Fire-fighting Measures for Container Carriers" for evaluation of additional fire-fighting measures implemented on a voluntary basis. The Society will affix the applicable class notations, corresponding to individual fire-fighting measures, to the container carriers that satisfy the Guidelines' requirements.

This report presents an overview of the requirements for the additional fire-fighting measures provided in the Guidelines.

Fig. 1 Container carrier

2. OVERVIEW OF ADDITIONAL FIRE-FIGHTING MEASURES

2.1 General Requirements

The general requirements mainly specify the strengthening of equipment and machinery required by the SOLAS Convention, such as fire pumps and fire hoses. The concrete requirements are as follows.

(1) Fire control stations: Fire control stations for controlling container fires are to be arranged. These fire control stations are to be provided with ① Information on openings for cargo holds and related information, ② Training manuals, ③ At least ten UHF radios, ④ Stopping devices for mechanical ventilation systems for cargo holds, ⑤ Electrical stopping devices for reefer containers, ⑥ Audible and visual alarms for fire detection systems for cargo holds and/or weather deck cargo spaces, ⑦ Water pressure indicators for fixed water spray systems for cargo holds and/or weather deck cargo spaces (in case fixed water spray systems are installed), and ⑧ Remote control systems for fixed water spray systems for cargo holds and/or weather deck cargo spaces (in case fixed type water spray systems are installed).
The fire control stations may be utilized as fire control stations specified in the existing ClassNK Rules for the Survey and Construction of Steel Ships (hereinafter, the Rules), etc.

(2) Fire pumps: The total capacity of fire pumps is to satisfy the maximum water quantity when using firefighting systems required to use simultaneously by the Rules and the Guidelines.

(3) Fire mains: Fire main lines are to be provided with isolation valves at intervals of not more than 40 meters. Fire hydrants are to be provided for each cargo hold, either one hydrant on both sides of the deck, or one double-mouth type hydrant located at or near the centerline of the ship.

(4) Fire hoses: At least ten fire hoses are to be provided for weather deck cargo spaces. The total number may include fire hoses required by the Rules. Fire hoses are to be provided equally on both sides of the deck.

(5) Water mist lances and mobile water monitors: Water mist lances and mobile water monitors already required in the Rules are to be provided.

(6) Indication of carriage of dangerous goods: In cases where dangerous goods classified as Class 4.3 in accordance with the International Maritime Dangerous Good Code (IMDG Code) or dangerous goods reactive to water are being carried, the relevant loading information is to be indicated at fire control stations.

2.2 Additional Fire Detection Systems for Cargo Holds

2.2.1 Smoke and Heat Detection Systems

For continuous detection of smoke/heat or both in spaces where smoke or heat may accumulate in cargo holds, the following detection systems, for example, are to be provided in the cargo holds.

- Sample extraction smoke detection systems whose detection interval is shorter than the interval specified in the Rules
- Laser smoke detection systems
- Thermography camera systems
- Optical image systems

The following spaces are some examples of requiring continuous detection.

- Void spaces, not loaded with containers, in cargo holds
- Inlets and outlets where smoke may accumulate or pass
- Upper parts in cargo holds
- Spaces provided with equipment for reefer containers (if provided)

2.2.2 Thermal Monitoring Systems

Thermal monitoring systems which are capable of continuously detecting the temperature in cargo holds are to be provided for early detection of heat increases or fires inside containers. As an example of the installation locations of these systems, transverse bulkheads of cargo holds is assumed.

2.3 Additional Fire Detection Measures for Weather Deck Cargo Spaces

2.3.1 Fire Patrols

In order to conduct fire patrols effectively, the equipment for fire patrols is to be provided below, and implementation procedures are to be established.

- Periodical fire patrols provided with portable thermal sensors and UHF radios are to be carried out in accordance with

approved fire training procedures.

- At least two portable thermal sensors for fire patrol use are to be provided in the fire control stations specified in section 2.1.

2.3.2 Thermal Monitoring Systems – Whole Area

Thermal monitoring systems are to be provided for continuous monitoring of the temperature of the whole weather deck cargo spaces. Since these systems are to be capable of monitoring the containers loaded at the highest position, the assumed installation positions are such as bridge deck or funnels (not affected by exhaust gas).

2.3.3 Thermal Monitoring Systems – Local Area

Thermal monitoring systems are to be provided for continuous monitoring of the local temperature of weather deck cargo spaces. The assumed installation positions are at or around lashing bridges.

2.4 Additional Water Spray Systems Installed in Cargo Holds

Water spray systems are to be provided to prevent from spreading fires to other holds and adjacent spaces. Water spray nozzles are to be arranged so as to prevent the spread of a fire in a cargo hold to the upper weather deck and adjacent cargo holds over hatch covers, bulkheads, etc. The following nozzle arrangements are examples.

- Uniformly distributing at 5 liters/min/m^2 to hatch covers, hatch coamings and upper surface areas of the top tiers containers in cargo holds.
- Uniformly distributing at 2 liters/min/m^2 to the end walls of the container in cargo holds and the upper one-third parts of the fore/aft bulkheads in way of cargo holds.

In addition, drainage systems are to satisfy the following.

- Drainage systems are to be sized to no less than 125% of the total capacity of both the water spray system and the water supply from fire hoses.
- Stop valves for drainage systems are to be controllable from positions outside of cargo holds. In addition, such positions are to be easily accessible during cargo hold fires.
- Strainers or grating are to be provided for bilge wells to prevent clogging.
- Eductor systems using the main fire pumps may be provided when the capacity of such pumps is a sufficient amount of water necessary for other fire-fighting activities.

In addition, water level detection systems are to be provided, detecting the water level with a function indicating the water level.

2.5 Additional Fixed Water-Based Systems Installed in Weather Deck Cargo Spaces

2.5.1 Fixed Water Curtain Systems

Fixed water curtain systems are to be provided to prevent fire from spreading in weather deck cargo spaces. The following arrangements are assumed as examples of water spray nozzles.

- Distributing at 2 liters/min/m^2 to deckhouse and engine room case end-walls where is faced to container bays.
- Distributing at 2 liters/min/m^2 to the end wall surface of maximum loadable containers stowed in a bay. (Water spray systems /water curtain systems may be installed at all container lashing bridges for distributing water to all coverage areas.)

2.5.2 Fixed Water Monitor Systems

Fixed water monitor systems, that can protect the entire container bay on deck, are to be provided for fires in weather deck cargo spaces. These systems are to be capable of protecting the upper area of containers stowed on top tiers covered at 2 liters/min/m^2 by at least two monitors. The two monitors located at the fore/aft near the fire may be used simultaneously.

Fig. 2 shows the image of the water systems described in the sections 2.4. and 2.5.

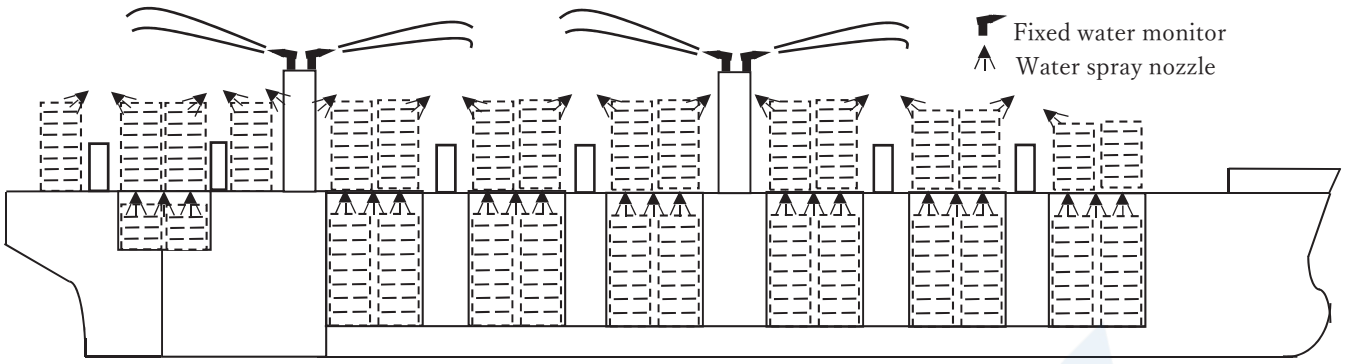

Fig. 2　Image of water systems

2.6　Flooding of Cargo Holds

Systems for flooding cargo holds are to be provided. In principle, simultaneous flooding of multiple cargo holds is not assumed. In cases where fixed flooding system is installed, it is desirable that the system is capable of reaching the design flooding height within 24 hours.

The following auxiliary devices are also to be provided for the flooding systems.

(1) Water Level Detecting Systems: Water level detecting systems are capable of detecting the water level in the flooding cargo holds and have a function for indicating water level are to be provided. System operation is not to be affected by heat generated by cargo hold fires.

(2) Water Ingress Prevention Means: Other cargo holds and surrounding spaces are to be designed to prevent water from entering into other spaces when the flooding is done for fire-fighting purposes.

Sufficient study must be given to the hull strength and stability in the set flooding condition. The requirements to be considered when providing flooding systems are as follows.

(1) Design Flooding Level: Designed flooding level is to be allowable in consideration of hull girder strength, primary supporting hull structural strength and local strength. In case where the design flooding level is below the tops of cargo holds, the design flooding level is to be clearly mentioned in the stability documents.

(2) Stability: Stability is to be mentioned in cases where cargo holds are flooded. The prerequisite conditions for stability calculations are as follows.

- Each cargo hold is flooded under the condition of loading containers into the cargo hold.
- Flooding level is the above-mentioned design flooding level.
- For the free surface effects of flooding water in a cargo hold, the flooding level with the most severe free surface effects is to be applied. In addition, the flooding level used is to be between the bottom level of the cargo hold and the design flooding level. In such cases, free surface effects are to be calculated under the condition of empty cargo holds (no containers in the cargo hold).
- The specific gravity used for calculations is to be the specific gravity of the actual liquid used for the flooding purpose.
- Flooding rate of the cargo holds is to be 0.7 or a value deemed appropriate by the Society.

(3) Strength Requirements: Hull girder collapse and other serious damage to the cargo hold structure are to be avoided, even when a cargo hold is flooded.

(4) Longitudinal Strength: Longitudinal strength under the flooding condition is to be assessed for each cargo hold. The flooding rate is to be taken as 0.7 when calculating the calm sea water bending moment for flooding. However, other values may be used when their appropriateness can be verified.

(5) Primary Structural Support Strength: Primary structural support strength is to satisfy the requirements for the water ingress condition in Chapter 8 of the Rules, Part 1, Part C in consideration of the water head for the design water flooding level.

(6) Local Strength: Plates and stiffeners are to satisfy the requirements for the water ingress condition in Chapter 6 of the Rules, Part 1, Part C in consideration of the water head for the design water flooding level.

Emergency Technical Assistance Service (ETAS): Ships provided with flooding systems are to be registered for Emergency Technical Assistance Service (ETAS).

3. CLASSIFICATION CHARACTERS

"Additional Fire-fighting Measures for Container Carrier (XX)" (abbreviated AFC (XX) is affixed to the classification characters of container carriers adding the measures described in Chapter 2. The additional fire-fighting measures corresponding to "XX" are shown in Table 1.

Table 1 Affixation of class notation for additional fire-fighting measures

Class Notation	Detail
AFC(G)	***A**dditional **F**ire-Fighting Measures for **C**ontainer Carrier (**G**eneral) (**AFC(G)**)*: Affixed to the classification characters for ships provided with the additional fire-fighting measures specified in **2.1.**
AFC(DH)	***A**dditional **F**ire-Fighting Measures for **C**ontainer Carrier (**D**etection of Cargo **H**olds) (**AFC(DH)**)*: Affixed to the classification characters for ships provided with the additional fire detection systems in cargo holds specified in **2.2.**
AFC(DH-SH)	The class notation ***AFC(DH-SH)*** is affixed to the classification characters for ships provided with a combination of **S**moke Detection Systems and /or **H**eat Detection Systems as additional fire detection systems in cargo holds.
AFC(DH-TM)	The class notation ***AFC(DH-TM)*** is affixed to the classification characters for ships provided with **T**hermal **M**onitoring Systems as additional fire detection systems in cargo holds
AFC(DD)	***A**dditional **F**ire-Fighting Measures for **C**ontainer Carrier (**D**etection for Weather **D**eck Cargo Spaces) (**AFC(DD)**)*: Affixed to the classification characters for ships provided with additional fire detection systems for weather deck cargo spaces specified in **2.3**.
AFC(DD-FP)	The class notation ***AFC(DD-FP)*** is affixed to the classification characters for ships provided with measures for **F**ire **P**atrols as an additional fire detection measure on weather deck cargo spaces.
AFC(DD-TMW)	The class notation ***AFC(DD-TMW)*** is affixed to the classification characters for ships provided with **T**hermal **M**onitoring Systems - **W**hole Area as additional fire detection measures on weather deck cargo spaces.
AFC(DD-TML)	The class notation ***AFC(DD-TML)*** is affixed to the classification characters for ships provides with **T**hermal **M**onitoring Systems - **L**ocal Area as additional fire detection measures on weather deck cargo spaces.
AFC(WH)	***A**dditional **F**ire-Fighting Measures for **C**ontainer Carrier (**W**ater Spray Systems Installed in Cargo **H**olds) (**AFC(WH)**)*: Affixed to the classification characters for ships provided with additional water spray systems in cargo holds specified in **2.4.**
AFC(WD)	***A**dditional **F**ire-Fighting Measures for **C**ontainer Carrier (Fixed **W**ater-Based Systems Installed in Weather **D**eck Cargo Spaces) (**AFC(WD)**)*: Affixed to the classification characters for ships provided with additional fixed water-based systems in weather deck cargo spaces specified in **2.5.**
AFC(WD-C)	The class notation ***AFC(WD-C)*** is affixed to the classification characters for ships provided with Fixed Water **C**urtain Systems as additional fixed water-based systems in weather deck cargo spaces.
AFC(WD-M)	The class notation ***AFC(WD-M)*** is affixed to the classification characters for ships provided with Fixed Water **M**onitor Systems as additional fixed water-based systems in weather deck cargo spaces.
AFC(FH)	***A**dditional **F**ire-Fighting Measures for **C**ontainer Carrier (**F**looding of Cargo **H**olds)(**AFC(FH)**)*: Affixed to the classification characters for ships that conform to the requirements for flooding of cargo holds specified in **2.6.**

4. CONCLUSIONS

The Society issued the Guidelines summarizing additional fire-fighting measures to improve the safety against cargo fires on container carriers. While also monitoring the discussion in the IMO, the Society will update the Guidelines as necessary and provide useful Guidelines for additional fire-fighting measures for container carriers. We hope that the Guidelines make container carriers improve fire safety and proactive implementation of safety-related initiatives in the maritime industry.

Structural Strength Rules Applied to Container Ships

Kinya ISHIBASHI*, Kei SUGIMOTO*, Tomohiro SUGIMOTO**

1. INTRODUCTION

ClassNK (hereinafter, the Society) completed a comprehensive revision of Part C of the Rules for the Survey and Construction of Steel Ships (hereinafter, Part C) [1] in 2022 [2]. Based on the knowledge of ship hull structures accumulated in ship classification work over a period of more than 100 years, in this comprehensive revision, the Society conducted research and development on the element technologies of load, corrosion, yielding, buckling, fatigue, etc. necessary in strength evaluations of the hull structure of ships in a rule development project that began in 2017, and adopted the results of the project in the revised rules. The former Rules, while based on load and strength formulae with a theoretical basis, frequently applied empirical engineering techniques, in which appropriate safety factors were derived by investigating the hull scantling necessary to avoid damage in each ship type or structure using records of damage up to the time. In contrast, following the comprehensive revision, the Rules are now based on techniques that accurately estimate and evaluate strength criteria, etc. which are directly tied to the rough sea states which ships encounter, the hull response under those rough sea states, and the condition of corrosion and occurrence of damage of ships in service, making it possible to use the design method called “design by analysis.” Therefore, although Part C of the Rules is applied to various ship types, including container ships, LNG carriers, general cargo ships, etc., the basic strength requirements are unified independent of the ship type. On the other hand, structural requirements specific to a certain ship type, or requirements for problems related to structural strength which are specific to a particular ship type are also necessary in some cases. Container ships have a comparatively large number of requirements of this type.

In response to both the recent sharp increases in fuel costs and the environmental regulations, slow steaming has been adopted. However, this has reduced container shipping efficiency, and progressively larger-scale container ships are being constructed in ways that compensate for this issue. In the 1990s, 9,000 TEU container ships were the largest scale vessels, but 23,000 TEU vessels with a length of more than 400 meters have now appeared.

Because extremely high strength, extremely thick steel plates of YP47 steel with a thickness of 100 mm are used in the upper deck plates and hatch side coamings of large container ships, it has become possible to reduce the amount of steel used in spite of the huge size of the hull structure. For this reason, there tends to be a relative decrease in the stiffness of the hull structure, and it has been pointed out that the effects of elastic vibration of the hull structure, i.e., whipping and springing, become greater. Moreover, since extremely thick steel plates are used under very high tensile stress conditions, the possibility of brittle fracture, which is a dangerous damage mode, has also been noted.

The Society developed the criteria for ensuring safety for these structural strength problems which are specific to large container ships through joint research, etc. with related industries and research institutes. The developed criteria are incorporated in Part C of the revised Rules, which are original structural rules of the Society, or adopted as Unified Requirements (URs) of the International Association of Classification Societies (IACS), through the efforts made by the Society.

This paper presents an overview of Part C of the Rules for the Survey and Construction of Steel Ships, focusing on container ships, and explains the content, history and technical background of the Society’s original strength requirements which are applied exclusively to container ships.

2. DESIGN LOADS OF CONTAINER SHIPS

The wave loads that act on a ship’s hull structure depend largely on the sea conditions which the ship encounters. Structural rules generally consider the sea states in the North Atlantic Ocean, which is thought to have the most severe sea conditions

* Research Institute, ClassNK
** Rule Development Department, Rule Development and ICT Division, ClassNK

among the sea areas that ships navigate. It is possible to estimate waves loads that capture the distinctive characteristics of individual ships by combined use of wave load analysis tools such as the strip method, 3-dimensional panel method, etc.

However, due to practical consideration such as manhours, it would be difficult to use wave load analyses in the design of each individual ship. Therefore, simplified formulae using the principal particulars, etc. of ships are necessary, and several formulae have been established in the structural rules. On the other hand, simplified formulae inherently involve a trade-off between simplicity and accuracy. Thus, the Society has been studying for many years to develop techniques for ensuring a good balance of simplicity, accuracy and transparency of the technical background, and formulated and published the results of our research as the “Guidelines for Container Carrier Structures” in the early 2000s. In addition to the equivalent design wave concept later adopted in the Common Structural Rules (CSR) of the IACS, these Guidelines also provide design torsional loads that occurs in ships with large hatches.

Following the release of the Guidelines, the Society responded to the increasing scale of container ships and twin-island container ships, and also continuously performed tank tests, series calculations by numerical analysis, etc. to address the problem of whipping, which is an elastic vibration phenomenon caused by impact loads due to slamming (see Fig. 1 and Fig. 2). A major revision of the rules for container carriers was carried out from 2015 to 2016, and the related design loads were also refined.

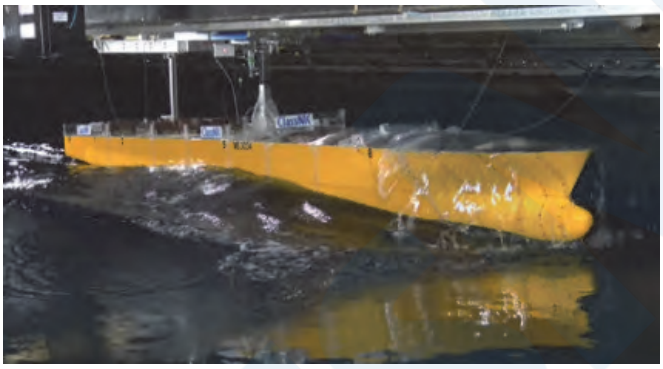

Fig. 1　Tank test of whipping

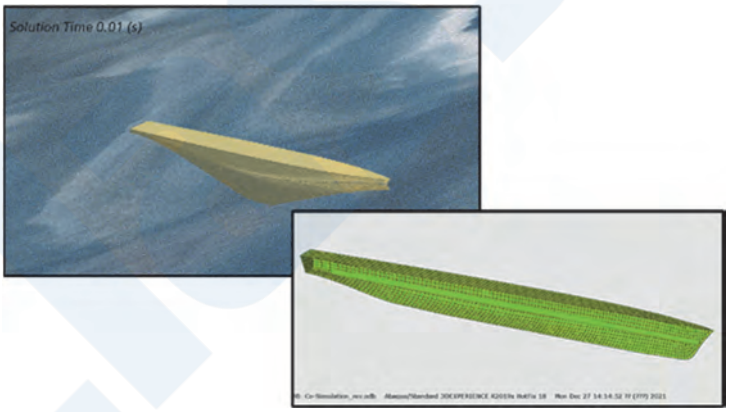

Fig. 2　Reproduction of whipping by analysis (coupled analysis using CFD and LS-dyna)

In the comprehensive revision projects of Part C carried out from 2017 to 2022, the simplified formulae were reviewed to make the design loads closer to the real phenomena, and concepts including the equivalent design wave were adopted throughout (see Fig. 3). Since the design loads for the equivalent design wave, etc. had already been introduced in the revision of Guidelines for Container Carriers in 2015-2016, no large changes are made in the concepts for container ships, but significant changes are made in the forms of the load formulae themselves.

In the above-mentioned comprehensive revision, a physical consideration based on theoretical formulae was carried out for the loads of acceleration and hydrodynamic pressure obtained by direct load analysis, the controlling factors were extracted for each component and their effects were investigated, and finally a careful verification was conducted with a large number of ships, not limited to container ships, based on the procedure of performing simplification. Through this process, design loads with high accuracy and greater generality have been successfully developed. In this project, ship operational effect (in addition,

effect of a route that is applied in a fatigue strength assessment), which had been handled conventionally by an empirical engineering approach, is also clarified by a big data analysis, and those effects are specified in the rules in an explicit form. (For the details of this work, which was carried out in the said project, please refer to papers No. 3 and No. 5in this issue of ClassNK Technical Journal [3) 4) 5)].)

The comprehensive revision improved the transparency of the relationship between sea states and design loads, etc., and in the future, use is expected in various situations, not limited to structural rules.

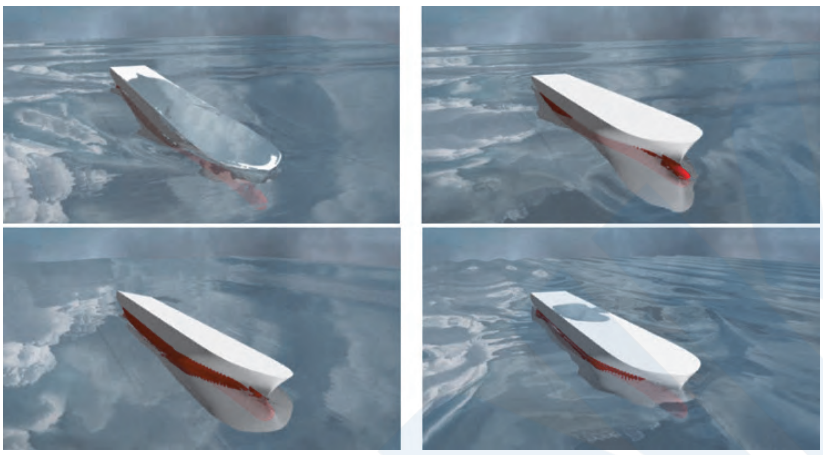

Fig. 3 Four equivalent design waves (top left: HM, top right: FM, bottom left: BR, bottom right: BP)

3. HULL GIRDER ULTIMATE STRENGTH CONSIDERING WHIPPING AND LATERAL LOAD EFFECTS

Based on hull failure accidents involving large container ships which have occurred in recent years, the Committee on Large Container Ship Safety [6)] of Japan's Ministry of Land, Infrastructure, Transport and Tourism (MLIT), consisting of experts dispatched from shipbuilding companies and shipping companies, researchers and persons of learning and experience, and the Society's Investigative Panel on Large Container Ship Safety [7)] conducted various investigations and examinations, and presented recommendations on safety measures for container ships and action plans to be implemented in the future. The Society' Rules make it possible to guarantee structural safety more reliably for large container ships by developing original own strength requirements in line with the recommendations and action plan.

Hull girder ultimate strength refers to the maximum bending moment that a ship's hull treated as a single beam, can withstand without structural failures. Generally, when considering hull girder ultimate strength, it is assumed that only vertical bending moment acts on the ship's hull, and to the influence of the other loads acting on the hull is taken into account with a certain constant safety factors. However, particularly in large container ships, it is known that hull girder ultimate strength decreases significantly as a result of superposing the vertical bending stress and the stresses caused by the double bottom bending due to out-of-plane loads of sea pressure acting on the outer plates (shell plating) of the ship's bottom (Fig. 4). It is also known that the decrease ratio due to the superimposition also changes significantly depending on the design of the individual ship.

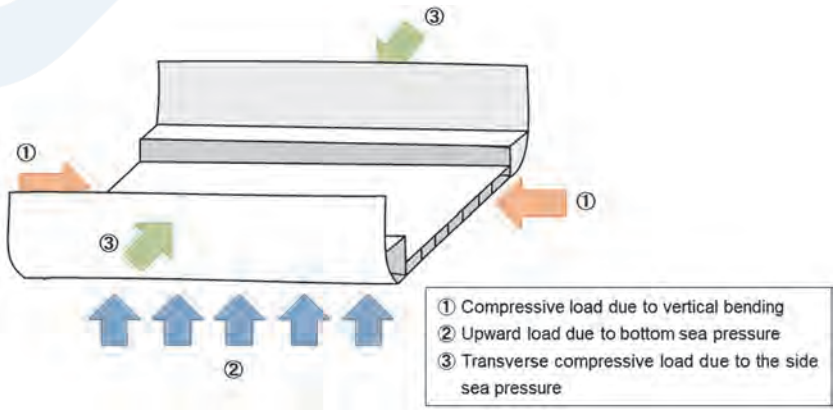

Fig. 4 Types of loads acting on bottom structure of container ships

Therefore, in the Society's Rules, the effects of these lateral loads are not expressed by safety factors with fixed values, but assessments can be carried out corresponding to the design of the individual ship. Concretely, the Rules adopt the simplified calculation method expressed by the following formula, which is derived by a comparative verification with a nonlinear finite element (FE) analysis that can directly consider the effects of lateral loads.

$$M_{U\_DB} = \alpha_U \sigma_{US\_avg} Z_B \times 10^3 \qquad (1)$$

M_{U_DB}: Hull girder ultimate strength considering the effects of lateral loads (kNm)
α_U: Correction factor derived by comparison with a nonlinear FE analysis (1.25)
Z_B: Section modulus at the ship's bottom (m^3)
σ_{US_avg}: Average ultimate strength for ship longitudinal loads of stiffened panels in the bottom shell plating (N/mm^2). The compressive stresses in the ship longitudinal direction and ship transverse direction acting on the bottom shell plates are derived from a cargo hold analysis, and the ultimate strength of the stiffened panels is obtained by considering the effects of the superposition of these stresses.

Vertical bending moment caused by elastic vibration of hull girders due to whipping is superimposed by the vertical bending moment induced by waves (see Fig. 5).

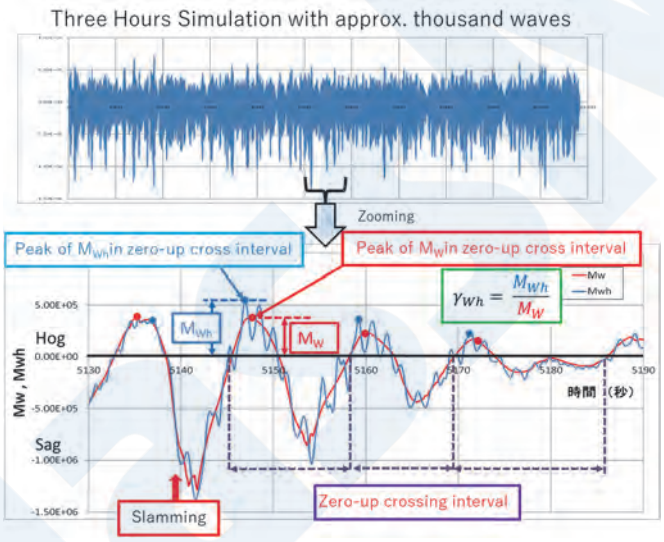

Fig. 5 Superposition of whipping moment

To determine the extent of the superimposed effect of the vertical bending moment, numerical simulations and tank tests using multiple sample ships were conducted as described above in Chapter 2. Based on these findings, a safety factor for the wave-induced vertical bending moment is set so as to enable a conservative assessment of the whipping effect for any container ship. Finally, the hull girder ultimate strength considering the effects of whipping and lateral loads is assessed as follows:

$$M_{Smax} + \gamma_{Wh} M_{W-Hog} \leq M_{U\_DB} \qquad (2)$$

M_{Smax}: Vertical bending moment in still water (kNm)
M_{W-Hog}: Vertical bending moment in waves (kNm)
γ_{Wh}: Safety factor considering whipping (1.5)

4. EFFECT OF ELASTIC VIBRATION IN FATIGUE STRENGTH ASSESSMENTS

Because elastic vibration of the hull girders is superimposed on the cyclic stresses generated by the vertical bending moment

in waves, the stress range and number of cycles increase, and this also affects fatigue strength [8) 9)].

It is difficult to distinguish whether the vibrational phenomena that appear in a ship's hull are caused by springing or whipping. However, it is thought that the vibrational phenomena in sea states with a small significant wave height are caused by springing and those in sea states with a large significant wave height are caused by whipping.

In the design process, a fatigue assessment is typically carried out based on the stress range and the number of cycles caused by wave loads and it is difficult to directly consider the cyclic stresses due to superposition of elastic vibration and the resulting increase in the number of cycles. Moreover, it is also difficult to say that conducting a nonlinear elastic vibration response simulation is realistic. It is considered a convenient and rational approach to take into account the influence of elastic vibrations by multiplying a coefficient that considers the effect of elastic vibrations on the cumulative fatigue damage caused by ordinary wave loads. [10)].

Therefore, in order to understand the nature of the elastic vibration that occurs in actual ships, the ship on-board measurement data for the vertical bending stress of two container ships (8600 TEU, 14000 TEU) were evaluated. The fatigue damage for the measured data for each 1-hour period were evaluated for the measured waveform *WV*, in which elastic vibration is superimposed, and the waveform *W* caused by ordinary wave loads with vibration component removed. The service routes of the 8600 TEU container ship were Asia-Europe and Asia-Europe-North America,via Cape of Good Hope, and back to Asia, while 14000 TEU vessel operated between Asia and Europe. The 8600 TEU container ship navigated severer sea areas.

Because the inverse of the slope of the S-N curve used in the assessment is 3, the fatigue damage is assumed to be proportional to the 3rd power of the stress range. The ratio of the sum of the 3rd powers for the stress ranges in *WV* and *W* for 1-hour period is equivalent to the ratio of the increase in the fatigue damage due to superposition of elastic vibration in welded joints.

$$C_{vib\_k} = \frac{\sum_{i=1}^{N_{WV\_k}} \Delta\sigma_{WV\_k,i}^{3}}{\sum_{j=1}^{N_{W\_k}} \Delta\sigma_{W\_k,j}^{3}} \qquad (3)$$

Fig. 6 shows the relationship of the significant values of the stress range due to an ordinary wave for a 1-hour period, and the ratio of the increase in the fatigue damage due to superposition of elastic vibration. The dotted lines in the figures indicate the increase ratio of fatigue damage for the entire measurement period. This ratio was 2.25 for the 8600 TEU container ship and 1.51 for the 14000 TEU container ship.

Larger variations in the increase ratio of the fatigue damage were observed as the stress range due to ordinary wave loads become smaller because the main factor is elastic vibration caused by springing, and in this case, relatively large vibration is superimposed in comparison with the stress range of ordinary wave loads. On the other hand, in the region of large stress ranges due to ordinary wave loads, where the main factor is elastic vibration caused by whipping, the variations are also small and appear to roughly converge near the average value.

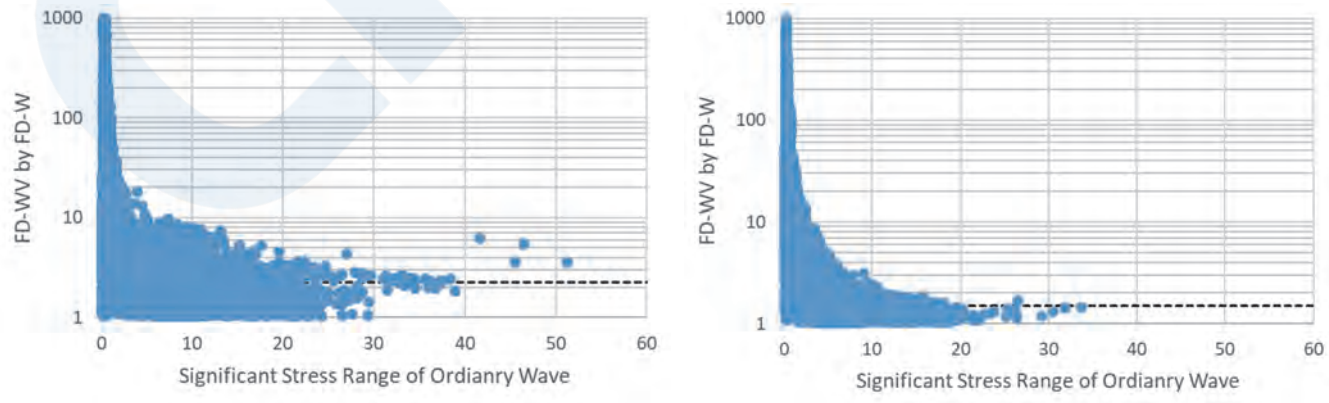

(a) 8600 TEU container ship (b) 14000 TEU container ship

Fig. 6 Increase ratio of fatigue damage by superposition of elastic vibration for 1-hour period

Fig. 7 shows the result when the significant values of the stress range due to ordinary wave loads are divided into 0.5 MPa

increments, and the expected value of increase ratio of the cumulative fatigue damage for each increment is taken. The dotted lines in these figures show the average values for the two container ships, which are 2.51 and 1.63, respectively. These results show that the values are almost constant irrespective of the significant values of the stress ranges and the type of vibration phenomenon, that is, springing or whipping. Based on this, by using the expected value of the increase ratio in cumulative fatigue damage as an influence coefficient, it is considered possible to take the effects of elastic vibration into account, without distinguishing springing and whipping..

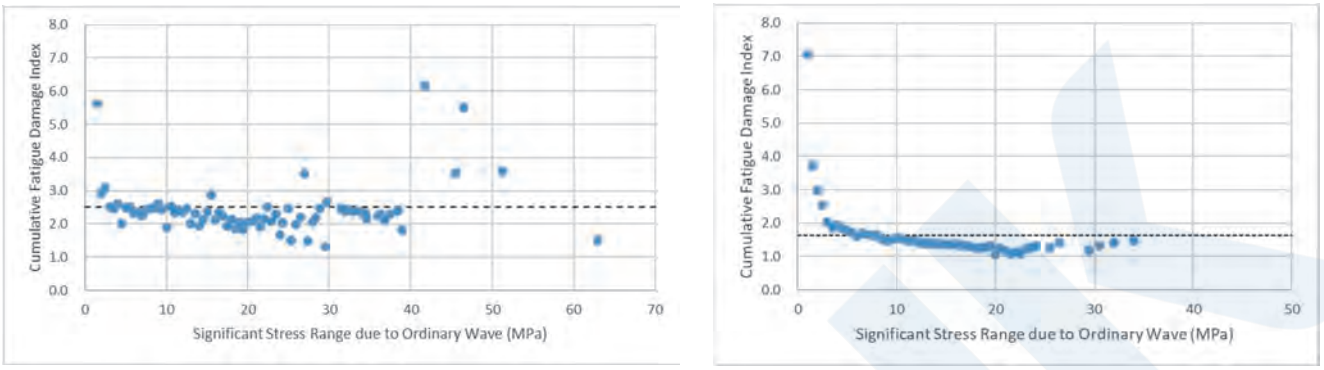

(a) 8600 TEU container ship　　(b) 14000 TEU container ship

Fig. 7　Expected values of increase ratio of fatigue damage by superposition of elastic vibration in increments of 0.5 MPa of significant value of stress range

From the results described above, it is found that the influence coefficient of elastic vibration can be evaluated by performing elastic vibration simulations under sea states with a certain significant wave height. Therefore, in addition to the ship on-board measured data for the two container ships discussed above, elastic vibration simulations were carried out 10 times for the three container ships shown in Table 1, and the influence coefficients of elastic vibration were obtained as average values.

Based on the simulation results, the obtained influence coefficient for elastic vibrations is believed to be consistent with the results from on-board measurement, indicating generally good agreement. As for the ratio of increase in fatigue damage in cases where elastic vibrations occur, it can be considered to be approximately twice the fatigue damage caused by ordinary wave loads.

Table 1　Ships used in elastic vibration simulations and increase ratio of fatigue damage by elastic vibration

	CC-1	CC-2	CC-3
L (m)	350	300	200
Vs (kt)	21.85	27.25	22.50
C_{vib}	2.09	2.15	2.08

Based on a study of the effects of elastic vibration on fatigue strength, the following items are considered:

(1) Elastic vibration occurs under $\pm 30°$ head sea conditions.
(2) Elastic vibration is superimposed onto the cyclic stress caused by the vertical bending moment.
(3) In cases where elastic vibration is superimposed, the fatigue damage increases by approximately twice, regardless of whether it is springing or whipping and irrespective of the significant wave height.
(4) Stress assessment of the design loads in fatigue design is conducted for the long-term expected values of response for all wave directions.
(5) In finite element analysis by the direct method, the combined loads of the each load component are applied as the design load.
(6) Long-term cumulative fatigue damage is calculated based on the long-term distribution of the stress range for linear response.

Based on these items, how the influence of elastic vibration should be considered in the cumulative fatigue damage evaluated in the design stage was studied. In this study, the fatigue damage at the intersection between girders and longitudinal stiffeners

of the target ships was examined as an example. In this evaluation, the vertical bending moment, horizontal bending moment, dynamic wave pressure and response amplitude operator of acceleration in the three directions X, Y and Z were used. The vertical bending moment, horizontal bending moment, stress range by wave and internal pressure at the evaluation position were calculated by using beam theory, and the combined stress considering the phases of the respective load components were obtained. When considering the effects of elastic vibration, a simplified evaluation was carried out by considering a multiplication factor for stress ranges that doubles the fatigue damage when elastic vibration occurred. Specifically, the response amplitude operator of the vertical bending moment in $\pm 30°$ head seas was multiplied by a factor of $\sqrt[3]{2}$. ISSC-1964 was used for the wave spectrum, and the distribution in the $\cos^2$ direction was considered. For the long-term predictions, the response values for all headings and the wave scatter diagram in IACS Rec.34 were used.

Long-term predictions were made for the stress range considering only ordinary wave loads (i.e., excluding stress due to elastic vibration) and for the case which also considers superposition of the stress due to elastic vibration on the vertical bending moment for $\pm 30°$ head seas, and the distributions of the stress range were obtained. Fig. 8 shows the long-term distribution of the stress range of a deck longitudinal, in which vertical bending stress is dominant, and Fig. 9 shows the long-term distribution of the stress range for a side longitudinal near the ship bottom, where both vertical bending stress and local bending stress are large.

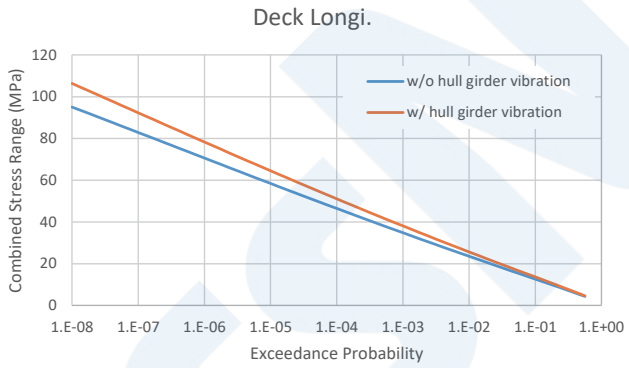

Fig. 8 Long-term distribution of stress range of deck longitudinal

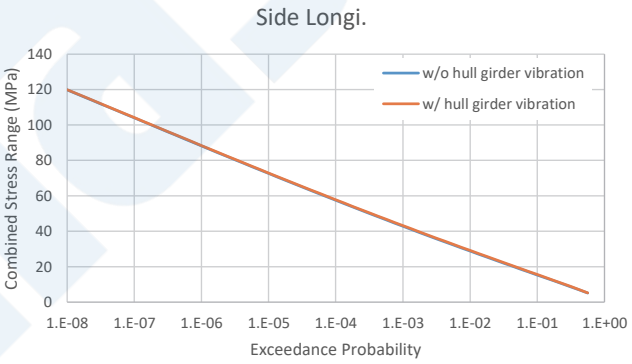

Fig. 9 Long-term distribution of stress range of side longitudinal near the ship bottom

Fig. 10 (a) shows the cumulative fatigue damage normalized by the longitudinal in which the largest cumulative fatigue damage occurred, and Fig. 10 (b) shows the increase ratio of the cumulative fatigue damage considering the effect of elastic vibration. The increase ratio of the cumulative fatigue damage differs depending on the longitudinals.

Fig. 11 shows the results of a comparison of the vertical bending stress and full stress for all load components (including elastic vibration) using the average values of the long-term distribution of the stress range when elastic vibration is superimposed. In the cases where the stress values of the members are substantially determined by the vertical bending stress (DL-1, BL-1, SL-2, IBL-1, IBL-14), the increase ratio of the fatigue damage is approximately 1.2 to 1.3, but when other load components are included, there is almost no increase in the fatigue damage. In other words, even in cases where elastic vibration is superimposed

on vertical bending stress, it is considered to have a little influence on fatigue strength in members where the stress state is determined in combination with other load components, and in members where fatigue strength is determined only by vertical bending stress, the effects of elastic vibration can be considered by increasing the cumulative fatigue damage of 1.3.

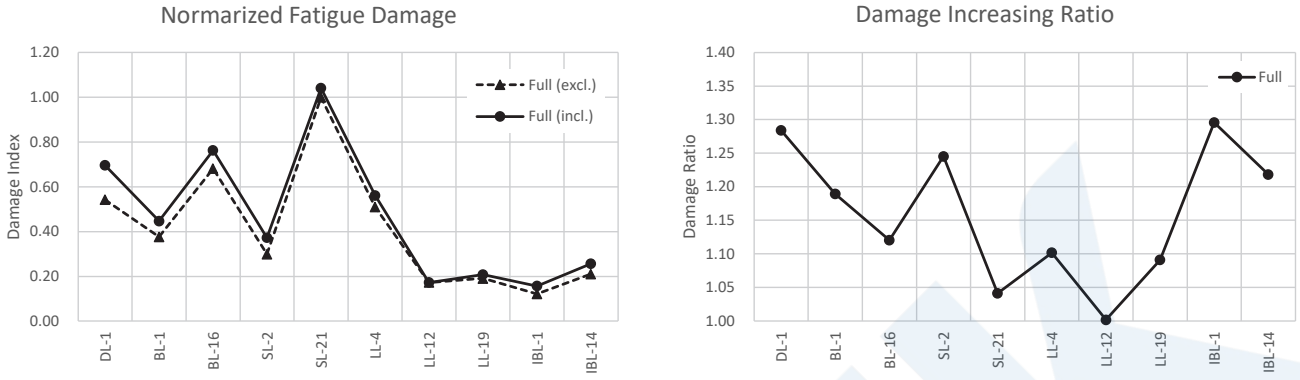

(a) Cumulative fatigue damage (normalized by SL-21)

(b) Increase ratio of fatigue damage

Fig. 10 Comparison of cumulative fatigue damage including/excluding effects of elastic vibration (DL: deck longitudinal (upper deck girder), BL: bottom longitudinal, SL: side longitudinal, LL: longitudinal on longitudinal bulkhead, IBL: inner bottom longitudinal)

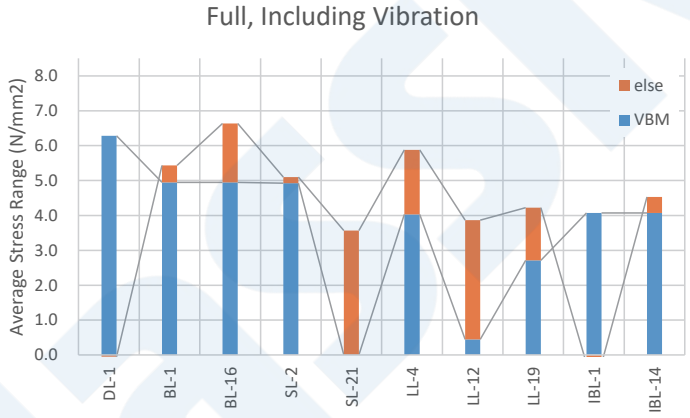

Fig. 11 Comparison of vertical bending stress component (vertical bending moment: VBM) and stress for all load components, including elastic vibration

The above-mentioned study can be summarized as follows.

- The expected value of the increase ratio of the cumulative fatigue damage in the short-term response in which elastic vibration occurs is approximately twice in the case of container ships, and is independent of the significant wave height and irrespective of springing or whipping.
- When elastic vibration is considered to occur in head sea states with directions of ±30°, the increase ratio of the long-term cumulative fatigue damage is approximately 1.3.
- When other load components are combined, the effect of elastic vibration is negligible.

Accordingly, it was decided that the effect of elastic vibration in fatigue strength assessments should be considered by multiplying the cumulative fatigue damage for ordinary wave loads by 1.3.

5. EXTERMELY-THICK STEEL PLATES AND CRACK ARREST BEHAVIOR

Accompanying the increasingly large scale of container ships from the 2000s, extremely thick steel plates with thicknesses of 50 mm to 100 mm and high yield point YP47 steel are adopted in hatch side coamings, strength decks (upper deck) and

certain other members. However, at the same time, research results indicating the possibility that brittle cracks initiating from welded joints of extremely thick steel plates could lead to large scale damage were reported, and it became clear that there were also several issues with these materials. In view of the seriousness of this problem, the Society carried out various surveys and research studies with the generous cooperation from the industry, and issued "Guidelines on the Application of YP47 Steel for Hull Structures of Large Container Carrier" in October 2008 and "Guidelines on Brittle Crack Arrest Design" in September 2009 in advance of others worldwide. (Fig. 12 shows a schematic diagram of brittle crack arrest design, and Fig. 13 shows a photograph of a related experiment.)

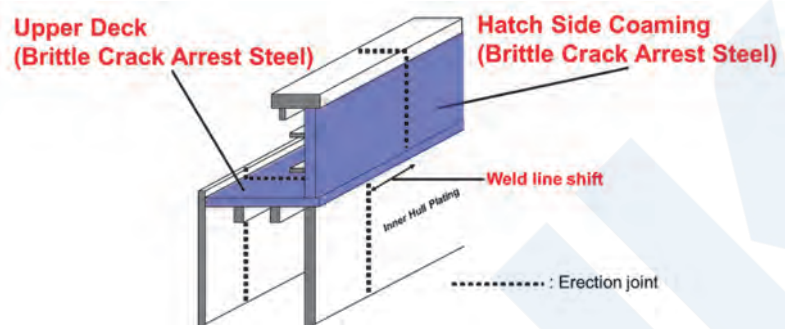

Fig. 12 Schematic diagram of brittle crack arrest design

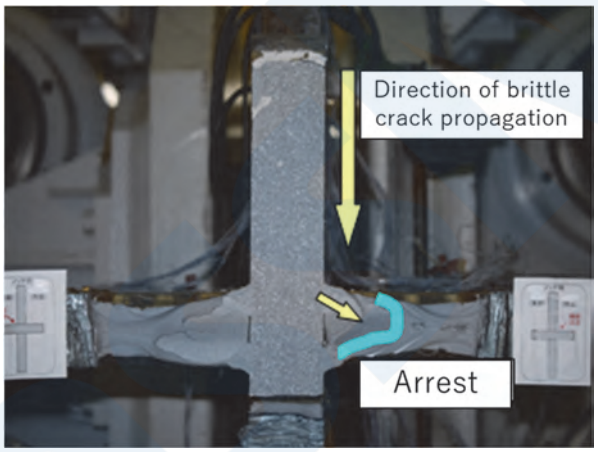

Fig. 13 Brittle crack propagation and arrest test simulating actual structure

In the IACS as well, discussions on brittle crack arrest design as a brittle fracture prevention measure for container ships using extremely thick steel plates were held under the leadership of the Society. The requirements for the use of extremely thick steel plates were studied based on the above-mentioned design guidelines developed by the Society, and these were adopted as the IACS Unified Requirement (*UR) S33 Requirements* for Use of Extremely Thick Steel Plates in Container Ships. At the same time, requirements based on the Society's Guidelines for YP47 steel were also adopted as IACS UR W31 for YP47 Steels and Brittle Crack Arrest Steels.

The Society also actively conducted ongoing research following the establishment of these URs in 2013. As brittle crack prevention measures, the IACS's URs do not provide concrete requirements for the brittle crack arrest properties when steel plates with thicknesses exceeding 80 mm are to be used as brittle crack arrest steel, and these requirements had been handled separately by each classification society. The Society conducted continuing joint research with industry, carried out large-scale experiments, numerical calculations, etc., and derived the arrest properties necessary in brittle crack arrest steel with plate thicknesses exceeding 80 mm. The Society then approached the IACS, leading to the adoption in 2019 of UR S33 (Rev. 2) and UR W31 (Rev. 2) [11], which reflected the results of the research by the Society.

Furthermore, active efforts were being made to research not only the properties of steel plates and related design methods but also the matter related to inspections. UR S33 (Rev. 3) [12], which was adopted in 2020, contains requirements that allow the use of advanced non-destructive testing techniques in place of the conventional ultrasonic testing for the all weld lines of butt joints between hull blocks of longitudinal hull girder members. For example, phased array ultrasonic testing (phased array UT) has

been recognized as a method for this purpose. The Society conducted research on phased array UT in cooperation with industry and issued its own “Guidelines for Non-destructive Inspection by Phased Array Ultrasonic Testing” [13] in March 2020. These Guidelines summarize the requirements for nondestructive inspections by phased array UT, concrete flaw detection requirements, etc.

Thus, the Society’s work is not limited to strength requirements, which occupy a large part of structural rules, but also includes efforts that make it possible to reflect state-of-the-art technologies at all times, even in different frameworks such as brittle crack arrest design, etc.

6. CONCLUSION

During the last quarter century, demand for container ships has expanded in line with the growth of the global economy and increased volume of international trade, and container ships have come to dominate a significant share in the classification of ship types. Although container movement has decreased since 2022 due to the effects of the invasion of Ukraine and rising commodity prices, the volume of container ship construction will continue to increase in the future.

While closely monitoring the trends in connection with the structural design and damage of container ships in the future, the Society will continuously conduct technology development related to structural strength evaluation, and will do its best to make it possible to create proactive rules, rather than rules established after accidents occur (i.e., rules as feedback), and carry out rule development that enables safe and rational design in the future.

REFERENCES

1) Nippon Kaiji Kyokai: Rules for the Survey and Construction of Steel Ships, Part C, 2023.
2) Ishibashi, K., et al.: Overview of Changes and Comprehensive Revision of Part C of the Rules for the Survey and Construction of Steel Ships, ClassNK Technical Journal, No. 5, pp. 75-82, 2022.
3) Matsui, S., et al.: Development of Simplified Formula for Froude-Krylov Force of 6-DOFs Acting on Monohull Ship, ClassNK Technical Journal, No. 3, pp. 93-112, 2021.
4) Shinomoto, K., et al.: Development of Closed Formula for Wave Load Based Upon Long-Term Prediction – Heave Acceleration and Pitch Angle –, ClassNK Technical Journal, No. 3, pp. 113-125, 2021.
5) Miratsu, R., et al.: Evaluation of the Ship Operational Effect Based on Actually Encountered Sea States of Ships, ClassNK Technical Journal, No. 5, pp. 93-99, 2022.
6) Ministry of Land, Infrastructure, Transport and Tourism (MLIT): Final Report of the Committee on Large Container Ship Safety, 2015.
7) Nippon Kaiji Kyokai: Final Report of the Investigative Panel on Large Container Ship Safety, 2014.
8) Heggelund, S. E., Storhaug, G. and Oma, N.: Consequence of Whipping and Springing on Fatigue and Extreme Loading for a LNG Vessel Based on Onboard Measurements, Proc. of PRADS 2010
9) Storhaug, G., Choi, H. K., Moan, T. and Hermundstad, O.: Consequence of Whipping and Springing on Fatigue for a 8600TEU Container Vessel in Different Trades Based on Model Tests, Proc. of PRADS 2010
10) Fricke, W. and Paetzold, H.: Experimental Investigation of the Effect of Whipping Stresses on the Fatigue Life of Ships, Proc. of IMSDC 2012
11) IACS：Unified Requirement W31 (Rev.2), 2019
12) IACS：Unified Requirement S33 (Rev.3), 2020
13) Nippon Kaiji Kyokai: Guidelines for Non-destructive Inspection by Phased Array Ultrasonic Testing, 2020.

Simplified Operational Guidance for Preventing Parametric Rolling*1

— Extension of Grim's Effective Wave Concept —

Naoya UMEDA*, Yuta UCHIDA**

1. INTRODUCTION

Since the case of the C11 class post-Panamax containership in head waves in 1998 [1], many accidents involving the loss of onboard containers due to the large heel of containerships in head, quartering and following waves have been reported [2]. Most large heels cannot be explained by a linear theory and are presumed to be due to parametric rolling. Parametric rolling typically means that only if the wave height exceeds a threshold, one roll cycle occurs during two encounter wave cycles, and the actual roll period is close to the natural roll period of the ship. In the C11 class containership accident, about 800 containers were lost or damaged due to a large heel of about 40°. Similar large parametric roll motions have also been observed in model experiments.

Although parametric rolling has been widely known in the theoretical research field [3], it was often regarded as a phenomenon that occurs in regular waves but may be unrealistic in irregular waves [4]. However, after Paulling et al. [5] observed parametric rolling of a free-running containership model in natural astern waves in San Francisco Bay in 1974 and Umeda et al. [6] realised parametric rolling of a free-running containership model in artificial short-crested irregular following waves in a model basin, parametric roll in following and quartering waves was recognised as a real threat to actual containerships at sea. Therefore, the International Maritime Organization (IMO) in 1995 [7] circulated operational guidance for following and quartering seas, which includes ship-independent guidance for parametric rolling focusing on the ratio of the encounter wave period to the ship's natural roll period. Later, partly as a result of a document from the United States [8] on the C11 class containership accident, the IMO in 2002 [9] started to develop means for preventing parametric rolling that also included head waves. Initially, the operational guidance in 1995 was expanded in a straightforward manner in 2007 to deal with parametric rolling in head waves [10]. In 2020, Interim Guidelines on the Second Generation Intact Stability Criteria including parametric rolling [11] were approved for trial use, and in 2022 the related Explanatory Notes [12] providing detailed calculation procedures were published. These new criteria, which are based on physics, deal not only with design but also with operational aspects, and provide simple two-level vulnerability criteria for ship design. If a ship under a certain condition fails to comply with them, its safety level may be demonstrated by probabilistic use of time-domain numerical simulation in short-crested irregular waves. Generally speaking, containerships and car carriers may often find it difficult to comply with these assessments because of their transom stern and exaggerated bow flare [13]. Thus, if the design measure is impractical, safe operation based on ship-dependent and physics-oriented operational guidance is required. For this purpose, full-probabilistic operational guidance and a simplified version can be utilised. The former is not always practical due to the high computational cost in terms of time. Although the example of the latter in the explanatory notes specifies only the ship speed, actual operation to avoid danger should also include the ship's course.

For practical use, operational guidance specifying not only the ship's speed but also its course is preferable. Therefore, this article attempts to provide a methodology to develop practical operational guidance for avoiding parametric rolling.

2. APPROACH ADOPTED FOR VULNERABILITY CRITERIA

The first level vulnerability criterion in the second generation intact stability criteria is the condition for the occurrence of parametric rolling regardless of the sea state. The second level consists of first and second checks: The former uses the weighted average of the occurrence conditions in typical sea states, while the latter uses the probability of sea states resulting in a parametric roll amplitude exceeding the critical magnitude. If any one of these three criteria is satisfied, the ship under the

*1 This article describes the details of the content read at the Spring Meeting of the Japan Society of Naval Architects and Ocean Engineers held in November 2022 [19].

* Professor emeritus, Osaka University

** Graduate School of Engineering, Osaka University

specified loading condition is judged as not vulnerable to parametric rolling. Among the three, only the second check of the second level vulnerability criteria can explicitly specify the critical heel angle, which depends on the lashing system, for example, the tier number of the lashing bridge. Since the second check of the second level vulnerability criteria seems most suitable for operational applications, this article will in principle attempt to adopt this methodology.

In this method, if a short-term sea state defined by the Bretschneider wave spectrum with the significant wave height and mean wave period is given, its spatial waveform is approximated by a regular wave using the Grim effective wave concept, and its 1/3 maximum largest amplitude is then used as the effective wave amplitude for estimating the GZ variation in a regular longitudinal wave. The parametric roll amplitude is determined by the encounter wave period depending on the ship speed and heading by numerically solving the uncoupled roll motion equation in the time domain. Here, the ship speed is set to the navigational speed, and the heading is uniformly distributed; that is, the effect of the wave heading on GZ variation is ignored as a conservative estimate. As a result, the encounter wave period can be calculated by changing the ship speed with the directional cosine of the wave heading. Finally, the probability of sea states with computed roll amplitudes larger than the critical heel angle is calculated by using the wave scatter diagram. If the obtained probability exceeds the acceptable value, the ship under the subject loading condition is judged vulnerable to parametric rolling failure.

3. SIMPLIFIED OPERATIONAL GUIDANCE IN THE IMO INTERIM GUIDELINES AS AN EXAMPLE

An example of the simplified operational guidance for parametric rolling is shown in paragraph 4.5.6.2.3 of the Interim Guidelines on the Second Generation Intact Stability Criteria. The parametric roll amplitude in longitudinal waves is calculated for the significant wave height, the zero-crossing mean wave period and the ship speed by using the method for the second check of the second level vulnerability criteria. If the amplitude is larger than 25°, the Guidelines request the ship master to avoid dangerous conditions defined by the significant wave height, the zero-crossing mean wave period and the ship speed, regardless of the wave heading. Although the ship speed is represented by "v_s" without definition in the Guidelines, judging from the text nearby, it could be read as the actual ship speed. If so, this guidance does not provide a dangerous ship course other than a dangerous ship speed.

On the other hand, section 4.5.6.2 of the IMO Interim Guidelines explicitly states that any guidance can be used if its required safety level is higher than that estimated by the full-probabilistic guidance using a numerical simulation in the time domain. Therefore, more advanced guidance specifying both the dangerous speed and course should be developed.

4. GENERALISATION OF THE GRIM EFFECTIVE WAVE CONCEPT

The second check of the second level vulnerability criteria utilises the Grim effective wave concept [14] to replace irregular waves with regular ones. Grim's paper only provides a formula for long-crested irregular longitudinal waves. However, the operational guidance is expected to be used for actual ship operational conditions, which means short-crested irregular waves with ship headings different from the main wave direction. Therefore, a formula for short-crested irregular quartering waves is derived here.

Normally, in a seakeeping theory, a ship response such as ship motions in irregular waves is handled stochastically under the assumption that the relationship between the incident wave and the ship response is linear. This means the spectrum of the ship responses in irregular waves can be estimated by the product of the incident wave spectrum and the response amplitude operator squared. Then, the significant amplitude of ship response is calculated by the Rayleigh distribution with the 0^{th} moment of the ship response spectrum. However, in the case of restoring variation due to waves, the relationship between incident waves and the restoring variation is nonlinear. In the example shown in Fig. 1 for a small trawler in regular waves whose length is equal to the ship length and crest or trough is located at the ship centre, the relationship between the incident wave amplitude and the wave-induced righting arm GZ at the heel angle of 10° has different slopes for the wave crest (negative value of the horizontal axis) and trough (positive value). Since the transom stern can be out of water when a wave trough is at the ship's stern, the waterplane breadth at the stern can be zero. On the other hand, when a wave crest is at the ship's stern, the waterplane breadth at the stern can be slightly larger than the calm-water value. In addition, when the relative wave elevation exceeds the deck edge level, the waterplane breadth can change nonlinearly. As a result, the restoring variation due to waves differs from the basic

assumption used in a seakeeping theory. On the other hand, the restoring variation can be evaluated even hydrostatically with the relative wave profile, and therefore can be regarded as nonlinear but without memory. The Grim effective wave concept utilises this fact.

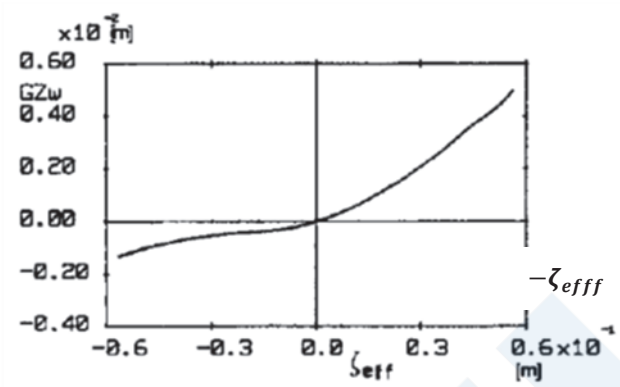

Fig. 1 GZ variation due to a regular wave whose length is equal to the ship's length and the crest or trough is located at the ship's centre for a small trawler at the heel angle of 10° [15)]

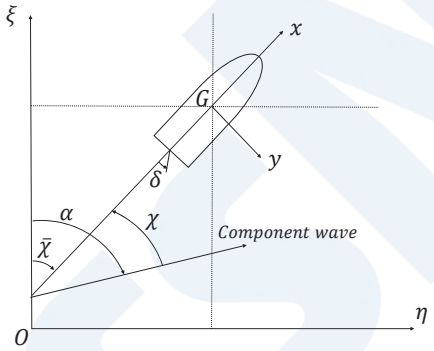

Fig. 2 Coordinate systems

As shown in Fig. 2, the space-fixed coordinate system O- ξ,η and the body-fixed coordinate system G- x,y are used. Here, the O-ξ axis indicates the main wave direction, α is the direction of a component wave, G is the centre of ship gravity (ξ_G, η_G) and $\bar{\chi}$ is the ship's heading from the main wave direction. Thus, the following relation exists.

$$\begin{aligned} \xi &= \xi_G + x\cos\bar{\chi} - y\sin\bar{\chi} \\ \eta &= \eta_G + x\sin\bar{\chi} + y\cos\bar{\chi} \end{aligned} \tag{1}$$

The wave elevation ζ_w as a function of position and time is represented as follows:

$$\zeta_w(\xi,\eta,t) = \int_{-\frac{\pi}{2}}^{\frac{\pi}{2}}\int_0^{\infty}\sqrt{2S(\omega,\alpha)d\omega d\alpha}\cos\left(\omega t - \frac{\omega^2}{g}\xi\cos\alpha - \frac{\omega^2}{g}\eta\sin\alpha + \psi\right)$$

$$= \sum_{i=1}^{N} a_i\cos\left[\omega_i t - \frac{\omega_i^2}{g}\{\xi\cos\alpha_i + \eta\sin\alpha_i\} + \psi_i\right] \tag{2}$$

$$= \sum_{i=1}^{N} a_i\cos\left[\omega_i t - \frac{\omega_i^2}{g}\{(\xi_G + x\cos\bar{\chi} - y\sin\bar{\chi})\cos\alpha_i + (\eta_G + x\sin\bar{\chi} + y\cos\bar{\chi})\sin\alpha_i\} + \psi_i\right]$$

where t is a time, ψ is a random value between 0 and 2π, $S(\omega,\alpha)$ is the incident wave spectrum, and the component wave

amplitude in discretisation is $a_i = \sqrt{2S(\omega,\alpha)d\omega d\alpha}.\ (i = 1, \cdots N)$

The effective wave is represented by Fig. 3 and Eq. (3).

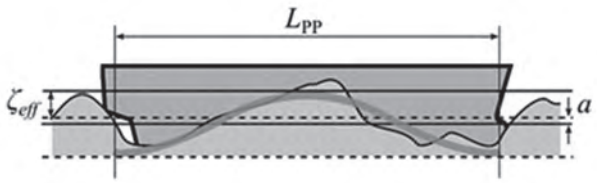

Fig. 3　Profile of the Grim effective wave

$$\hat{\zeta}_{eff}(x,t) = a(t) - \zeta_{eff}(t)\cos\frac{2\pi}{L}x \tag{3}$$

The effective wave can be determined by the least square method within the range of ship length -L/2<x<L/2 and its centre line y=0. Here, L indicates the ship length. Thus, the following value, J, should be minimised.

$$\begin{aligned}
\mathrm{J} &= \int_{-L/2}^{L/2}\left\{\zeta_w(\xi,\eta,t) - \hat{\zeta}_{eff}(x,t)\right\}^2 dx \\
&= \int_{-L/2}^{L/2}\left\{\sum_{i=1}^{N} a_i cos\left[\omega_i t - \frac{\omega_i^2}{g}\{(\xi_G + xcos\bar{\chi})cos\alpha_i + (\eta_G + xsin\bar{\chi})sin\alpha_i\} + \psi_i\right]\right. \\
&\qquad \left. - \left[a(\xi_G,\eta_G,\bar{\chi},t) - \zeta_{eff}(\xi_G,\eta_G,\bar{\chi},\ t)\cos\left(\frac{2\pi}{L}x\right)\right]\right\}^2 dx \\
&= \int_{-L/2}^{L/2}\left[\left\{\sum_{i=1}^{N} a_i cos\left[\omega_i t - \frac{\omega_i^2}{g}\{(\xi_G + xcos\bar{\chi})cos\alpha_i + (\eta_G + xsin\bar{\chi})sin\alpha_i\} + \psi_i\right]\right\}^2 - 2\left\{\sum_{i=1}^{N} a_i cos\left[\omega_i t\right.\right.\right. \\
&\qquad \left.\left.\left. - \frac{\omega_i^2}{g}\{(\xi_G + xcos\bar{\chi})cos\alpha_i + (\eta_G + xsin\bar{\chi})sin\alpha_i\} + \psi_i\right]\right\}\left\{a(\xi_G,\eta_G,\bar{\chi},t)\right. \\
&\qquad \left. - \zeta_{eff}(\xi_G,\eta_G,\bar{\chi},\ t)\cos\left(\frac{2\pi}{L}x\right)\right\} - \{a(\xi_G,\eta_G,\bar{\chi},t)\}^2 \\
&\qquad + 2\left\{a(\xi_G,\eta_G,\bar{\chi},t)\zeta_{eff}(\xi_G,\eta_G,\bar{\chi},\ t)\cos\left(\frac{2\pi}{L}x\right)\right\} - \left(\zeta_{eff}(\xi_G,\eta_G,\bar{\chi},\ t)\right)^2\cos^2\left(\frac{2\pi}{L}x\right)\ \Bigg]dx
\end{aligned} \tag{4}$$

Therefore, the following formula should be satisfied.

$$\begin{aligned}
0 &= \frac{\partial J}{\partial \zeta_{eff}} \\
&= 2\int_{-L/2}^{L/2}\left\{\sum_{i=1}^{N} a_i cos\left[\omega_i t - \frac{\omega_i^2}{g}\{(\xi_G + xcos\bar{\chi}))cos\alpha_i + (\eta_G + xsin\bar{\chi})sin\alpha_i\} + \psi_i\right]\right\}\ \cos\left(\frac{2\pi}{L}x\right)\ dx + \\
&\quad 2\left\{a(\xi_G,\eta_G,\bar{\chi},t)\int_{-\frac{L}{2}}^{\frac{L}{2}}\cos\left(\frac{2\pi}{L}x\right)dx\right\} - 2\int_{-L/2}^{L/2}\zeta_{eff}(\xi_G,\eta_G,\bar{\chi},\ t)\ \cos^2\left(\frac{2\pi}{L}x\right)\ dx \\
&= 2\int_{-L/2}^{L/2}\left\{\sum_{i=1}^{N} a_i cos\left[\omega_i t - \frac{\omega_i^2}{g}\{(\xi_G)cos\alpha_i + (\eta_G)sin\alpha_i\}\right\} - \frac{\omega_i^2}{g}\{(xcos\bar{\chi})cos\alpha_i + (xsin\bar{\chi})sin\alpha_i\} + \right. \\
&\quad \left.\psi_i\right]\right\}\ \cos\left(\frac{2\pi}{L}x\right)\ dx - 2\int_{-L/2}^{L/2}\zeta_{eff}(\xi_G,\eta_G,\bar{\chi},\ t)\ \cos^2\left(\frac{2\pi}{L}x\right)\ dx
\end{aligned} \tag{5}$$

$$=2\int_{-L/2}^{L/2}\left\{\sum_{i=1}^{N} a_i cos\left[\omega_i t-\frac{\omega_i^2}{g}\{(\xi_G)cos\alpha_i+(\eta_G)sin\alpha_i\}-\frac{\omega_i^2}{g}xcos(\bar{\chi}-\alpha_i)+\psi_i\right]\right\}\ \cos\left(\frac{2\pi}{L}x\right)\ dx-\zeta_{eff}L$$

$$=2\int_{-L/2}^{L/2}\left\{\sum_{i=1}^{N} a_i cos\left[\omega_i t-\frac{\omega_i^2}{g}\{(\xi_G)cos\alpha_i+(\eta_G)sin\alpha_i\}+\psi_i\right]cos\left(-\frac{\omega_i^2}{g}xcos(\bar{\chi}-\alpha_i)\right)\right\}\ \cos\left(\frac{2\pi}{L}x\right)\ dx-$$

$$\zeta_{eff}L$$

Using the following relation,

$$\int_{-L/2}^{L/2} cos\left(-\frac{\omega_i^2}{g}xcos(\bar{\chi}-\alpha_i)\right)\cos\left(\frac{2\pi}{L}x\right)\ dx$$

$$=\frac{1}{2}\int_{-L/2}^{L/2} cos\left(-\frac{\omega_i^2}{g}xcos(\bar{\chi}-\alpha_i)+\frac{2\pi}{L}x\right)+cos\left(-\frac{\omega_i^2}{g}xcos(\bar{\chi}-\alpha_i)-\frac{2\pi}{L}x\right)\ dx \quad (6),$$

$$=\frac{-2\frac{\omega_i^2}{g}cos(\bar{\chi}-\alpha_i)sin\left(\frac{\omega_i^2 L}{2g}cos(\bar{\chi}-\alpha_i)\right)}{\left(\frac{\omega_i^2}{g}cos(\bar{\chi}-\alpha_i)\right)^2-\left(\frac{2\pi}{L}\right)^2}$$

the Grim effective wave ζ_{eff} is obtained as follows:

$$\zeta_{eff}(\xi_G,\eta_G,\bar{\chi},\ t;L)=\frac{4}{L}\sum_{i=1}^{N} a_i\frac{1}{\left(\frac{2\pi}{L}\right)^2-\left(\frac{\omega_i^2}{g}cos(\bar{\chi}-\alpha_i)\right)^2}$$

$$\cdot\left(\frac{\omega_i^2}{g}cos(\bar{\chi}-\alpha_i)\right)\ \ sin\left\{\frac{\omega_i^2}{2g}cos(\bar{\chi}-\alpha_i)\right\}$$

$$\cdot cos\left[\omega_i t-\frac{\omega_i^2}{g}\{\xi_G cos\alpha_i+\eta_G sin\alpha_i\}+\psi_i\right]$$

$$=\sum_{i=1}^{N} a_i\frac{\left(\frac{\omega_i^2 L}{g}cos(\bar{\chi}-\alpha_i)\right)sin\left\{\frac{\omega_i^2 L}{2g}cos(\bar{\chi}-\alpha_i)\right\}}{\pi^2-\left(\frac{\omega_i^2 L}{2g}cos(\bar{\chi}-\alpha_i)\right)^2} \quad (7)$$

$$\cdot cos\left[\omega_i t-\frac{\omega_i^2}{g}\{\xi_G cos\alpha_i+\eta_G sin\alpha_i\}+\psi_i\right]$$

$$=\int_{-\frac{\pi}{2}}^{\frac{\pi}{2}}\int_0^{\infty}\sqrt{2S_{eff}(\omega,\alpha;L,\bar{\chi})d\omega d\alpha}\cdot cos\left[\omega t-\frac{\omega^2}{g}\xi_G\cos\alpha-\frac{\omega^2}{g}\eta_G\sin\alpha+\psi\right]$$

where

$$S_{eff}(\omega,\alpha;L,\bar{\chi}) = S(\omega,\alpha)\cdot\left[\frac{\left(\frac{\omega^2 L}{g}cos(\bar{\chi}-\alpha)\right)sin\left\{\frac{\omega^2 L}{2g}cos(\bar{\chi}-\alpha)\right\}}{\pi^2-\left(\frac{\omega^2 L}{2g}cos(\bar{\chi}-\alpha)\right)^2}\right]^2 \quad (8).$$

As shown above, the spectrum of the effective wave amplitude $S_{eff}(\omega,\alpha;L,\bar{\chi})$ can be calculated as a function of the frequency ω and the angle α when the ship length L and the wave heading $\bar{\chi}$ are given. When the denominator of Eq. (8) is zero, in other words, the length of the relevant component wave is equal to the ship's length, the spectrum density of the effective wave amplitude coincides with the spectrum density of the incident wave. Thus, this is consistent with the definition of the Grim effective wave. The specific density of the effective wave amplitude decreases when the wave heading increases from that of a pure following wave. When $\bar{\chi}-\alpha=\pi/2$, the spectrum density of the effective wave amplitude becomes zero. This formula coincides with that in Umeda & Yamakoshi [15].

Furthermore, by using the following formula,

$$\frac{\partial J}{\partial a}=0 \quad (9),$$

the mean value of the effective wave a can be obtained as follows:

$$a(\xi_G,\eta_G,\bar{\chi},\ t;L) = \int_{-\frac{\pi}{2}}^{\frac{\pi}{2}}\int_0^{\infty}\sqrt{2S_a(\omega,\alpha;L,\bar{\chi})d\omega d\alpha}\cdot cos\left[\omega t-\frac{\omega^2}{g}\xi_G\cos\alpha-\frac{\omega^2}{g}\eta_G\sin\alpha+\psi\right] \quad (10)$$

where its spectrum $S_a(\omega,\alpha;L,\bar{\chi})$ is given by

$$S_a(\omega,\alpha;L,\bar{\chi}) = S(\omega,\alpha)\cdot\left[\frac{sin\left\{\frac{\omega^2 L}{2g}cos(\bar{\chi}-\alpha)\right\}}{\frac{\omega^2 L}{2g}cos(\bar{\chi}-\alpha)}\right]^2 \quad (11).$$

When the denominator of Eq. (11) is zero, in other words, $\bar{\chi}-\alpha=\pi/2$, the spectrum density of the mean value of the effective wave becomes the spectrum density of incident waves.

5. ESTIMATION METHOD FOR RESTORING VARIATION USING THE GRIM EFFECTIVE WAVE CONCEPT

Once the Grim effective wave is given, the restoring variation due to waves can be estimated as follows. First, the righting arm in a regular longitudinal wave is calculated. Here, the wavelength is equal to the ship's length, and the wave crest or trough is situated at the ship's centre. The incident wave is assumed not to be disturbed by the ship, which is known as the Froude-Krylov assumption. Then, the incident wave pressure is integrated over the ship's submerged surface. Sinkage and trim should be iteratively determined with the ship's weight. The profile of an incident wave propagating in the direction of ξ, that is, ζ_w, and its pressure p are given by Eqs. (12) and (13), respectively.

$$\zeta_w(\xi,t) = \zeta_a cosk(\xi-ct) \quad (12)$$

$$p(\xi,\zeta,t) = \rho g\zeta - \rho g\zeta_a e^{-k\zeta}cosk(\xi-ct) \quad (13)$$

Here, the ζ-axis is pointed downward, ζ_a is the wave amplitude, k is the wave number and c is the wave celerity. Since the wave amplitude is not small in actual cases, the following practical formulae are often used.

$$p(\xi,\zeta,t) = \rho g\zeta - \rho g\zeta_a e^{-k\{\zeta-\zeta_w(\xi,t)\}}cosk(\xi - ct) \tag{14}$$

$$p(\xi,\zeta,t) = \rho g\zeta - \rho g\zeta_a e^{-kd}cosk(\xi - ct) \tag{15}$$

where d indicates the ship's mean draught. Further, the following expression can be obtained by expanding the exponential function into the Taylor expansion and ignoring higher-order terms.

$$\begin{aligned} p(\xi,\zeta,t) &\approx \rho g\zeta - \rho g\zeta_a(1-kd)cosk(\xi - ct) \\ &\approx \rho g\{\zeta - \zeta_a cosk(\xi - ct)\} \end{aligned} \tag{16}$$

In this case, the righting arm can be hydrostatically calculated with a sinusoidal wavy surface. Comparisons among the above formulae and a captive model experiment indicate that Eq. (16) is sufficient for practical purposes [16) 17)].

Repeating the above calculations for different wave amplitudes, GZ and GM can be obtained as functions of the effective wave amplitude so that they are represented as $GZ(\zeta_{eff})$ and $GM(\zeta_{eff})$, respectively. Thus, if the time series of ζ_{eff} is provided, the time series of $GZ(\zeta_{eff})$ and $GM(\zeta_{eff})$ can also be obtained. If the probability density function of the effective wave amplitude is given, stochastic representative values of the effective wave amplitude, such as the significant amplitude and the zero-crossing mean period, can be directly obtained by the transformation of random variables [18)].

Nevertheless, in the IMO Interim Guidelines on the Second Generation Intact Stability Criteria [11)], the 1/3 maximum amplitude of the effective wave amplitude is used for the input to the righting arm calculation in a regular wave for simplicity. More precisely, the 1/3 maximum amplitude obtained from the spectrum of the righting arm transformed from the effective wave amplitude with the narrow band assumption should be used as the amplitude of the effective wave for the righting arm calculation [18)]. Further, a probabilistic differential equation can be solved for the effective wave amplitude as a random process [19)].

6. ESTIMATION METHOD OF PARAMETRIC ROLL BY USING RESTORING VARIATION

Numerical simulation in the time domain is adopted in the IMO Interim Guidelines on the Second Generation Intact Stability Criteria [11)]. However, the obtained time series can exhibit roll motions other than the principal parametric roll assumed in the first level vulnerability criterion, such as chaos, as shown in the explanatory notes [12)]. Thus, expert knowledge may be required to handle the output properly. In addition, adding the direct roll excitation terms in the equation of motions in oblique waves may make the output even more complicated. Therefore, in this article, the averaging method is used to solve Eq. (17).

$$\ddot{\phi} + 2\alpha\dot{\phi} + \gamma\dot{\phi}^3 + {\omega_\phi}^2\phi + {\omega_\phi}^2 l_3\phi^3 + {\omega_\phi}^2 l_5\phi^5 + {\omega_\phi}^2(F + M\cos\omega_e t)\{\phi - (1/\pi^2)\phi^3\} = E\sin\omega_e t \tag{17}$$

where ϕ is the roll angle, α is the linear roll damping coefficient, γ is the cubic roll damping coefficient, ω_ϕ is the natural roll frequency, l_3 and l_5 are nonlinear restoring coefficients, F is the ratio of the mean value of GM variation to the calm-water GM and M is the ratio of the amplitude of GM variation to the calm-water GM. E represents the direct roll excitation moment with r as the effective wave coefficient, which can be calculated as follows:

$$E = \zeta_a r k {\omega_\phi}^2 sin\chi \tag{18}$$

The averaging method is applied to Eq. (17), assuming the following solution form.

$$\phi = A\,cos\left(\frac{\omega_e}{2}t - \varepsilon_1\right) + B\,sin(\omega_e t - \varepsilon_2) \tag{19}$$

where A, B, ε_1 and ε_2 are constants, the first term represents the subharmonic motion related to the parametric roll, and the second term indicates the harmonic motion related to the synchronous roll. The detailed formulae to be solved in order to determine A, B, ε_1 and ε_2 are provided by Sakai et al. [20]. It is noteworthy here that the averaging method without the direct excitation term [21) 22)] is still useful because the second term is not particularly significant under conditions where parametric roll is important.

For the wave encounter frequency, which is the same as the frequency of restoring variation, the Interim Guidelines [11] use the linear wave dispersion of a regular wave whose length is equal to the ship length. Following the Grim effective wave concept, the wave encounter frequency should be estimated as the zero-crossing mean frequency of restoring variation estimated from the probability density function of restoring variation transformed from the Gaussian probability density function of the effective wave amplitude. However, according to a numerical study by Sakai et al. [23], the difference between the two methods seems small.

7. EXAMPLE OF APPLICATION OF SIMPLIFIED OPERATIONAL GUIDANCE

It appears to be possible to develop simplified operational guidance specifying the dangerous speed and course for a ship by following the methodology mentioned above and using the incident wave spectrum observed by onboard wave radar [24]. An example of the operational guidance prepared in this manner is shown in Figs. 4 and 5 as polar charts. Here, the averaging method with the direct excitation term is used as the solution method, and roll damping is estimated by using Ikeda's simplified method [25] with correction of its forward speed effect [26]. The subject ship is the C11 class containership, which has a natural roll period of 25.7 s. The assumed mean wave period, T01, is 12.5 s with the significant wave heights of 5 m and 7 m. The Bretschneider wave spectrum with a cosine squared directional distribution is used as the wave spectrum. The polar radius indicates the Froude number, and the polar angle shows the ship heading from the main wave direction. The region where the 1/3 maximum parametric roll amplitude exceeds 25° is shown in red as the dangerous zone.

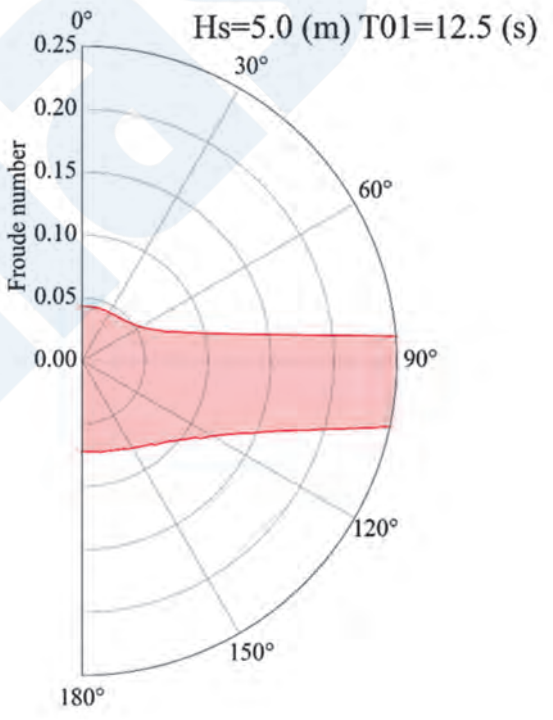

Fig. 4 Polar plot of simplified operational guidance for parametric rolling of the C11 class containership under a significant wave height of 5 m and mean wave period of 12.5 s

A dangerous zone exists in the operational condition where the encounter period is about half the ship's natural roll period. It exists at almost zero speed regardless of the heading angle, and extends to a higher speed region in beam waves. While the amplitude of the effective wave in regular beam waves is zero, short-crested irregular beam waves involve component waves encountering the ship with smaller heading angles, and thus are sufficient to cause a parametric roll.

When the significant wave height increases, the dangerous zone becomes somewhat broader. At the significant wave height of 5 m, an increase in the ship speed to a Froude number of 0.05 or higher in head waves effectively prevents parametric roll. At the significant wave height of 7 m, an increase to a Froude number of 0.07 or higher in head waves effectively prevents parametric roll.

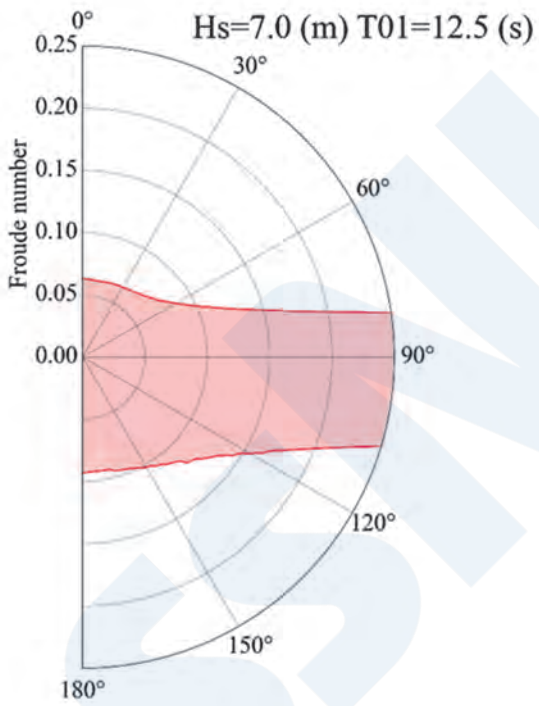

Fig. 5 Polar plot of simplified operational guidance for parametric rolling of the C11 class containership under a significant wave height of 7 m and mean wave period of 12.5 s

8. CONCLUSION

A method for developing simplified operational guidance for parametric rolling specifying the dangerous ship speed and dangerous course in short-crested irregular waves is proposed as an extension of the IMO vulnerability criteria using the generalised Grim effective wave concept. Examples of its application are provided as polar plots.

ACKNOWLEDGEMENTS

This study was partly carried out as a research activity of the Goal-based Stability Criteria Project of the Japan Ship Technology Research Association in fiscal year 2022 with funding by the Nippon Foundation.

REFERENCES

1) France, W. N., Levadou, M., Treakle, T.M., Paulling, J.R., Michel, R W.K and Moore, C., (2003): An Investigation of Head-Sea Parametric Rolling and its Influence on Container Lashing Systems, Marine Technology, 40(1), 1-19.
2) IMO (2023): Proposal for a new output on prevention of loss of containers at sea, submitted by Australia, Belgium, Chile, Denmark, France, Germany, Kingdom of the Netherlands, Morocco, Republic of Korea, Spain and IUMI, MSC 107/17/12.

3) Watanabe, Y. (1934): Dynamic Properties of the Transverse Instability of a Ship due to Pitching, Journal of Zosenkyokai, 53, 51-70, in Japanese.
4) Kerwin, J.E. (1955): Note on Rolling in Longitudinal Waves, International Shipbuilding Progress, 2(16), 597-614.
5) Oakley, O. H., Paulling, J. R., Wood, P. D. (1974): Ship Motions and Capsizing in Astern Seas, Proceedings of the 10th Symposium on Naval Hydrodynamics, 297-350.
6) Umeda, N., M. Hamamoto et al. (1995): Model Experiments of Ship Capsize in Astern Seas, Journal of the Society of Naval Architects of Japan, 177, 207-217.
7) IMO (1995): Guidance to the Master for Avoiding Dangerous Situations in Following and Quartering Seas, MSC/Circ. 707.
8) IMO (2002): Head-Sea Parametric Rolling and Its Influence on Container Lashing Systems, submitted by USA, SLF 45/6/7.
9) IMO (2002): Report to the Maritime Safety Committee, SLF 45/14, 20-25.
10) IMO (2007): Revised Guidance to the Master for Avoiding Dangerous Situations in Adverse Weather and Sea Conditions, MSC.1/Circ. 1228.
11) IMO (2020): Interim Guidelines on the Second Generation Intact Stability Criteria, MSC.1/Circ.1627.
12) IMO (2022): Explanatory Notes to Interim Guidelines on the Second Generation Intact Stability Criteria, MSC.1/Circ.1652.
13) IMO (2017): Selecting Calculation Methods and Standards for the Vulnerability Criteria for Parametric Roll, Pure Loss of Stability and Dead Ship Stability Failures Based on Sample Calculations, SDC 5/INF.4, Annex 17.
14) Grim, O. (1961): Beitrag zu dem Problem der Sicherheit des Schiffes im Seegang, Schiff und Hafen, 6, 490-497.
15) Umeda, N. and Yamakoshi, Y. (1994): Probability of Ship Capsizing due to Pure Loss of Stability in Quartering Seas, Naval Architecture and Ocean Engineering, 30, 73-85.
16) Umeda, N. (1985): Pure Loss of Stability in Following Waves, Journal of Fishing Boat Association, 258, 60-67.
17) Paulling, J.R. (1961): The Transverse Stability of a Ship in a Longitudinal Seaway, Journal of Ship Research, 4(4), 37-49.
18) Umeda, N. and Y. Yamakoshi (1986): Experimental Study on Pure Loss of Stability in Regular and Irregular Following Seas, Proceedings of the 3rd International Conference on Stability of Ships and Ocean Vehicles, Gdansk, 1, 93-99.
19) Umeda, N., Sakai, M. and Okamoto, H. (2022): Some Remarks on Simplified Operational Guidance for Parametric Rolling, Conference Proceedings of the Japan Society of Naval Architects and Ocean Engineers, 35, 437-440.
20) Sakai, M., Umeda, N., Yano, T., Maki, A., Yamashita, N., Matsuda, A., Terada, D. (2018): Averaging methods for estimating parametric roll in longitudinal and oblique waves, Journal of Marine Science and Technology, 23(3), 2, 413-424.
21) Umeda N., Hashimoto H., Vassalos D., Urano S., Okou K. (2004): Nonlinear dynamics on parametric roll resonance with realistic numerical modeling. International Shipbuilding Progress, 51(2/3), 205-220.
22) Maki, A., Umeda, N., Shiotani, S. and Kobayashi, E. (2011): Parametric rolling prediction in irregular seas using combination of deterministic ship dynamics and probabilistic wave theory, Journal of Marine Science and Technology, 16(3), 294-310.
23) Sakai, M., Umeda, N., Maki, A. (2019): Encounter frequency effect on the simplified design criteria against parametric roll, Ocean Engineering, 182, 21-27.
24) Yano, T., Umeda, N., Hirayama, K., Baba, M., Sakai, M. (2023): Wave Radar Application to the Simplified Parametric Roll Operational Guidance at Actual Sea. In Spyrou, K.J., Belenky, V.L., Katayama, T., Bačkalov, I., Francescutto, A. (eds.) Contemporary Ideas on Ship Stability. Fluid Mechanics and Its Applications, Vol. 134, Springer, Cham, 323-333.
25) Kawahara, Y., Maekawa, K., Ikeda, Y. (2011): A Simple Prediction Formula of Roll Damping of Conventional Cargo Ships on the Basis of Ikeda's Method and Its Limitation. In Almeida Santos Neves, M., Belenky, V., de Kat, J., Spyrou, K., Umeda, N. (eds.) Contemporary Ideas on Ship Stability and Capsizing in Waves, Fluid Mechanics and Its Applications, Vol. 97, Springer, Dordrecht, pp. 465-486.
26) Ikeda, Y. (2004): Prediction Methods of Roll Damping of Ships and Their Application to Determine Optimum Stabilisation Devices, Marine Technology, 41, 89-93.

Damage of SOx Scrubber Discharge Water Lines

Machinery Department, Plan Approval and Technical Solution Division, ClassNK

1. INTRODUCTION

Regulation 14 of Annex VI of the MARPOL Convention gradually strengthens regulation of the sulfur content in fuel oil used on board ships. However, under Regulation 4 of the Convention, the use of fuel oil with a sulfur content exceeding the regulatory value is permitted if the ship is equipped with an exhaust gas cleaning system (SOx scrubber) approved by the flag government as an equivalent measure to the use of fuel oil with a low sulfur content that complies with the regulation (compliant fuel). Since the limit for open sea areas was reduced from 3.50 % to 0.50 % in 2020, not only use of a compliant fuel, but also installation of a SOx scrubber has been considered and adopted as a response. Under these circumstances, as the number of vessels equipped with SOx scrubbers has increased, ClassNK (hereinafter, the Society) received several reports of seawater leakage from corrosion-damaged distance pieces fitted to hull structures on SOx scrubber discharge water lines. Although the Society issued technical information (TEC-1205 and 1214) in 2020 on measures to prevent this type of damage, similar incidents are still being reported. Therefore, we are publishing this Technical Journal article to share the results of statistical evaluations of the factors presumed to be responsible for this damage and the countermeasures to be taken.

2. OVERVIEW

SOx scrubbers remove the sulfur content from exhaust gas by spraying the exhaust gas with washwater. In open type SOx scrubbers, which are widely used, the washwater sprayed in the SOx scrubber tower reacts with the exhaust gas and is discharged overboard.

According to the damage reports received to date, seawater leakage has been observed either on or adjacent to welded parts between distance pieces and their associated flanges (see Fig. 2), as well as between distance pieces and bluff bodies (see Figs. 3 and 4), as shown in Fig. 1. These reports indicate that the corrosion apparently initiates at welded parts and then continues to progress until it finally leads to seawater leakage into the engine room. Peeling of the painted surfaces of butt-welded parts of distance pieces (see Fig. 5) has also been observed.

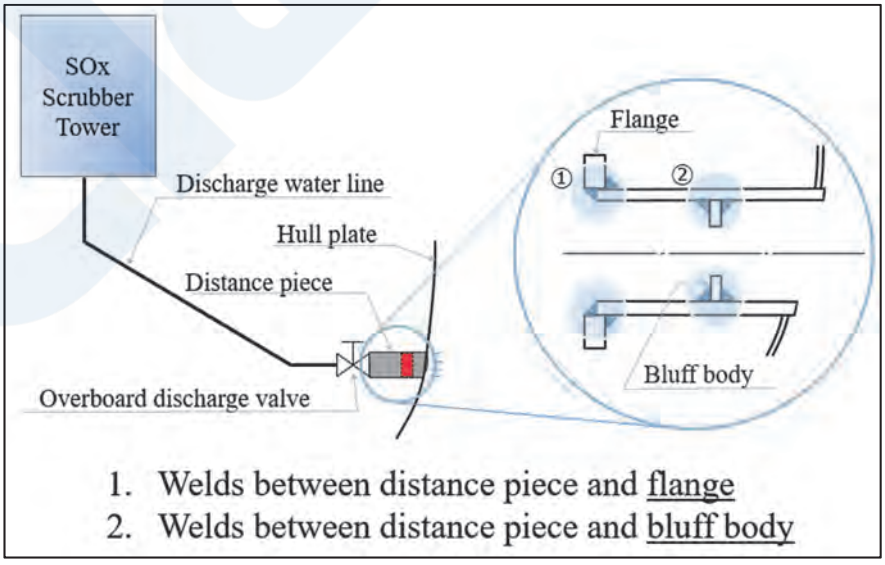

Fig. 1 Schematic of SOx scrubber discharge water system

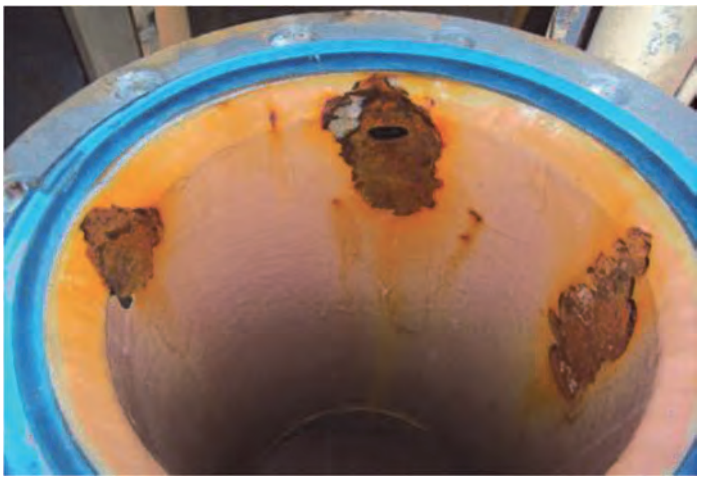

Fig. 2　Corrosion around welded parts between distance piece and flange

Fig. 3　Corrosion around welded parts between distance piece and bluff body

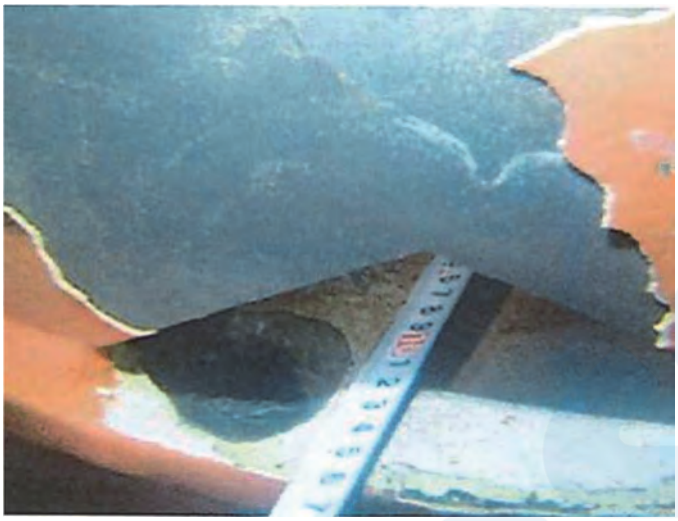

Fig. 4　Corrosion around welded parts between distance piece and bluff body

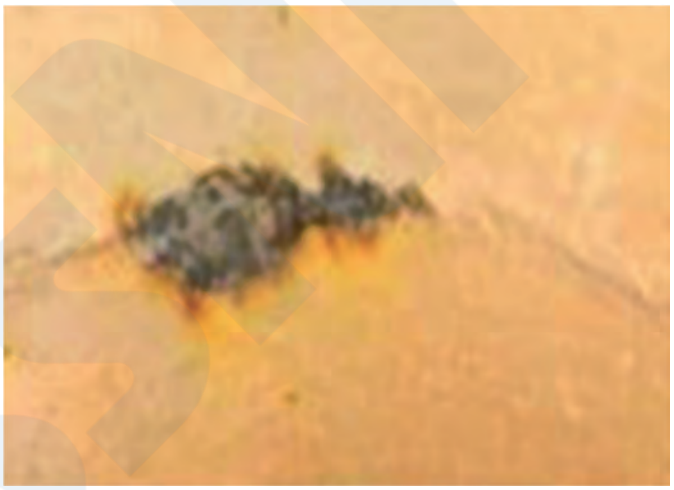

Fig. 5　Paint peeling at butt-welded parts of distance piece of discharge water system

3.　POSSIBLE CAUSES

The following is a list of the possible causes estimated since this damage became apparent, based on the nature of the SOx scrubber system and the trends of damage cases reported to the Society.

3.1　Acidity (pH) of Discharge Water

During the desulfurization process in the SOx scrubber tower, the sulfur content in the exhaust gas is dissolved in the sprayed washwater and discharged overboard. Therefore, discharge water with a high acidity of pH 3 to 4 may flow through the distance piece on SOx scrubber discharge water lines, depending on the amount of washwater and the desulfurization performance of the SOx scrubber. Although corrosion-resistant paint is generally applied to the inner surface of the distance piece, corrosion is thought to occur in areas where the paint has peeled off and the distance piece is directly exposed to the highly acidic discharge water.

3.2　Flow Velocity of Discharge Water

In order to satisfy the regulatory value for the sulfur content in exhaust gas, it is necessary to remove the sulfur content sufficiently from the exhaust gas by spraying a large amount of washwater in the SOx scrubber tower. When a large amount of washwater is sprayed, it is presumed that the distance piece on SOx scrubber discharge water lines will become less corrosive due to the decreased acidity of the discharge water after the exhaust gas is cleaned. On the other hand, the flow velocity of the discharge water increases because of the large amount of washwater and discharge water. This increase in the flow velocity

could be an environmental factor that facilitates paint peeling.

3.3 Bluff Body

Based on the EGCS guideline established by IMO (Resolution MEPC.340(77)), the pH of discharge water after exhaust gas cleaning must recover to 6.5 or higher in seawater 4 m from the overboard discharge port. To meet this standard, some SOx scrubber manufacturers install a bluff body in the distance piece on SOx scrubber discharge water lines to diffuse the discharge water so it is more easily diluted by the seawater outside the vessel. If a bluff body is installed, the connection between the distance piece and the bluff body will be narrower, which is expected to worsen workability in terms of space. This suggests that the quality of welding and painting work could deteriorate, resulting in a condition in which the paint is easily peeled off. In addition, the bluff body decreases the cross-sectional area where discharge water passes, which causes a sudden increase in the flow velocity of the discharge water and a turbulence flow, which is assumed to result in easier peeling of the paint on the distance piece.

3.4 Installation Environment

When SOx scrubbers are retrofitted after ships enter service, the time available for installation is limited compared to installation during newbuilding, and for this reason, it is assumed that workers may not fully comply with the installation procedures specified by the paint manufacturer to prevent corrosion of the distance piece.

In addition, in a retrofit facility environment, it may be difficult for workers to install the equipment with sufficient quality because of the small workspace and unstable scaffolding.

Recently, in many cases, measures such as dispatching a site supervisor or a professional engineer for SOx scrubber installation have been taken at the time of retrofitting to ensure sufficient installation quality. However, in the early stages of SOx scrubber adoption, it is highly possible that the quality of the painting work was not sufficient because the importance of painting quality was not recognized, or because a site supervisor could not be dispatched due to COVID19.

Especially, the painting work at the edge of the surface, where the paint is applied in a linear pattern or in dots as though with a stylus as a finishing touch, may result in a decrease in the adhesion of the paint. Therefore, the painting work at these areas should be done with the utmost care.

3.5 Solid Substances

Seawater is generally used as the washwater sprayed in SOx scrubber towers, and there have been reports of solid substances caused by salt from the sprayed seawater accumulating in the SOx scrubber tower and exhaust gas pipes. When solids occur, they are eventually discharged overboard, but may cause physical damage to the inner surface of the distance piece on SOx scrubber discharge water lines.

4. DATA ON FLOW VELOCITY AND ACIDITY OF DISCHARGE WATER

Fig. 6 shows the relationship between the data on the flow velocity and pH of discharge water and the presence of damage on vessels equipped with SOx scrubbers in ClassNK vessels. These data were extracted from a population of damage cases reported to the Society and cases in which no damage occurred, so there is no bias among SOx scrubber manufacturers. The data for the percentage of damaged vessels per flow velocity range show that the percentage of damaged vessels increases as the flow velocity increases (from 24 % to 67 %). However, there were cases where damage occurred even though the flow velocity was low, and conversely, cases where damage did not occur even though the flow velocity was high (the same was true for pH), suggesting that damage was not caused by one factor alone, but by a combination of several factors.

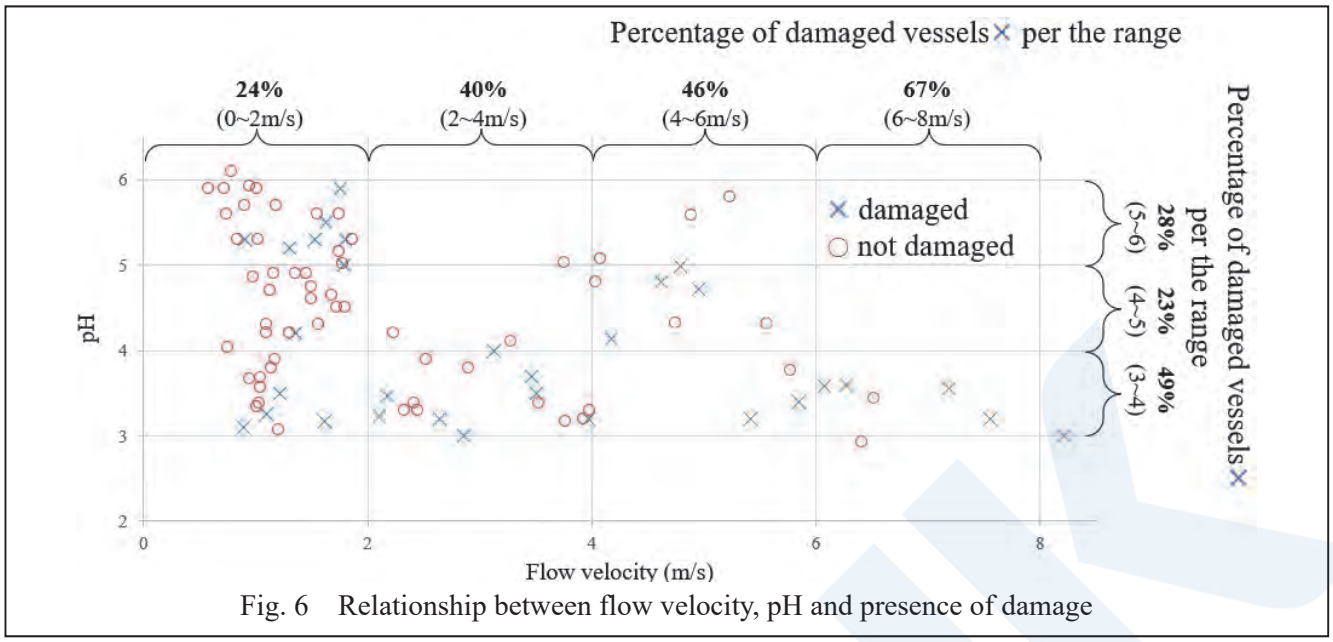

Fig. 6　Relationship between flow velocity, pH and presence of damage

5.　STATISTICAL TEST

Based on our investigations, the following factors have been postulated as causes of the damage to distance pieces: (1) acidity (pH) of discharge water, (2) flow velocity of discharge water, (3) bluff body, (4) installation environment and (5) solid substances. However, since it was found that this damage was not uniformly caused by a specific factor, the above-mentioned factors should be considered to be only intuitive estimation factors.

Therefore, the following factors (1) to (4) were compared in the damaged and non-damaged groups to determine whether any statistically significant differences existed by using statistical tests (i.e., a significant difference test) from the data of ClassNK vessels, and the relationship between those factors and the damage was investigated. The results showed that there are some statistical relationships between these factors and this type of damage, as shown below.

(1) Acidity of discharge water (pH)*
　There is a significant difference. More damage occurs as the pH increases.
(2) Flow velocity of discharge water*
　There is a significant difference. More damage occurs as the flow velocity increases.
(3) Presence of bluff body**
　There is a significant difference. More damage occurs when bluff bodies are present than when bluff bodies are absent.
(4) Installation environment (i.e., whether the scrubber was installed during newbuilding or during retrofitting after the ship entered service)**
　There is a significant difference. Vessels that are retrofitted with scrubbers after entering service are more likely to be damaged than those in which scrubbers are installed at the time of newbuilding.

*　Based on t-test: Test method to determine if there is a significant difference in the relevant subjects for each population.
**　Based on $\chi 2$ (chi-square) test: Test method to determine if there is a significant difference between the observed and expected values.

(Supplementary information)
Generally, a statistically significant difference is considered to exist if the criterion value (p value) is less than 0.05. The values of each of the above-mentioned items were as follows; (1) p=0.0110 (2) p=0.0027 (3) p=0.0300 (4) p=0.0008. This study did not consider the effects of the condition of the paint, the type of paint or the shape of the bluff body.

6. COUNTERMEASURES

These results suggest that measures which take these factors into account may reduce the risk of damage. The following are the advantages, disadvantages and points to note about the measures that are currently considered effective. It should be noted that the following measures are for reference purposes only, and their effectiveness is not guaranteed in all cases. Therefore, you are requested to independently investigate their effectiveness on a case-by-case basis and study their applicability carefully with the concerned parties when such measures are to be applied.

6.1 Paint

If an appropriate corrosion-resistant paint is applied and the installation quality is adequate, painting is considered to be sufficiently effective as a corrosion countermeasure. In order to prevent corrosion due to inadequate painting quality, it is important to pay special attention to pre-painting procedures and paint application, and to ensure that the procedures specified or recommended by the paint manufacturer are followed.

6.2 GRE Lining

Linings made of GRE (Glass fiber Reinforced Epoxy) or GRVE (Glass fiber Reinforced Vinyl Ester) have excellent corrosion resistance, and can be expected to provide pinhole-less performance. However, GRE or GRVE lining requires a certain construction period because the lining material must be dried repeatedly. In addition, as in the case of paint, sufficient attention should be paid to quality control at the installation site.

A GRE sleeve is also adopted in some cases to solve the problems of drying time and installation quality. In this case, the GRE is formed into a sleeve in advance at the manufacturing factory prior to the installation on board, and the sleeve is inserted inside the distance piece and bonded with a special paint on board.

6.3 Stainless Steel Pipe

When stainless steel is used as the material of the distance piece, the risk of corrosion is considered to be less affected by installation quality because the pipe itself has high corrosion resistance.

However, because the hull plates will be made of a different material than the distance piece, appropriate painting or other measures to prevent electrolytic corrosion will be required. If stainless steel is used, it should be noted that approval of the welding procedure specification for stainless steel is required.

6.4 Change of Bluff Body Shape

If the shape of the obstruction plate installed on the distance piece is changed from a bluff body to an orifice type, the workability around the installation area will be improved, and as a result, the quality of welding and painting work will be improved, and the risk of corrosion occurring around the point will be reduced. However, when the shape of the bluff body is changed, recalculation by CFD or other means is required to confirm that the pH standard of the discharge water specified in Section 3.3 is satisfied.

7. CONCLUSION

The authors believe that the information contained in this Technical Journal article will be a useful reference for shipowners, ship management companies, etc., and will make it possible to take effective preventive actions as needed.

We recommend that shipowners and ship management companies share the above-mentioned information with the ship masters of vessels on which SOx scrubbers are installed, and instruct them to pay greater attention to external inspections of discharge water lines (especially those around distance pieces from engine rooms) and carry out the said periodical inspections more frequently, and also arrange to inspect the internals of distance pieces when the opportunity presents itself, e.g., by arranging divers for hull cleaning.

We will continue to contribute to the safe operation of ships and the preservation of the marine environment by actively collecting and disseminating information to those concerned.

Update of Wave Statistics Standards for Classification Rules*1

Håvard Nordtveit AUSTEFJORD*, Guillaume de HAUTECLOCQUE**, Michael JOHNSON***, Tingyao ZHU****

1. INTRODUCTION

The world's commercial shipping in global service is designed to structurally withstand a severe wave environment defined by the International Association of Classification Societies (IACS) - namely IACS "Rec. No. 34 rev1" (2001), which provides details of the North Atlantic Ocean, principally in the form of a scatter diagram giving the occurrence statistics of combinations of significant wave height (H_s) and average zero up-crossing wave period (T_Z).

IACS has faced some criticism of Rec. No. 34 rev1 (2001) because the underlying statistical data originates in historical 'eyeball' observations from ships. Whilst these data were the best available at the time, studies have shown inaccuracies in human estimates. The effect of weather avoidance is embedded in the data but unquantifiable, and any bias, for example due to fixed shipping routes or ship types, cannot be identified either. Furthermore, the last observations included date back to 1984, so there is also concern that long term changes since that time are missing.

In recent years numerical wave modelling has improved greatly in quality and has also become more readily available to the engineering community. Furthermore, the International Maritime Organization (IMO) has made the public broadcast of ship positions (Automatic Identification System, AIS) mandatory; this was intended as an aid to navigation local to any particular ship, but the aggregation of such records globally has provided an enormously valuable dataset. These two developments led IACS to propose a project team in 2018 to consider updating Rec. No. 34, with the idea that the AIS tracking data could be combined with co-located wave model data for the North Atlantic to produce an unbiased wave scatter diagram. The project team has submitted its work to IACS "Rec. No. 34 rev2"; this paper makes public much of the technical work performed in order to establish this updated recommendation.

In this paper, the geographical area of review and the sources of ship track and wave model data are first presented. The method to calculate a 'raw' scatter diagram is given, together with work underlying the recommendation for spectra shape and spreading. This is followed by a description of a smoothing process employed to sanitise the raw scatter diagram. Results are then presented, showing how, for a testing database of 70 different ship types, ship responses (ship motion, accelerations, and wave loads) are expected to change when comparing the new "Rec. No. 34 rev2" with the old "Rec. No. 34 rev1 (2001)". Finally, known limitations of the approach are identified and discussed.

2. DATA SOURCE

2.1 Wave Hindcast

The sources underlying the Rec. No. 34 rev1 scatter-diagram are visual observations from ships, last published in 1986[1)]. Whilst some corrections were applied, those visual observations have been reported to have limited accuracy, especially concerning wave period[2)]. Since Rec. No. 34 rev1, significant progress has taken place. Numerical hindcast analyses are nowadays common practice, and several reliable global datasets are publicly available. Based on the analysis of different datasets[3)], the IOWAGA (Integrated Ocean Waves for Geophysical and other Applications) dataset from Ifremer (Institut Français de Recherche pour l'Exploitation de la Mer) is used in this work[4)]. As the IOWAGA dataset does not store full spectra, it is complemented with ERA5 (ECMWF Reanalysis v5) dataset[5)] from ECMWF (European Centre for Medium-Range Weather

*1 This paper has been originally published in the Proceedings of 9th International Conference on Marine Structures. The permission to reproduce this paper in this Journal has been obtained from the Technical Programme Committee of the conference.

* Det Norske Veritas, Oslo, Norway
** Bureau Veritas, Paris, France
*** Lloyds Register, Southampton, UK
**** Nippon Kaiji Kyokai (ClassNK), Tokyo, Japan

Forecasts) in section 5.

2.2 Ship Position

As Rec. No. 34 is supposed to reflect waves encountered by ships, it is important to consider realistic combinations of routes and wave data[6) 7) 8)]. The best way to do this is to combine millions of in-voyage locations with individually co-located wave data. This naturally gives a full representation of the routing effect in a 'routed' scatter-diagram. Voyages of over twenty thousand vessels were established by cleaning and resampling AIS data to the same temporal resolution as the hindcast wave data.

The fleet is limited to cargo and passenger vessels longer than 90m. This means most commercial seagoing ships are included. Excluded are many fishing vessels, offshore vessels, naval ships, and ships operating at fixed locations e.g. FPSOs.

The time period analysed ranged from 2013 to 2020 (seven full years). The collection of voyages was made in the North-Atlantic, as defined by Fig. 1. The choice of this area is further discussed in section 7. Coastal traffic near islands was discarded (~50 nautical miles).

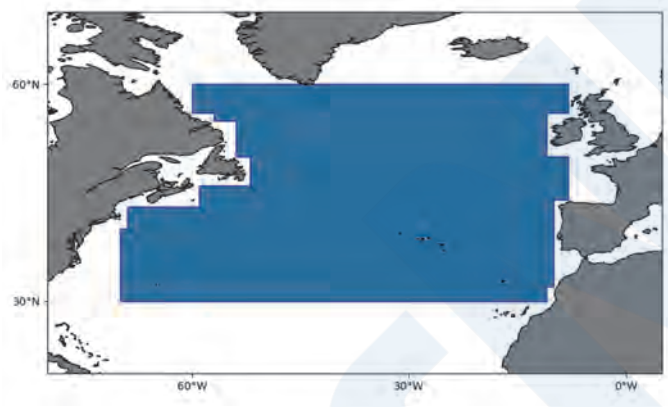

Fig. 1 Definition of North-Atlantic area for this work.

2.3 Database of Ship Responses

The final objective of the new wave statistics standard is a better long-term prediction of ship responses. It is thus important to have this in mind when evaluating the different assumptions and compromises made on the way to this new wave standard. To tackle this, a database of 3D linear seakeeping responses was used.

The vessels included are presented in Table 1. For each vessel, 3D BEM linear calculation[9)] is performed. The transfer functions are output for the quantities listed in Table 2. The RAOs are calculated with a 5° heading resolution, and are available at four speeds: 0 knots, 5 knots, Froude number of 0.1 and 75% of the service speed.

Table 1 Ship database, number of ships investigated for each type and loading condition.

Ship type	Full	Ballast
Tanker	16	11
Bulk and Cargo	19	16
Container-vessel	21	10
LNG	5	0
LPG	5	0
RoRo	3	0
Passenger-ship	5	0
Total	**74**	**37**

Furthermore, for each response, a characteristic period T_c is calculated thanks to the available regression in[10)]; the characteristic length L/α from[10)] is converted to period: $T_c^2 = (2 * \pi * L\ ) /\quad (g * \alpha)$. Note that in this work, the characteristic period is not used for any quantitative derivation; but only to display results in a scale allowing for physical interpretation.

Fig. 2 and Fig. 3 illustrate this responses dataset, showing two RAOs, with very different characteristic periods: the vertical

bending moment of a long ship with large T_c, and the horizontal bending moment of a short ship (low T_c).

Table 2 Type of ship responses included in the dataset.

RAO label	Description
VBM	Vertical Bending Moment amidship
HBM	Horizontal Bending Moment amidship
VSF	Vertical Shear Force, aft quarter
Pitch	Pitch motion
Acc. Surge	Surge acceleration
Acc. Sway	Sway acceleration
Pressure wl	Waterline pressure amidship
Roll	Roll motion

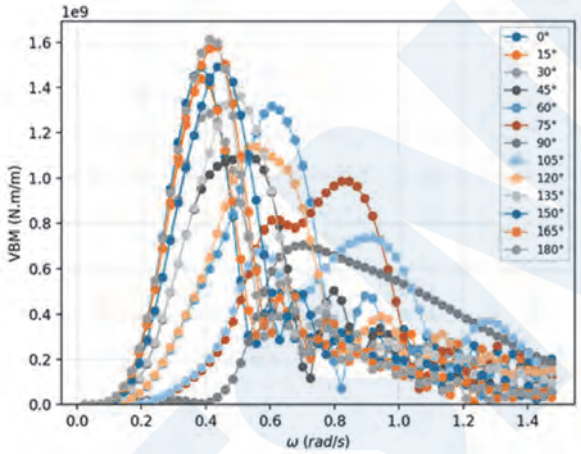

Fig. 2 VBM RAOs, long ship, L = 370m, T_c =18s.

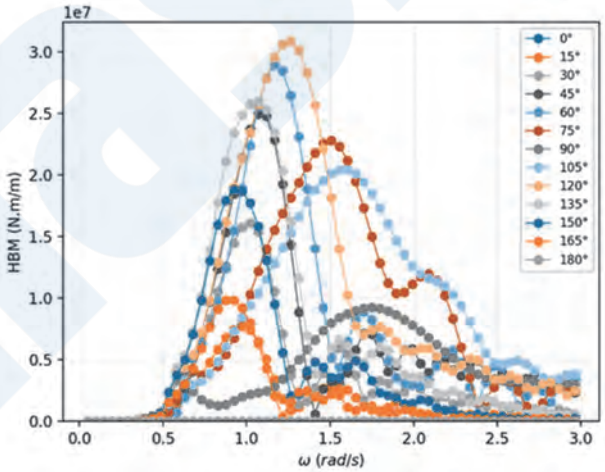

Fig. 3 HBM RAOs short ship, L = 90m, T_c=6s.

3. DISCRETE SCATTER-DIAGRAM

The approach for deriving discrete scatter diagrams with bad weather avoidance is summarised as follows:

- Download AIS and IOWAGA hindcast data within the North-Atlantic area for a period of 7 years (from June 1st 2013 to June 30th 2020).
- Clean and resample AIS data to 3-hour resolution, including outlier removal and interpolation to fill gaps in the records. Match each AIS data point to the nearest hindcast data point.

- Place encountered significant wave heights H_s and mean wave periods (T_{0m1}) in 0.1m and 0.1s bins. Here, $T_{0m1}(=2\pi(m_{-1}/m_0)$ is a mean wave period (s), where m_n is the spectral moment of order n.

4. STATISTICAL MODEL

The previous section introduced the process followed by the IACS working group to derive the Rec. No. 34 rev2 scatter-diagram from the combination of vessel tracks and hindcast wave data.

The empirical scatter-diagram obtained from AIS and hindcast data is fitted with a statistical model. It smooths out some of the sampling uncertainties, allows the possibility to extrapolate to unobserved wave periods and provides the scatter-diagram in a compact form (the scatter-diagram can be reconstructed at any desired resolution from a few coefficients).

The statistical model underlying Table 1 of the Rec. No. 34 rev2 is written as:

$$p(H_s, T_{0m1}) = p_H(H_s) * p_{T_{0m1}}(T_{0m1}|H_s) \qquad (1)$$

Where $p_H(H_s)$ is the marginal distribution of the significant wave height, and $p_{T_{0m1}}(T_{0m1}|H_s)$ the conditional distribution of the mean wave period.

4.1 Marginal Distribution of H_s

A mixture of Weibull distributions is used to model the marginal distribution. The coefficients (given in Table 3) are determined by MLE (maximum likely-hood estimate) based on the discrete scatter diagram.

$$P_H(H_s) = \chi\ F_{H,1}(H_s) + (1-\chi)F_{H,2}(H_s) = 1 - \chi\ \exp\left[-\left(\frac{H_s-\varepsilon}{\lambda_1}\right)^{\alpha_1}\right] - (1-\chi)\ \exp\left[-\left(\frac{H_s-\varepsilon}{\lambda_2}\right)^{\alpha_2}\right] \qquad (2)$$

Table 3 Hs distribution coefficients.

	Coefficient
$\boldsymbol{\alpha_1}$	1.4230
$\boldsymbol{\varepsilon}$	0.9360
$\boldsymbol{\lambda_1}$	1.8150
$\boldsymbol{\alpha_2}$	1.3940
$\boldsymbol{\lambda_2}$	2.8050
$\boldsymbol{\chi}$	0.9499

4.2 Conditional Model

The conditional mean wave period distribution is modelled as a split generalized normal distribution:

$$p_{T_{0m1}}(t|H_s) = \begin{cases} c \cdot e^{-\left[\frac{x_0-t}{\sigma_l}\right]^{d_l}} & for\ \ t<x_0 \\ c \cdot e^{-\left[\frac{t-x_0}{\sigma_u}\right]^{d_u}} & for\ \ t\geq x_0 \end{cases} \qquad (3)$$

With

$$c = \frac{1}{\sigma_l \Gamma\left(1+\frac{1}{d_l}\right) + \ \sigma_u \Gamma(1+\frac{1}{d_u})}$$

The parameters σ_u , σ_l and x_0 are fitted, for each H_s bin, by MLE. The dependency of those parameters with H_s are then fitted with the shapes described in equation (4) using least-square. Table 4 provides the coefficients thus obtained.

$$x_0(h_s) = l_0 + 1.0 * \ h_s + l_1 * \ h_s * \ \sqrt{h_s}$$

$$\sigma_u(h_s)$$

$$= \begin{cases} su_2 + su_1 * \left(1 - \cos\left(\frac{\pi * h_s}{su_0}\right)\right) * 0.5 \ \text{ for } \ h_s < su_0 \\ (su_2 + su_1) * \cos(\sigma_d * \pi) \text{ for } \ h_s \geq su_0 \\ \text{with} \quad \sigma_d = \frac{1}{1 + \ e^{-su_3 * (h_s \ - \ su_0)}} - 0.5 \end{cases} \tag{4}$$

$$\sigma_l(h_s) = sl_0 * h_s + sl_1$$

$$d_u = 2$$

$$d_l = 3$$

Table 4 Coefficients for conditional model.

	Coefficient
$\boldsymbol{l_0}$	5.427251
$\boldsymbol{l_1}$	-0.085340
$\boldsymbol{su_0}$	2.549443
$\boldsymbol{su_1}$	2.435955
$\boldsymbol{su_2}$	0.705177
$\boldsymbol{su_3}$	0.133225
$\boldsymbol{sl_0}$	0.018557
$\boldsymbol{sl_1}$	1.005918

Finally, discretisation is performed into 1m and 1s bins to get the final scatter-diagram. Values in each bin are calculated using midpoints, except for H_s = [0.0m, 1.0m] where exact integration is used. The obtained discretized scatter-diagram is given in appendix (Fig. 19).

4.3 Contribution Coefficients

Using the newly defined scatter-diagram, and working with the ship database introduced in 2.3, contribution coefficients can be calculated to show the sensitivity to the seas state of both extreme and fatigue loads. The knowledge of those contribution coefficients allows prioritisation of the relevant sea-states when simplified assessments are needed.

The contribution coefficients are calculated using the response dataset from section 2.3, assuming a JONSWAP spectrum with $\gamma = 1.5$ and a directional spreading of $\cos^3$.

From Fig. 4, the H_s of the sea-states contributing the most to the extreme are, roughly speaking, between, 7.5m and 16.5m. The characteristic period largely explains the variations observed: small T_C are associated with small H_s, large T_C with large H_s. As a simplification, hereafter, sea-states with H_s > 10m are considered as extreme sea-states.

The range of sea-states contributing to the fatigue damage are, on the other hand, lower; in the range [3m, 7m] (Fig. 5).

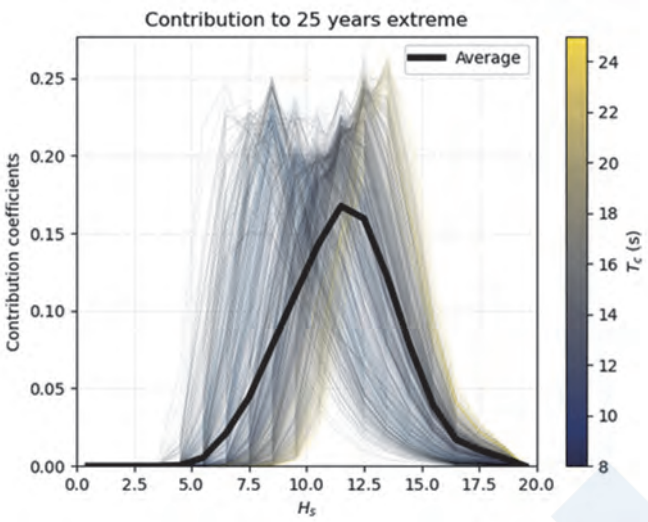

Fig. 4　Contribution coefficients for extreme.

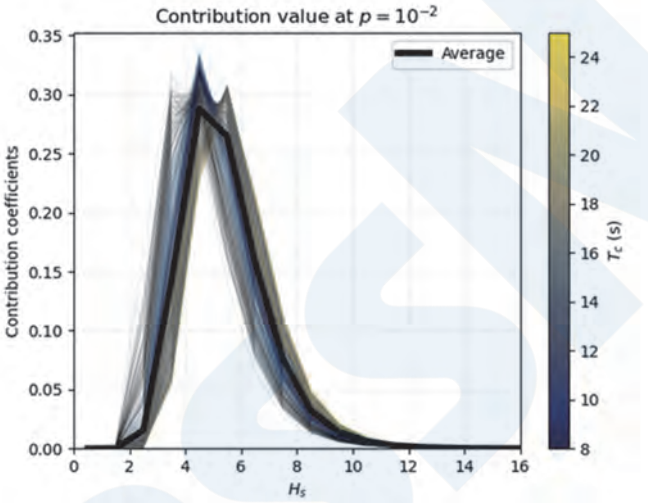

Fig. 5　Contribution coefficients for fatigue loads.

5.　SPECTRUM SHAPE

In Rec. No. 34 rev1, the spectral shape is a two parameters Pierson-Moskowitz spectrum (equivalent to JONSWAP with $\gamma = 1.0$), associated with cos² spreading. In the present studies, analysis of full directional spectra from hindcast data has shown that JONSWAP spectrum with $\gamma = 1.5$ and a cos³ spreading was more appropriate to represent extreme sea-states. Furthermore, this spectral shape provides accurate results for fatigue loads as well. This section gives some background justifications.

The full spectra data here analysed are from the model ERA5, at a single point located in the North Atlantic, over the period of 25 years (1990-2014).

Fig. 6 shows the shape of 306 sea-state spectra contributing the most to the 25-years extreme (~H_s > 10m), normalised according to T_{0m1}. The extreme sea states have remarkably constant shape and seem to be well represented by a JONSWAP spectrum with peakedness factor γ= 1.5. This value of 1.5 has been obtained by a least-square minimisation. It is also observed that matching T_{0m1} or T_p provides much better results than T_Z[11].

A slight trend of gamma increasing with H_s was observed; however, it was found that setting gamma as a function of H_s did not significantly improve the overall accuracy of ship responses. For simplicity and practicality, a fixed value γ=1.5 is then recommended.

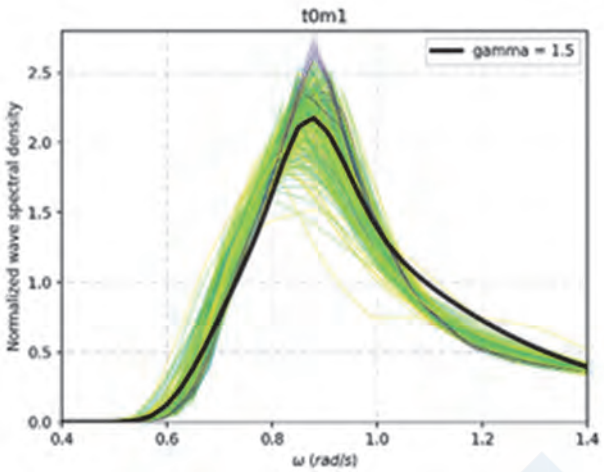

Fig. 6 Shapes of contributing spectra (H_s > 10m) and the chosen parameterized spectrum (JONSWAP, $\gamma = 1.5$), based on 25 years of hindcast data.

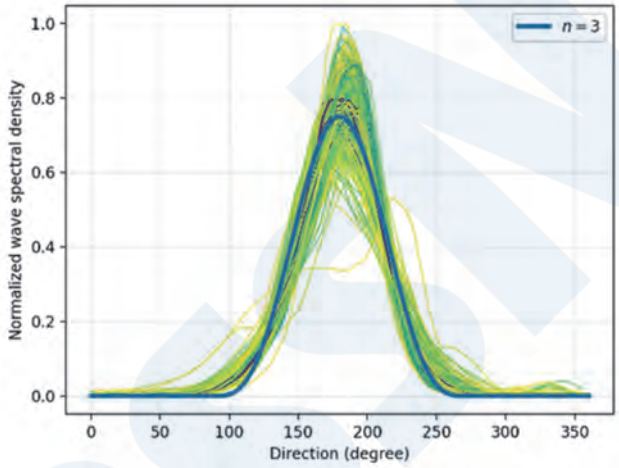

Fig. 7 Shapes of contributing spectra (H_s > 10m) as function of headings, together with the parametrized shape ($\cos^3$).

Similarly, Fig. 7 shows the directional shape of sea-states contributing to the extreme. As with the frequency shape, the directional spreading is very similar among the different sea-states and well approximated by a cos^n formulation with n=3.

Finally, to evaluate the accuracy loss induced by this simple parametrization, a validation is performed with the ship RAO dataset introduced section 2.3 and the ERA5 directional wave dataset introduced earlier in this section. The 25 years extreme values are calculated for all ship responses:

- Using full spectra (reference)
- Using $\gamma = 1.0$ and n = 2 (Rec. No. 34 rev1)
- Using $\gamma = 1.5$ and n = 3 (Rec. No. 34 rev2)

For extreme loads, the Rec. No. 34 rev1 shape results in a 7% quadratic error compared with the benchmark full spectrum case, which is reduced to 5% using Rec. No. 34 rev2 parameters.

Fatigue loads (at 10^{-2} probability as the reference value) are less sensitive to spectrum shape. With the same testing data set, Rec. No. 34 rev1 and Rec. No. 34 rev2 show a quadratic error of 2.7% and 3.2% compared with the benchmark case, respectively. Those errors are considered comparable and acceptable.

These findings are confirmed by a similar analysis conducted at several locations[11].

6. OPERATIONAL PROFILE

The Rec. No. 34 rev1 includes recommendations for how ships are assumed to operate in different sea conditions. Equal probability for all ship headings is specified, and zero speed is assumed when evaluating extreme wave loads (strength assessment).

In this section, using results from the combined AIS-hindcast dataset described in Section 2, the probability distributions of ship speeds and relative wave headings are estimated. All types of merchant ships over 90m navigating in the North Atlantic Area shown in Fig. 1 are considered.

The correlation between speed and heading with significant wave height is complex. In the following, it is assumed that the speed and heading can be investigated separately.

6.1 Heading

Accounting for the AIS-IOWAGA data including the entire range of H_s, we observe that the heading profile is equiprobable, as currently assumed in Rec No. 34 rev1 (Fig. 8). Uniform distribution is thus perfectly suited to fatigue calculations.

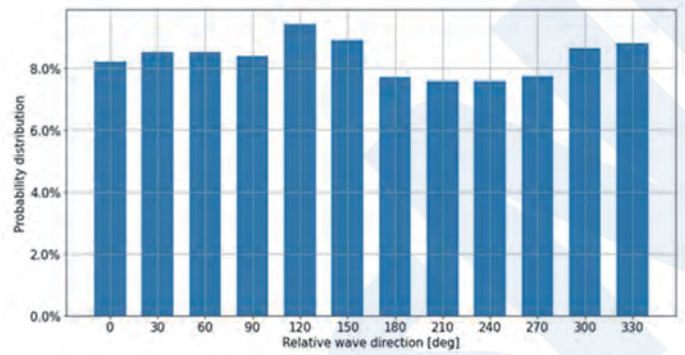

Fig. 8 Heading histogram, all data.

However, looking only at extreme sea-states, the picture is different: beam seas are less likely, as shown in Fig. 9. This figure presents the data in North-Atlantic only; it has been checked that using world-wide data which provides a similar picture. Two factors can explain this observation:

- Ship's captains avoid beam seas in harsh weather, to limit roll motion and increase stability.
- Harsh weather happens in locations where routes are mostly east-west, with dominant wave direction from west.

While the first explanation is considered as the main one, the below data cannot distinguish between the two effects. Whatever the cause, the practical effects are the same and evaluated on the ship response database.

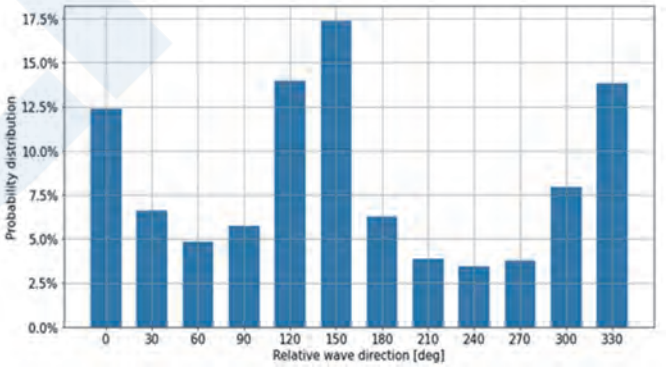

Fig. 9 Heading histogram, H_s > 10m.

Fig. 10 shows the relative differences between extreme responses considering the headings equiprobable, or with the same distribution as Fig. 9. A constant speed 5 knots has been assumed for simplicity. The effect is small, and keeping a constant probability for headings thus appears to be a good compromise between simplicity and accuracy.

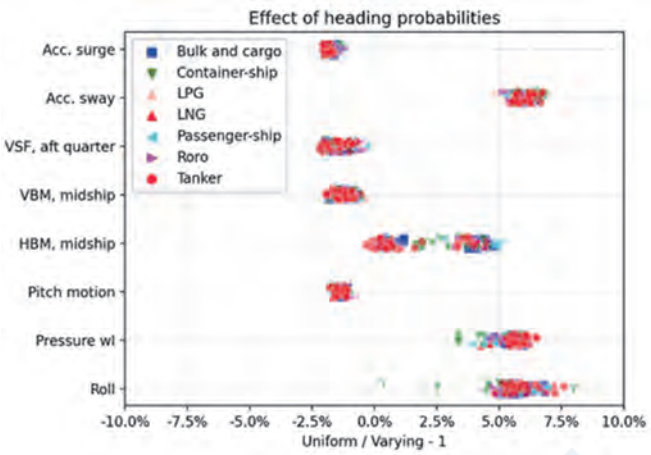

Fig. 10 Response sensitivity to heading distribution.

6.2 Speed

In the same fashion, the relationship between ship speed and heading is investigated. From Fig. 11 it is observed that speed in head seas reduces significantly with wave-height. The two most plausible reasons are:

- Voluntary speed reduction to limit ship motions.
- Involuntary speed reduction due to added resistance in waves.

Looking slightly deeper, it appears that the speed reduction is strongly dependent on the relative wave heading. Fig. 12 shows the speed reduction for each heading. It appears that the reduction is larger in head sea than in following sea.

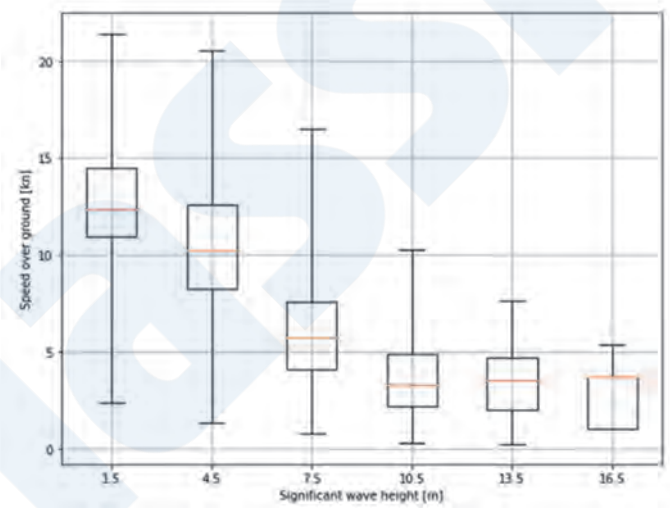

Fig. 11 Speed versus wave height in head sea, all ships.

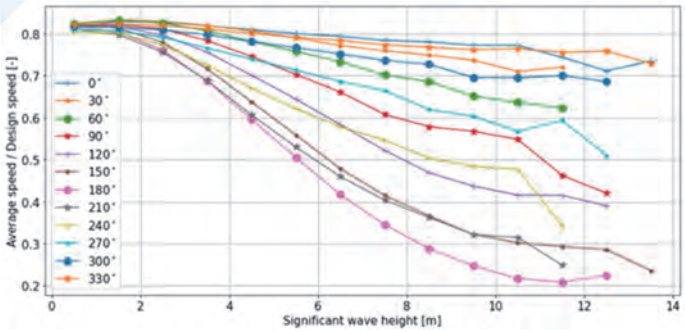

Fig. 12 Average ship speed as function of Hs and relative wave heading, 0 being following sea and 180 head sea.

To assess the sensitivity of long-term results to assumptions made on vessel speed, long-term calculations of extreme responses are performed using data from Fig. 12, simplified as follows to be compatible with the RAO dataset:

- 0.75 Vs for 0°, 30° and 330°.
- Froude number = 0.1 for 60°, 90°, 270° and 300°.
- 5 knots for 120°, 150°, 180°, 210° and 240°.

The results are then compared with the less refined assumption from the Common Structural Rules for bulk carriers and oil tankers[12]: fixed 5 knots. The headings are considered equiprobable in both cases.

From Fig. 13, it is observed that assuming a 5 knots speed for extreme has small effect on most of the responses. However, large difference may arise for roll motion and related quantities such as pressure on waterline. This is linked to the roll motion which can be large for low GM vessels in stern-quartering seas at high speed[13]. While this is relevant, the discrepancies are overestimated in our calculations, for three reasons:

- The GMs used in the ship response dataset are a lower bound (full, scantling GM). However, ships tend to operate on average at larger GM.
- In the ship response dataset, the roll damping is linear (6%) and does not vary with speed. In reality, lift damping as well as the quadratic effect would attenuate large roll angles at large speed.
- The fact that large roll angles are likely for low GM vessels in stern quartering seas is known and operational guidance are given to avoid those conditions[13]. The speed/heading/H_s statistics observed from AIS and hindcast do not include GM data, and do not allow this to be accounted for.

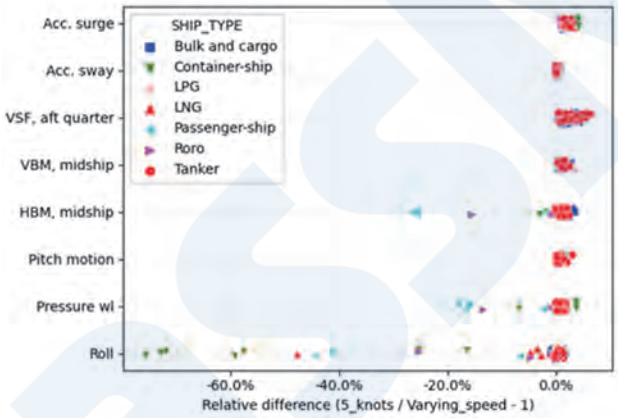

Fig. 13　Effect of fixed 5 knots assumption.

Filtering out ships having low GM with much larger roll motion at forward speed, we obtain Fig. 14, which shows that the 5 knots assumption is acceptable.

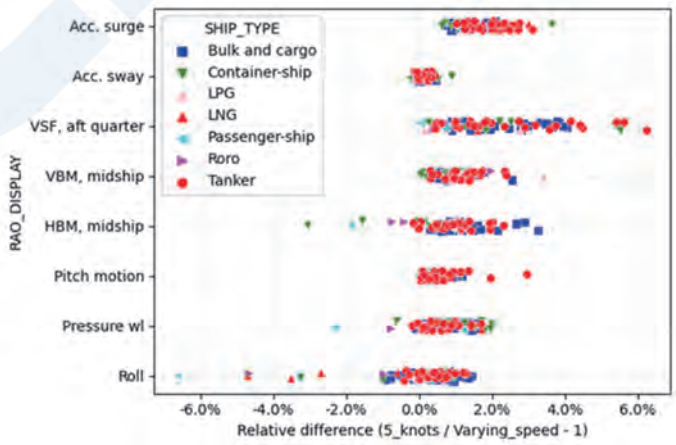

Fig. 14　Effect removing ship with high stern quartering roll.

For vessels with low metacentric height and operating without reduced speed in stern quartering seas appropriate speed and viscous damping need to be applied when evaluating roll related responses by numerical simulations. Furthermore, it is assumed that these effects can be considered in the development of rule formulae of roll motions by individual classification society.

6.3 Summary on Operational Profile

The uniform heading distribution currently used in the IACS Common Structural Rules for bulk carriers and oil tankers (CSR) and in Rec. No. 34 rev1 is thus confirmed and the continued use is justified in Rec. No. 34 rev2.

Using 5 knots for vertical shear force and bending moment and for loads in general for oil tankers and bulk carriers covered by CSR rules is mostly conservative. At most 1% non-conservatism is observed for roll motion of bulk carriers and tankers. It is therefore considered acceptable to use 5 knots as basis for vertical shear and bending in unified requirements S11 and S11A as well as loads in general for the CSR rules.

7. GEOGRAPHICAL AREA AND LOAD LEVEL

IACS Rec. No. 34 is based on wave data obtained from North Atlantic trade as this represents the most severe area ships tend to operate in. The basic idea of using a harsh design wave environment is that ships should not need to have geographical limitations on their operation.

Deciding on the exact polygon defining the North Atlantic is a subject for discussion. The wave characteristics are not uniform across the whole basin. Selecting a small area with harsher weather will result in a stricter scatter diagram than if the polygon is expanded to include less severe areas. To understand the consequence of the area selection an assessment of wave load level is made.

Hydrodynamic strip theory analyses were performed for 1500 vessels of different ship types and sizes. Each vessel was evaluated at multiple speeds between zero and full forward speed for relative wave directions with 30 degrees spacing.

AIS data for the world fleet is, in this study, limited to merchant vessels longer than 90 meters with a minimum of one year of data. The resulting 44000 vessels are matched with the closest hydrodynamic model in terms of vessel type, length, breadth and service speed. By matching the AIS data with IOWAGA hindcast data each vessel has a known series of wave height, period, relative direction and speed. This is used in long term response evaluation of the midship vertical bending moment at 1 year return period as well as the 10^{-2} exceedance probability.

Fig. 15 presents the ratio between 1-year moment from actual operation normalised by the 25-year design moment obtained using the Rec. No. 34 rev2. Fig. 16 shows the ratio of 10^{-2} moment between experienced and design load used for fatigue assessment in the IACS Common Structural Rules for bulk carriers and oil tankers (CSR).

Two variants of geographical areas are evaluated, one being somewhat smaller than the one finally selected. The smaller harsher area would slightly increase the 25-year extreme design wave loads, resulting in fewer vessels exceeding the 25-year design point. For fatigue the smaller area would easily result in no vessels exceeding the design value, meaning an over conservativism on fatigue loads. The effect of including the highly trafficked Bay of Biscay was considered but found not to make any difference to the loads, typically less than +/- 0.3% on extreme loads.

It is also observed that the different vessel types do not strictly encounter the same sea-states. The option to provide different scatter-diagrams for different types of vessels was considered and quickly discarded and considered not practical. On the other hand, the knowledge from Fig. 15 and Fig. 16 leaves the door open to further development of partial safety factors that would account for this observation.

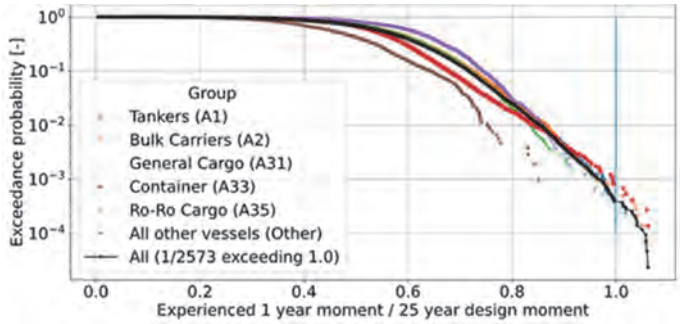

Fig. 15　Exceedance rate of 25-year extreme design moment per year.

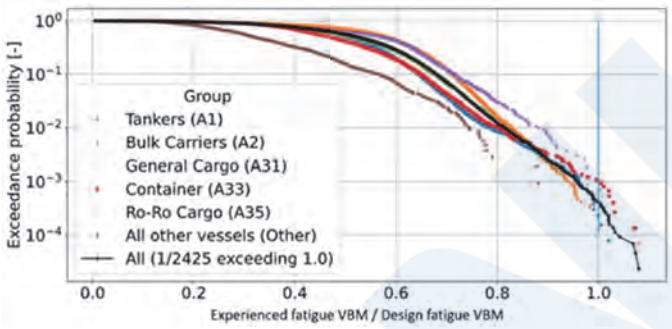

Fig. 16　Exceedance rate of 10^{-2} fatigue design moment.

This study gives an early idea of the level of the design load compared to what the world fleet experiences and may act as input when the final safety level including both load and capacity will be calibrated by IACS.

8.　CONSEQUENCE ASSESSMENT

The changes from Rec. No. 34 rev1 to rev2 are summarized in Table 5. The most significant change is the scatter-diagram itself, which induces relative lower loads. Then, the narrower spectrum and sharp spreading tend to slightly increase the loads respectively. Finally, the new definition of extremes (Return period (RP) =25 years, vs $p = 10^{-8}$) introduces a tiny reduction of the loads.

Table 5　Summary of changes.

	Rec. No. 34 rev1	**Rec. No. 34 rev2**
Scatter-diagram	Visual observation	Hindcast
Spectrum	Pierson-Moskowitz	JONSWAP $\gamma = 1.5$
Spreading	$\cos^2$	$\cos^3$
Extreme definition	$p = 10^{-8}$	RP= 25 years
Heading distribution	Uniform	Uniform
Fatigue reference	NA	$p = 10^{-2}$

The combined consequences of those updates are evaluated on the ship response dataset presented in Section 2.3, for extreme, and for fatigue loads.

Fig. 17 shows the consequences of extreme loads for both Rec. No. 34 rev1 and rev2 on all ship responses. Depending on the vessel and response type, the extreme loads are reduced from 10% to 30%. The characteristic period alone explains most of the variation: the reduction is relatively higher for responses with low characteristic period. Hence, for extreme loads, the new recommendation is – relatively – more favorable to short vessels.

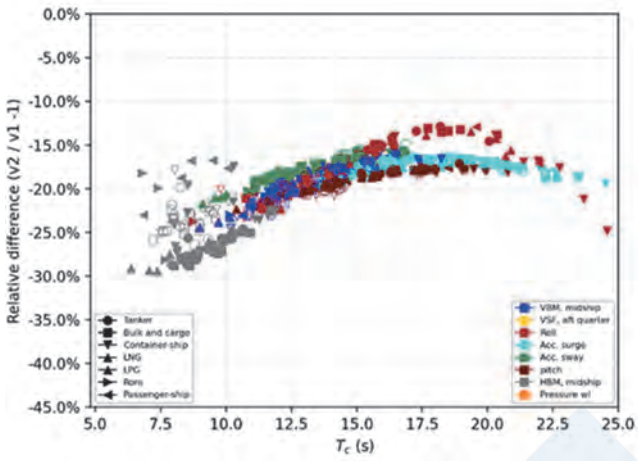

Fig. 17 Consequences on extreme loads.

Fig. 18 shows the consequence of fatigue loads, evaluated at $p = 10^{-2}$ for both Rec. No. 34 rev1 and rev2 on all ship responses. Compared to Rec. No. 34 rev1, the fatigue loads are significantly reduced in average, with reduction from -5% to -50%. As for extreme loads, the characteristic period of the response explains for most of the variation. On the other hand, this time, the Rec. No. 34 rev2 is, relatively, more favorable to long responses (i.e. long vessels).

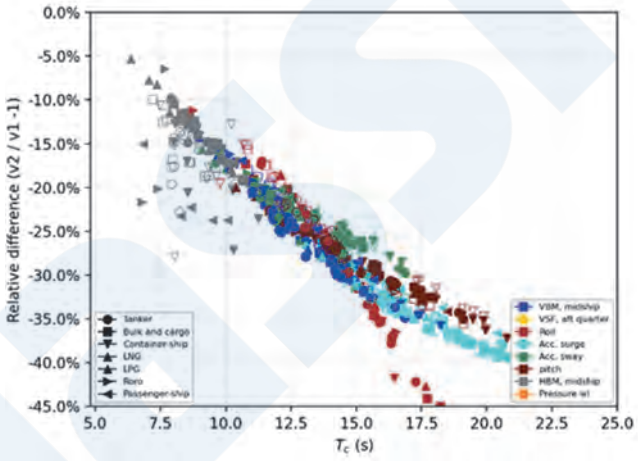

Fig. 18 Consequences on fatigue loads.

9. LIMITATIONS

Whilst the studies, techniques and data used by IACS to contribute to the up-issue of Rec. No. 34 are, at the moment of writing, considered state-of-the-art, there are known limitations. These are highlighted here.

9.1 Wave Models

IACS Rec. No. 34 rev2 relies heavily on numerical hindcast data. Although those have been validated through comparison with buoy data and satellite altimeters some uncertainties remain. Wave modelling is an active academic field and the accuracy of the global wave models is expected to continue to improve year on year.

9.2 Climate Change

The updated wave environment recommendations proposed by IACS are a present day snapshot and do not include any climate forecast change effects. The working group reviewed the work of the Intergovernmental Panel on Climate Change (IPCC), and found that there was a great deal of uncertainty about the effects relevant to shipping. However, even changes at the highest end of IPCC projections of +/- 0.5m (positive or negative) in extreme wave heights for the North Atlantic would be

expected to have negligible effect on the IACS Rec. No. 34 rev2 scatter diagram due to the robustness of the derivation procedure. Furthermore, ships in service will continue to avoid rough weather at the levels encapsulated in the new scatter diagram. In effect the IACS Rec. No. 34 rev2 scatter diagram does include some future-proofing.

9.3 Bad Weather Avoidance

The bad-weather avoidance embedded within this work represents the current performance level of global shipping. The technical quality, availability and take-up of routing services is increasing under current industry drive towards digitalisation. Therefore, the new recommendation might be regarded as including a slightly conservative bias as time goes on and those improvements become more definite.

9.4 Statistics

Synchronised weather data with ship position was limited to only 7 years. This was compensated by the fact that a huge number of ship positions was used, roughly 4500 ship-years, and that these later years were among the roughest recorded. The amount of data used is considered sufficient to correctly assess the 25 years ship responses, though this limitation is to be kept in mind when using the proposed scatter-diagram to estimate ship response at very low probabilities (i.e. very large return period). Even so, the new scatter diagrams are considered a huge improvement on Rec. No. 34 rev1 derived from eyeball observations.

Finally, the industry standard design approach that uses scatter-diagram is itself an approximation. By grouping time-series data into H_s-T_{0m1} bins, the serial correlation of sea-states is lost and can result in an overestimation bias[14]. Up to +5% conservatism on VBM is possible for large vessels.

10. CONCLUSIONS

A new wave standard is defined using state-of-the-art wave data sources combined with a ship position dataset. The wave scatter-diagram is significantly modified and includes the effect of bad-weather avoidance. Furthermore, the spectrum and spreading shapes are slightly narrower than in Rec. No. 34 rev1.

The change of wave loads is not homogenous: it depends on the type of loads and the type and size of the vessels. It thus, theoretically, optimises how the steel is distributed on a vessel, and across the fleet.

While Rec. No. 34 is an important document, it is only one piece acting as input to rule development. The average wave load reduction observed here will not necessarily translate directly into a reduction of the scantling. For instance, the current IACS unified requirement S11A for container vessels considers a routing factor to correct for the fact that Rec. No. 34 rev1 does not account properly for bad weather avoidance; this factor shall thus be adjusted when accounting for Rec. No. 34 rev2.

Further work is thus ongoing within IACS to update downstream documents, such as IACS URS11, IACS URS11A and the Common Structural Rules for bulk carriers and oil tankers[12].

ACKNOWLEDGMENTS

The work reported here was sponsored by the International Association of Classification Societies. The authors also wish to acknowledge the contributions to this work of Dr. Norio Yamamoto, ClassNK, Quentin Derbanne, Marine Lasbleis, BV, Dr. Eivind Ruth, Dr. Elzbieta Maria Bitner-Gregersen, Dr. Tormod R. Landet, all three of DNV, Dr. Zhenhong Wang, LR.

REFERENCES

1) Hogben, N: “Global Wave Statistics”, British Maritime Technology,1986.
2) Bitner-Gregersen, EM, Cramer, EH & Korbijn, F: “Environmental Description for Long-Term Load Response of Ship Structures”, the Fifth International Offshore and Polar Engineering Conference, 1995.
3) de Hauteclocque, G, Zhu, T, Johnson, M, Austefjord, H & Bitner-Gregersen, E: “Assessment of Global Wave Datasets for Long Term Response of Ships”, OMAE2020, Volume 2A: Structures, Safety, and Reliability, 2020.
4) Ardhuin, F, Hanafin, J, Quilfen, Y, Chapron, B, Queffeulou, P & Obrebski, M: “Calibration of the IOWAGA Global Wave Hindcast (1991–2011) Using ECMWF and CFSR Winds”, *12th International Workshop on Wave Hindcasting and*

Forecasting, Kohala Coast, Hawaii, 2011.

5) Hersbach, H, Bell, B, Berrisford, P, Horányi, A, Sabater, JMTN, Nicolas, J, Radu, R, Schepers, D, Simmons, A, Soci, C & Dee, D: "Global Reanalysis: Goodbye ERA-Interim, Hello ERA5", ECMWF Newsletter No. 159, pp. 17–24, 2019.
6) Eisinger, E, Bloch, H & Storhaug, G: "A Method for Describing Ocean Environments for Ship Assessment", Proc. 6th International Maritime Conference on Design for Safety, Hamburg, 2016.
7) Miratsu, R, Fukui, T, Matsumoto, T & Zhu, T: "Quantitative Evaluation of Ship Operational Effect in Actually Encountered Sea States", 2019. https://doi.org/10.1115/OMAE2019-95121.
8) Miratsu, R, Fukui, T, Matsumoto, T & Zhu, T: 2020, "Study on Ship Operational Effect for Defining Design Values on Ship Motion and Loads in North Atlantic", 2020. https://doi.org/10.1115/OMAE2020-18193.
9) Chen, XB: "Hydrodynamics in Offshore and Naval Applications - Part I", *Keynote lecture of 6th International Conference on Hydrodynamics*, Perth, Australia, 2004.
10) de Hauteclocque, G, Monroy, C, Bigot, F & Derbanne, Q: "New Rules for Container-Ships - Simplified Formulae for Wave Loads.", the Proceedings of 13th International Symposium on Practical Design of Ships and Other Floating Structures (PRADS2016), Copenhagen, Denmark, 2016.
11) de Hauteclocque, G & Lasbleis M: "Extreme Seastate Parametrization and Its Consequences on Ship Responses", the *Proceedings of 15th International Symposium on Practical Design of Ships and Other Floating Structures (PRADS2022)*, Dubrovnik, Croatia. 2022.
12) IACS: "Common Structural Rules for Bulk Carriers and Oil Tankers", 2014.
13) IMO: "Revised Guidance to the Master for Avoiding Dangerous Situations in Adverse Weather and Sea Conditions", 2007.
14) Mackay, E, de Hauteclocque, G, Vanem, E & Jonathan, P: "The Effect of Serial Correlation in Environmental Conditions on Estimates of Extreme Events", *Ocean Engineering*, Vol 242, 2021.

APPENDIX

Significant wave height, H_S (m)	Mean wave period, T_{0m1} (s)																Sum
	4.5	5.5	6.5	7.5	8.5	9.5	10.5	11.5	12.5	13.5	14.5	15.5	16.5	17.5	18.5	19.5	
0.5	6.82	202.00	333.61	187.76	45.59	4.74	0.21	0.00	0.00	0.00	0.00	0.00	0.00	0.00	0.00	0.00	780.73
1.5	0.33	2028.35	12750.82	11693.39	7215.76	3006.80	846.07	160.77	20.63	1.79	0.10	0.00	0.00	0.00	0.00	0.00	37724.81
2.5	0.00	3.38	2805.81	8517.74	7835.85	5885.37	3608.30	1805.81	737.71	246.00	66.96	14.88	2.70	0.40	0.05	0.00	31530.96
3.5	0.00	0.00	23.06	2742.51	4666.81	4100.83	2936.41	1713.38	814.68	315.65	99.66	25.64	5.38	0.92	0.13	0.01	17445.07
4.5	0.00	0.00	0.00	82.06	1759.81	2069.19	1715.42	1151.29	625.51	275.12	97.96	28.24	6.59	1.24	0.19	0.02	7812.64
5.5	0.00	0.00	0.00	0.08	149.74	811.81	791.81	609.66	375.67	185.26	73.12	23.09	5.84	1.18	0.19	0.02	3027.47
6.5	0.00	0.00	0.00	0.00	1.02	147.59	305.37	271.71	190.23	104.79	45.42	15.49	4.16	0.88	0.15	0.02	1086.83
7.5	0.00	0.00	0.00	0.00	0.00	4.77	88.62	107.20	86.26	53.35	25.36	9.27	2.60	0.56	0.09	0.01	378.09
8.5	0.00	0.00	0.00	0.00	0.00	0.02	9.40	38.70	36.80	25.95	13.63	5.33	1.55	0.34	0.05	0.01	131.78
9.5	0.00	0.00	0.00	0.00	0.00	0.00	0.20	9.34	15.15	12.51	7.39	3.12	0.94	0.20	0.03	0.00	48.88
10.5	0.00	0.00	0.00	0.00	0.00	0.00	0.00	0.81	5.73	5.96	4.08	1.90	0.60	0.13	0.02	0.00	19.23
11.5	0.00	0.00	0.00	0.00	0.00	0.00	0.00	0.02	1.29	2.68	2.23	1.18	0.40	0.08	0.01	0.00	7.89
12.5	0.00	0.00	0.00	0.00	0.00	0.00	0.00	0.00	0.11	1.01	1.14	0.72	0.27	0.06	0.01	0.00	3.32
13.5	0.00	0.00	0.00	0.00	0.00	0.00	0.00	0.00	0.00	0.22	0.51	0.42	0.18	0.04	0.00	0.00	1.37
14.5	0.00	0.00	0.00	0.00	0.00	0.00	0.00	0.00	0.00	0.02	0.19	0.21	0.12	0.03	0.00	0.00	0.57
15.5	0.00	0.00	0.00	0.00	0.00	0.00	0.00	0.00	0.00	0.00	0.04	0.09	0.07	0.02	0.00	0.00	0.22
16.5	0.00	0.00	0.00	0.00	0.00	0.00	0.00	0.00	0.00	0.00	0.00	0.03	0.04	0.01	0.00	0.00	0.08
17.5	0.00	0.00	0.00	0.00	0.00	0.00	0.00	0.00	0.00	0.00	0.00	0.01	0.02	0.01	0.00	0.00	0.04
18.5	0.00	0.00	0.00	0.00	0.00	0.00	0.00	0.00	0.00	0.00	0.00	0.00	0.01	0.01	0.00	0.00	0.02
Sum	7.15	2233.73	15913.30	23223.54	21674.58	16031.12	10301.81	5868.69	2909.77	1230.31	437.79	129.62	31.47	6.11	0.92	0.09	100000.00

Fig. 19 Rec. No. 34 rev2 scatter diagram.

Studies on In-Engine Combustion of Low and Zero-Carbon Fuels

Koji TAKASAKI*

1. INTRODUCTION

The development of marine engines that burn zero-carbon fuels such as hydrogen and ammonia is urgently needed to achieve the IMO target of significantly reducing greenhouse gas (GHG) emissions from international shipping. Methane and methanol, if synthesized in a carbon-neutral way, could also be considered net zero-carbon in the same sense as biofuels[1]. This paper describes the combustion of these five alternative fuels in engines.

Fig. 1 shows the classification of these fuels. It should be noted that LPG is not discussed in this paper. As the diagram shows, the molecules of methane and methanol contain carbon C, and combustion of these fuels produce CO_2. However, as they are considered "bridge fuels" to zero-carbon fuels, the amount of CO_2 produced (per calorific value) compared to marine gas oil (MGO) or heavy fuel oil (HFO) is reduced by about -25 % for methane and -10 % for methanol.

To achieve further CO_2 reductions from LNG- and methanol-fueled vessels, the carbon-neutral methane and methanol mentioned above need to be mixed with those fuels. Fig. 2 shows an example of the carbon-neutral methane production route[1], where synthetic methane is made from green hydrogen and CO_2 captured at power plants, steel mills, etc. If this means that CO_2 has been emitted on the land side, the methane synthesized by recycling the captured CO_2 would be defined as carbon neutral. Green methanol can also be made from this methane.

On the other hand, ammonia and hydrogen do not contain C and therefore do not produce CO_2, but marine engines that use them are still under development. This paper also introduces the development status of ammonia and hydrogen engines funded by the Green Innovation (GI) Fund of Japan's New Energy and Industrial Technology Development Organization (NEDO).

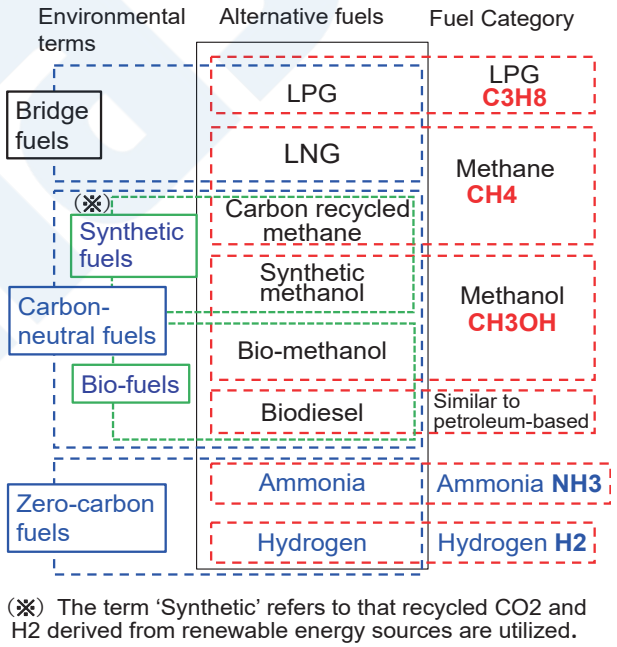

Fig. 1 Classification of alternative fuels
(Source: The Japan Association of Marine Safety)

* Professor (Emeritus), Kyushu University & Fellow, National Maritime Research Institute, Japan

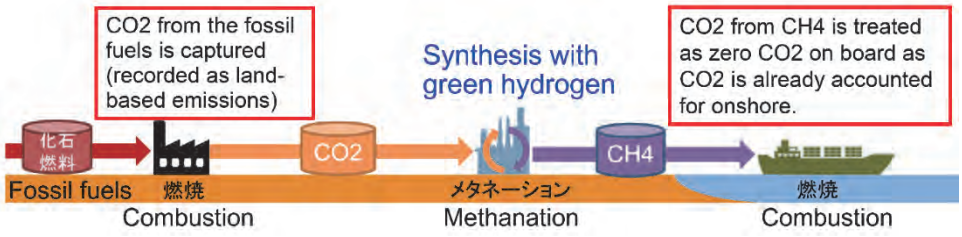

Fig. 2　Example of carbon-neutral methane production route[1)]

Table 1　Properties of zero-emission fuels for onboard liquid storage (extracted from MLIT website[1)])

	Hydrogen H2 (LH2)	Ammonia NH3	Carbon recycled (CR) synthetic methane CH4	CR synthetic methanol CH3OH	Biodiesel (FAME)
Lower Calorific Value (GJ/t)	**120.0**	**18.8**	**50.0**	**19.9**	**37.1**
Liquid density (t/m3)	**0.0708**	**0.7**	**0.422**	**0.79**	**0.885**
Volume ratio per calorific value (VLSFO ratio @ liquefied)	**4.42**	**2.86**	**1.78**	**2.39**	**1.14**
Boiling point (℃) at P atm.	**-253**	**-33**	**-161**	**65**	**345~354**
Storage method on board (liquid state)	Vacuum heat shielded tank	Type C (low temp. or pressurized)	Type C (low temp. or pressurized)	Tank with hull, normal temp. and press.	Tank with hull, normal temp. and press.
		Independent square tank / Membrane	Independent square tank / Membrane		
Properties stored on board (liquid state)	abt.-250 ℃、0.5 MPa	-30~-10 ℃、0.07~0.5 MPa	-160~-140 ℃、0.07~0.5 MPa	Normal temp. and press.	Normal temp. and press.

Table 2　Properties of alternative fuels (ClassNK)

State at fueling to engine	Liq. or Gas (3) NH3	Gas (4) CH4	Liq. (Standard)	Liq. (2) CH3OH	(Liq. (LPG)) (C3H8)	Gas (5) H2
	Ammonia	Methane	HFO	Methanol	Propane	Hydrogen
Gas specific gravity kg/m3 @ boiling point	0.876	1.820		1.206	2.385	1.340
Gas specific gravity kg/m3 @ 20℃	0.707	0.659		---	1.840	0.083
Liquid gravity kg/m3 @ 4℃	633.1	---	989 @15℃	805.9	523.2	---
Liquid gravity kg/m3 @ boiling point	682.3	422.5		748.7	580.8	70.8
Boiling point ℃ @ atmospheric pressure	-33	-161	---	65	-42	-253
Saturated vapor pressure barA @ 45 ℃	17.8	---	---	---	15.3	---
Self-ignition temperature ℃	630	537	250	385	450	585
Flash point ℃	---	-175	>60	12	-105	---
Lower flammable limit (fuel vol.%)	15	5.3	1	6	1.7	4
Upper flammable limit (fuel vol.%)	30	17	7	36.5	10.9	75
Minimum ignition energy mJ	45	0.274	0.24 (ガソリン)	0.174	0.240	0.017
Combustion speed cm/s	7	37	30 (ガソリン)	48	47	270
Lower calorific value MJ/kg	18.8	48.0	40.2	19.9	46.3	119.9

The properties of the five fuels are shown in Table 1, which is cited from the website of the GHG Zero Emissions Project[1)] of the Ministry of Land, Infrastructure, Transport and Tourism (MLIT). This is a selection of items relating specifically to liquid storage on board (tank capacity and type). Each tank capacity is determined by the calorific value per volume of liquid. The

current tank type and storage conditions are set as shown in the table according to the boiling point under atmospheric pressure.

The alternative fuel properties table published by ClassNK is shown as Table 2. This table is used as a basis for this paper. Explanations will be given in the following order: (1) biofuels, (2) methanol, (3) ammonia, (4) methane, (5) hydrogen. The paper refers to ignition and combustion characteristics of these fuels in marine engines, and discusses the harmful exhaust components from (3) ammonia.

(1) Biofuels, (2) methanol and (3) ammonia can maintain a liquid phase in the line from the tank to the engine, enabling diesel injection into the cylinder. (3) Ammonia becomes a gas at room temperature if not pressurized, and can also be supplied to the intake pipe of the four-stroke cycle engine that realizes Otto cycle premixed combustion.

On the other hand, (4) methane and (5) hydrogen are liquefied at very low temperatures in the tank, but are supplied as a gas phase to the engine. Diesel cycle or Otto cycle type engine can be applied with these two fuels. The characteristics of the two types of engines in combustion of natural gas will be reviewed later. Both types are also applicable for hydrogen combustion and are being developed with support from the GI Fund mentioned above.

2. COMBUSTION OF BIOFUEL (FAME)

Types of biofuels include (1) crude biofuels such as palm oil and rapeseed oil, (2) fatty acid methyl esters (FAME), which are converted from crude biofuels to reduce viscosity to the level of marine diesel oil (MDO), (3) HVO (Hydrotreated Vegetable Oil), paraffinic hydrocarbons that are further hydrotreated so that their characteristics are no different from those of mineral oils and (4) bio-methanol and bio-ethanol.

Since HVO is a high-grade fuel that is also used for aircraft and is not expected to be diverted to ships, this section focuses on FAME. In general, FAME is not inferior to MDO in density and viscosity, or in self-ignition and combustion characteristics.

The calorific value of FAME is lower than that of heavy fuel oil (HFO) due to the presence of about 10 % oxygen in the fuel molecule. As shown in Table 1, the calorific value of FAME is around 37 (GJ/t) compared to that of HFO, which is normally 40 to 42 (GJ/t). However, this is hardly a problem when FAME is mixed with HFO (for example, B30 (30 % FAME + 70 % HFO)).

FAME has one problem, in that NOx increases by 10 to 20 % compared to MDO. However, a clear decision on this has already been made in MEPC 78 and this means that the increase in NOx due to biofuel mixing is no longer subject to regulation. This makes FAME a true “drop-in” fuel that can be used in marine diesel engines without adjustment.

For this reason, there is likely to be greater demand from shippers, but production volume is recognized as a challenge. There is global resistance to using food as fuel, and although FAME is now made from waste cooking oil and other raw materials, the amount is limited, and there are also concerns about competition with the aviation industry.

In terms of the handling of crude biofuels and FAME, some points such as the development of microbials require attention and long-term storage is prohibited. The Machinery Department of ClassNK has provided explanations on these points. (https://www.classnk.or.jp/hp/ja/info_service/bio/). The Maritime Bureau of MLIT also published Guidelines for the Handling of Biofuels on Ships in March 2023, and a member of the Research Institute of ClassNK is contributing to this effort (https://www.mlit.go.jp/report/press/content/001597437.pdf).

3. METHANOL COMBUSTION

The author conducted a visualization analysis of methanol spray combustion prior to the development of MAN's low-speed two-stroke methanol engine (2015)[2]. The properties of methanol (CH_3OH) and heavy fuel oil (HFO) are compared in Table 2.

Methanol has a boiling point of 65 °C at atmospheric pressure and is a liquid at room temperature, which means that high-pressure liquid injection as in conventional diesel engines is possible. However, half of its molecular weight consists of oxygen, and its calorific value per mass is less than half that of HFO. Therefore, when using methanol, about 2.4 times the volume, equal to twice the mass of HFO, must be injected to obtain the same power output.

This paper demonstrates that methanol shows good combustion characteristics despite its lower calorific value. As the self-ignition temperature is higher than that of HFO (Table 2), ignition of methanol spray requires pilot injection of diesel fuel. However, once ignited, it exhibits excellent combustion characteristics, as described below. The same point, i.e., it is necessary to distinguish between self-ignitability and combustibility, also applies to methane and hydrogen.

Fig. 3 shows an apparatus that can visualize the combustion of a single spray in high-pressure, high-temperature air like that in a diesel engine[2]. The spray flames of gas oil and methanol were photographed using this apparatus. The injection pressure patterns of both fuels are also shown in the figure. The color photograph at the top right is a direct photographic image, showing that the gas oil spray is burning emitting a luminous color. In the case of methanol, only the pilot gas oil at the tip of the spray has a luminous flame, and the methanol flame itself, which follows the pilot flame, is non-luminous and invisible by the direct photographic technique. The left shows an image of the same flame taken by shadowgraph, in which the methanol non-luminous flame is captured in black.

A luminous flame of gas oil gives the impression of good combustion, but in fact the opposite is true: The luminous flame is the emission from particles of soot as it is formed in the flame. In other words, the non-luminous flame of methanol indicates good combustion with less soot formation. No black carbon is emitted from actual methanol engines. It is also clear from the comparison of the heat release rates in the figure that methanol has faster combustion after the end of fuel injection, as the after-burning of methanol is shorter.

Data from the prototype engine (500 mm bore: 7S50ME-B9.3-LGI) tested at Mitsui Engineering & Shipbuilding in 2015[3] has shown similar or slightly better thermal efficiency than that by MDO and a reduction of about -30 % in NOx. A major advantage of using methanol is that engines of this type have already been developed and are in service. However, the challenge is the availability of carbon-neutral (green or bio-) methanol. Maersk, the largest container shipping company, which has sparked the development of methanol-fueled ships, is also reportedly making efforts to procure such methanol[4].

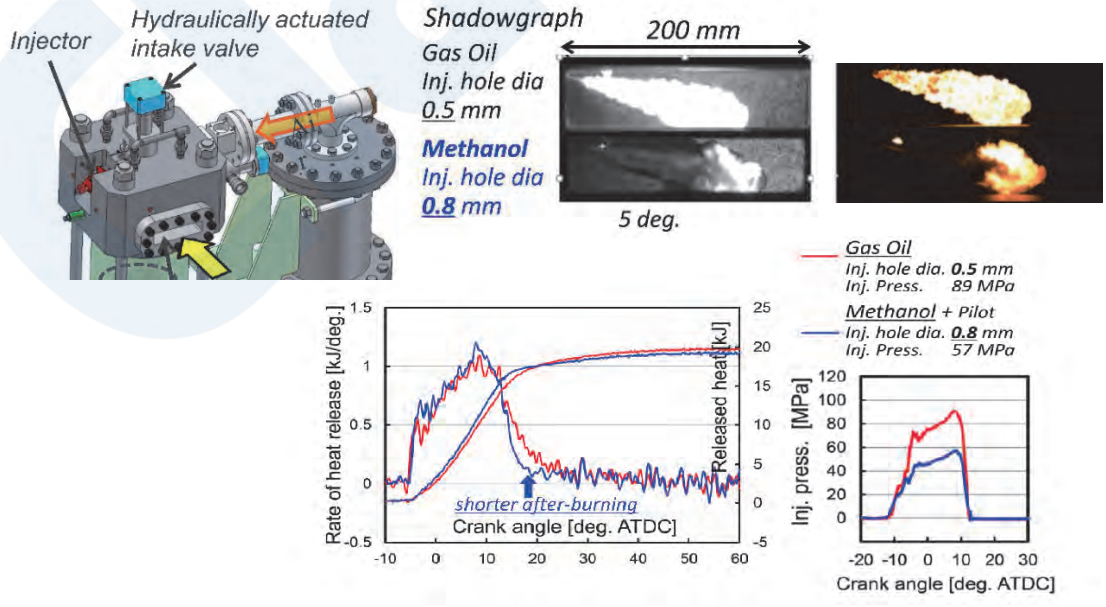

Fig. 3 Results of methanol spray combustion analysis (top left: combustion visualization apparatus (RCEM), top right: spray flame of gas oil and methanol, bottom: heat release rates of two fuels).

4. COMBUSTION OF AMMONIA

While the points requiring caution when handling ammonia are its toxicity and corrosiveness, some combustion-related issues must also be solved. This section describes the solution. Returning to Table 2, because the boiling point of ammonia at atmospheric pressure is -33 °C, it can be stored in onboard tanks in the liquid phase if pre-pressurized or cooled to a temperature lower than -33 °C.

There are two ways to supply ammonia to the engine. One is to keep the pre-pressure in the line and supply the ammonia to the engine in the liquid phase. According to MAN, in this case, the line pressure should be 8 MPa for safety reasons. The other way is to vaporize the ammonia and supply it as a gas. In the former case, the engine is a diesel type in which liquid ammonia is injected into the cylinder, while in the latter case, the engine is an Otto cycle type, in which gaseous ammonia is supplied to the intake pipe to form a mixture with air. Due to the presence of nitrogen in the ammonia molecule, it has a lower calorific value and must be injected in a volume about three times that of HFO, even in the case of liquid injection.

Ammonia is a fuel which simultaneously has both poor ignition and poor combustion characteristics, as the self-ignition temperature is the highest and combustibility represented by the combustion speed is the lowest among the fuels in Table 2. It is therefore expected that pilot injection with diesel fuel and combustion support by post-injection, etc., as described below, will be necessary. However, diesel fuel emits CO_2, so the target is to improve ammonia combustion with support by the minimum quantity of diesel fuel.

The National Project for “Development of ships with ammonia-fueled domestic engines” is introduced below. Fig. 4 shows an overview. The four-stroke engine for tugboats is designed as an Otto cycle type, in which gaseous ammonia is supplied to the intake pipe and forms a mixture of ammonia and air. On the other hand, the low-speed two-stroke engine for ocean-going vessels is designed as a diesel engine, in which ammonia is injected into the cylinder as a liquid. Although ammonia itself does not produce CO_2, but there are several challenges, in particular, generation of N_2O (nitrous oxide), a greenhouse gas about 300 times stronger than CO_2, which, if emitted to any degree, would drastically reduce the GHG reduction benefits of using ammonia fuel.

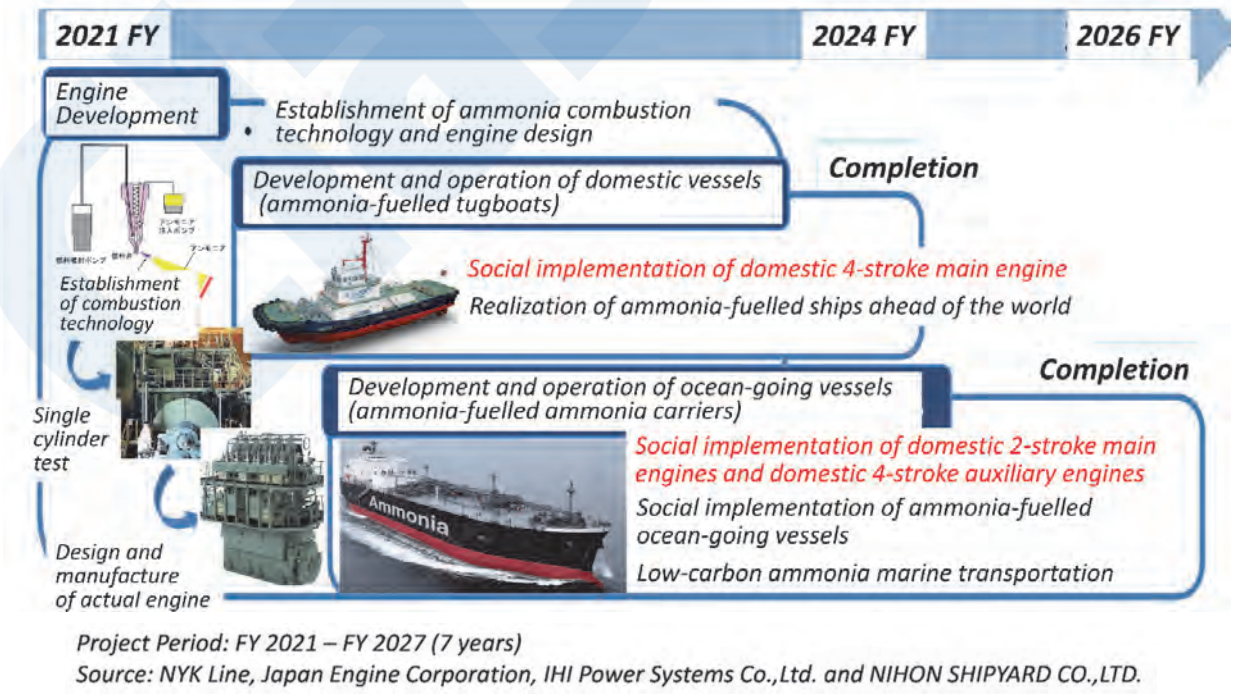

Fig. 4 Green Innovation Fund project, “Development of ships with ammonia-fueled domestic engines”
(*MLIT website: https://www.mlit.go.jp/maritime/content/001484436.pdf*)

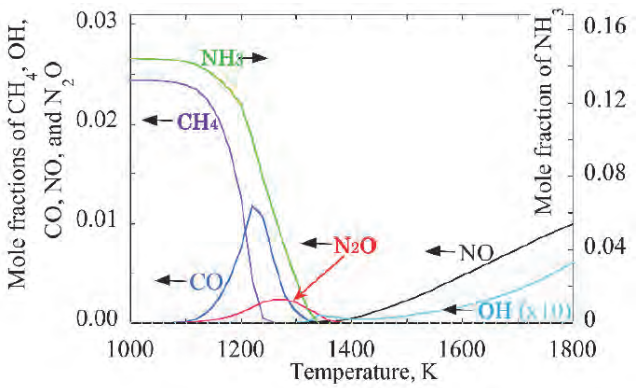

Fig. 5　Temperature range for formation of toxic exhaust components, including N_2O[5)]

Fig. 5 shows the result of a study by Prof. Kobayashi et al. at Tohoku University on the formation temperatures of toxic exhaust components, including N_2O[5)]. The figure shows that the temperature range at which N_2O is formed in the flame (about 1 300 K) is considerably lower than the normal range of the flame temperature where NO is formed. Unburnt ammonia also increases significantly at such lower temperatures.

To suppress N_2O formation, it seems important to avoid making conditions where combustion of the ammonia spray becomes inactive and the flame temperature drops. The following introduces the technology of stratified injection of diesel fuel oil and ammonia, which is being researched as a countermeasure jointly by the National Maritime Research Institute, Japan (NMRI) and Japan Engine Corporation.

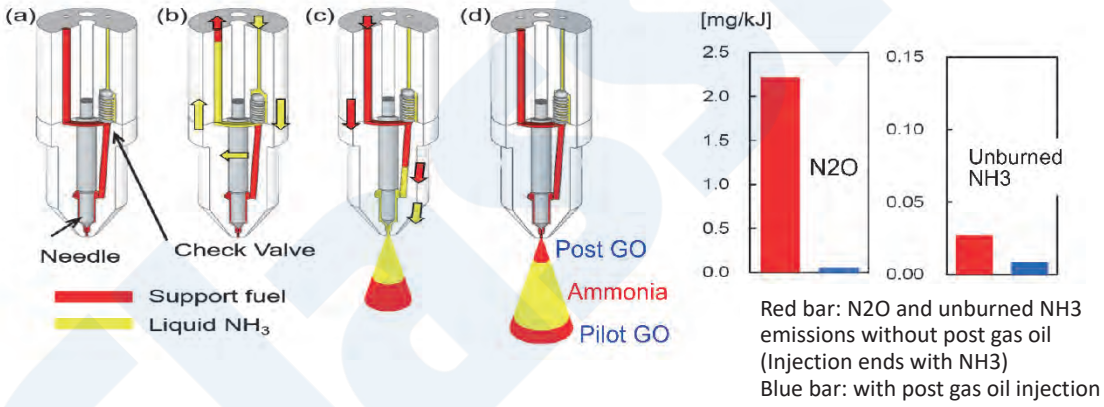

Fig. 6　Mechanism of stratified gas oil (GO) & ammonia injection system (left) and emission data from fundamental study by NMRI[6)] (right)

As shown in (d) on the left in Fig. 6, a small amount of gas oil is injected before and after ammonia injection. The first layer of gas oil acts as a pilot flame to ignite the ammonia, while the third (last) layer of gas oil acts as a post-fuel to activate ammonia spray combustion at the end of the combustion phase, keeping the flame hot and reducing N_2O[6)].

NMRI has clarified the effect of post-injection on exhaust components by experiments using a combustion chamber simulating the inside of a diesel cylinder. The right side of Fig. 6 shows an example of the experimental results, where the N_2O and unburned NH_3 emissions shown in red indicate the case without post-injection, which ends with ammonia combustion, and the emissions in blue indicate the case with post-injection. Post gas oil injection shows a dramatic effect in reducing N_2O, and unburnt NH_3 is also drastically reduced by post-injection. This system will be applied to a single-cylinder test engine of Japan Engine Corp. this year.

5. REVIEW OF NATURAL GAS (METHANE) COMBUSTION FOR HYDROGEN STUDY

Similar to natural gas engines, diesel cycle and Otto cycle combustion are also possible with hydrogen engines, which will be discussed below. Both types of combustion are reviewed in this section with natural gas. Currently, orders for LNG-fueled ships are increasing, and MAN's low-speed two-stroke diesel cycle engine is used as the main engine of K-Line's first car carrier, while WinGD's Otto cycle type is used as one of NYK's first vessel.

Fig. 7 shows the differences between the operation and combustion patterns of these two types of natural gas engines. The diesel cycle type shown as (A) in the figure is similar to a diesel engine, in which the piston compresses only air and then a pilot fuel and high-pressure (30 MPa) natural gas are injected. This is also known as the high-pressure type. For the Otto cycle type shown as (B) in the figure, natural gas with a pressure of about 1 MPa is supplied to the cylinder before compression by the piston starts, forming a mixture with air. The mixture is ignited by the pilot fuel after being compressed by the piston, and the flame spreads through the mixture (flame propagation). This is also called the low-pressure type because the supply gas pressure is much lower than in the former.

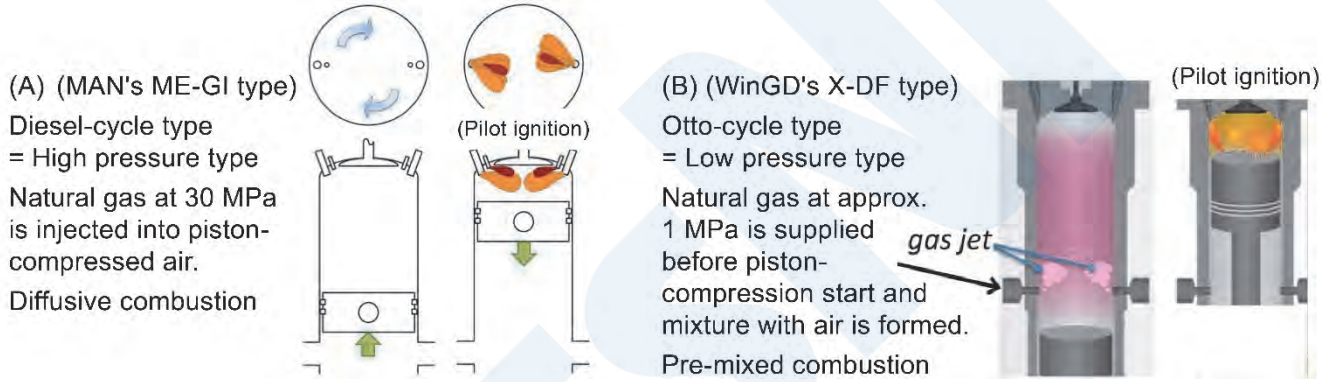

Fig. 7 Two operating patterns for low-speed two-stroke natural gas engines

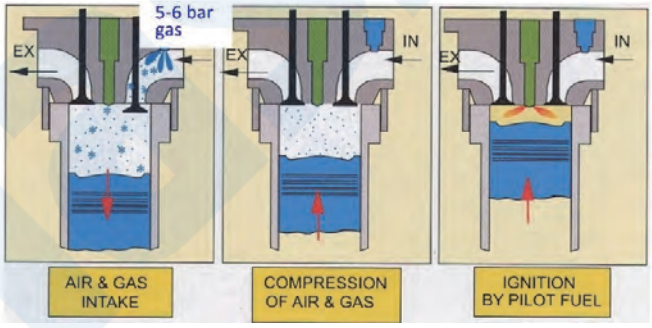

Fig. 8 Formation of air-gas mixture in medium- and high-speed 4-stroke natural gas engines (Otto cycle type)
(In 4-stroke hydrogen engines, hydrogen is supplied at the same position as above.)

So far, all medium- and high-speed four-stroke natural gas engines are of the Otto cycle type. As shown in Fig. 8, natural gas is supplied to the intake pipe to form a mixture with air. The hydrogen-fueled four-stroke engines described below are similar, with a hydrogen supply nozzle at the same position in the intake pipe. In practice, because the hydrogen engines are being developed on the base of natural gas engines, both hydrogen and natural gas nozzles are fitted, and an approach in which the amount of hydrogen is increased while that of natural gas is decreased is adopted.

Knocking and pre-ignition are concerns in Otto cycle type combustion. These problems are caused by the activity of the mixture. Pre-ignition is a phenomenon where, for example, the cylinder lubricating oil ignites the mixture during the compression stroke, as shown in Fig. 9. If pre-ignition occurs, the cycle fluctuations in cylinder pressure become extreme. The aforementioned X-DF solves this problem by applying EGR (Exhaust Gas Recirculation) to reduce the activity of the mixture.

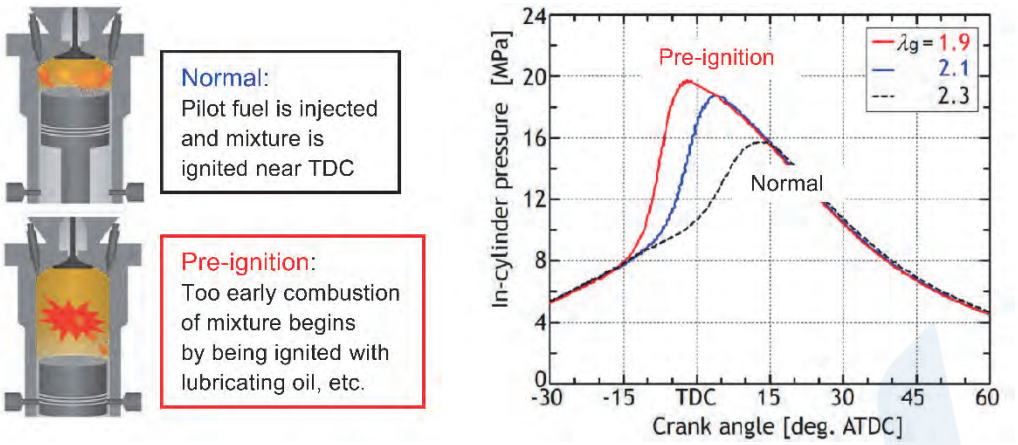

Fig. 9　Mechanism of pre-ignition (left) and cylinder pressure rise by pre-ignition of natural gas mixture (right) (In actual engines, random occurrence of pre-ignition leads to excessive cycle fluctuations.)

Hydrogen mixtures are even more active than methane (natural gas) mixtures. This means that the low minimum ignition energy and wide upper and lower flammable limits (fuel vol.% of the flammable range) of hydrogen in Table 2 should be noted. Even before the mixture is fully formed, the possibility of pre-ignition by lubricating oil particles or residual gases in the cylinder is increased.

Fig. 10 provides an overview of the aforementioned Green Innovation Fund project to develop marine hydrogen engines. In the development of medium- to high-speed four-stroke Otto cycle type hydrogen engines by KHI and YANMAR Co., Ltd. in the project, pre-ignition and knocking are suppressed applying not only EGR but also a leaner mixture than in the case of natural gas.

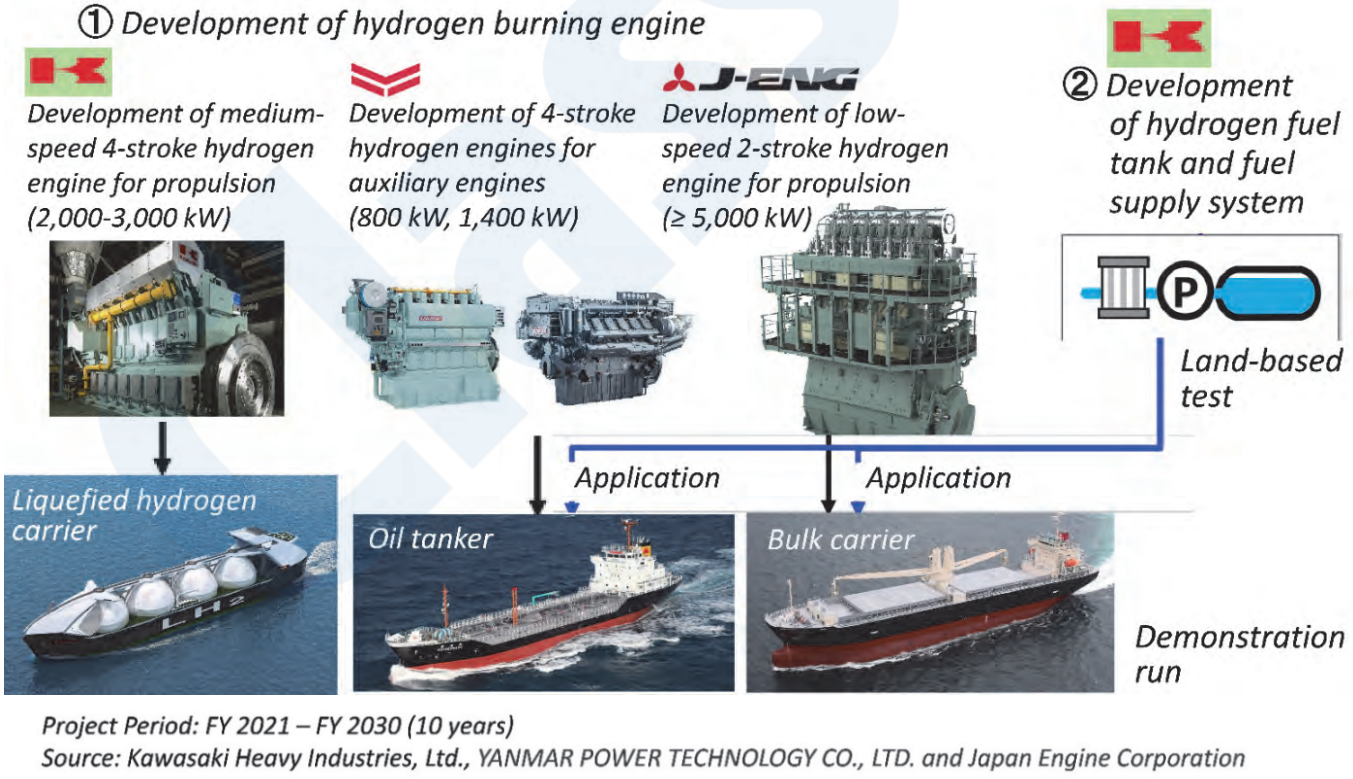

Project Period: FY 2021 – FY 2030 (10 years)
Source: Kawasaki Heavy Industries, Ltd., YANMAR POWER TECHNOLOGY CO., LTD. and Japan Engine Corporation

Fig. 10　Green Innovation Fund project, Development of marine hydrogen engines and MHFS (Marine Hydrogen Fuel System)　(*MLIT website: https://www.mlit.go.jp/maritime/content/001484436.pdf*)

6. COMBUSTION IN DIESEL CYCLE HYDROGEN ENGINE

In the project to develop marine hydrogen engines (Fig. 10), the diesel cycle was adopted in Japan Engine Corp.'s low-speed, two-stroke engine. This section presents the author's previous research on a diesel cycle type hydrogen engine, which has not been studied as much as the Otto cycle type. Based on the ratio of the molecular weights of hydrogen and methane (2 :16), the density of hydrogen is 1/8 that of methane. Table 2 shows that the calorific value per mass of hydrogen is 2.5 times that of methane, but when considered per volume of gas, a volume about three times larger than that of methane must be injected to obtain the same heat. However, in high-pressure injection, where the initial speed of injection is the sonic velocity, a sufficient volume of hydrogen can be injected at the same gas pressure without extremely enlarging the injection hole because the sonic velocity of hydrogen is about three times faster than that of methane.

The combustion of a hydrogen jet injected at high pressure was visualized by shadowgraphs using the apparatus shown in Fig. 3. As the self-ignition temperature of hydrogen is high, as shown in Table 2, it is ignited with pilot gas oil (5 % heat) in the first stage. The ignition image is shown in Fig. 11(a). The white flame is produced by the pilot gas oil, while the ignited hydrogen flame appears black as a non-luminous flame.

On the other hand, Fig. 11(b) shows the result of an attempt to self-ignite the hydrogen jet by raising the air temperature to higher than normal (estimated to be around 700 °C, although this has not been measured). From this photograph, it appears that the hydrogen jet self-ignites in the second frame (5.5°), after which the flame front penetrates in proportion to the square root of the elapsed time based on the momentum theory, like a normal diesel spray flame.

Fig. 11(c) compares the heat release rates of high-pressure jets of hydrogen and methane. Both are ignited by pilot gas oil. Both fuels are injected at the same pressure (30 MPa) and at the approximately the same timing, and both show an almost constant heat release rate in line with the injection rate. However, it can be seen that the hydrogen burns up earlier after the end of injection. In principle, the diesel cycle type does not suffer from pre-ignition and knocking like that in the Otto cycle type. Furthermore, the combustion rate can be controlled primarily by the fuel injection rate, which is an advantage over the Otto cycle type.

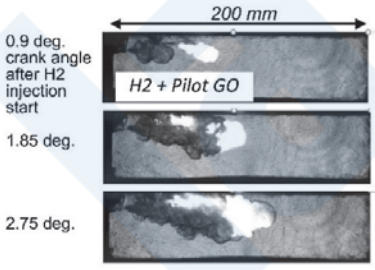

(a) Ignition of high-pressure hydrogen jet by gas oil pilot

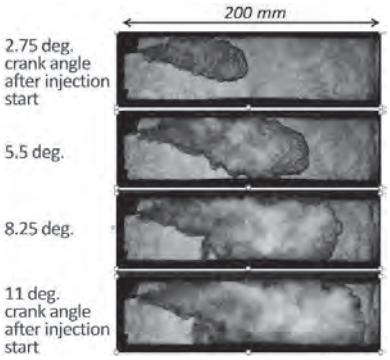

(b) Self-ignition and combustion of high-pressure hydrogen jet in high-temperature air

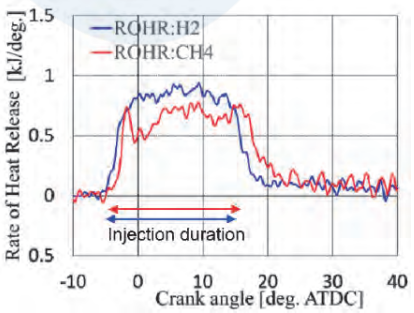

(c) Comparison of heat release rates of hydrogen and methane (both ignited by gas oil pilot)

Fig. 11 Combustion analysis of high-pressure hydrogen jet (30 MPa hydrogen jet into 8 MPa air)

7. CONCLUSION

Which of the fuels introduced above is the most realistic future marine fuel? At this moment, they are expected to coexist in the world based on the following advantages and disadvantages.

- Biofuels are “drop-in” fuels and have no combustion problems, but the quantity of raw materials is the main issue.

- The same applies to carbon-neutral methanol, which requires a pilot fuel for ignition but has good combustion characteristics. The development of methanol engines has already been completed. However, as far as building a global supply chain for carbon-neutral methanol which would only be used as a marine fuel, one challenge is how much supply and demand will emerge compared to hydrogen and ammonia, which are also used on land.

- N_2O-related challenges are anticipated in the case of ammonia combustion, but the results of the forthcoming engine running tests are waited for further research and development.

- The development of hydrogen engines is progressing well, supported by the existing technology of natural gas engines.

As the above-mentioned zero-carbon or carbon-neutral fuels will be several times more expensive than heavy fuel oil, subsidies and other measures will be needed in order to achieve widespread use. In this regard, Japan has proposed a “Feebate” mechanism to the IMO MEPC as an economic approach.

REFERENCES

1) MLIT (Ministry of Land, Infrastructure, Transport and Tourism, Japan) website (2022):
Toward Achieving Net Zero GHG Emissions from International Shipping by 2050.
Shipping Zero Emission Project, March 2022, https://www.mlit.go.jp/maritime/content/001484436.pdf
2) Takasaki, et al.: CIMAC 2016, Paper No. 91.
3) Mitsui Zosen Technical Review, No. 218, 2017.
4) For example, Merkmal, 3. March 2022, https://merkmal-biz.jp/post/6674
5) Okafor, et al.: Fuel; 287: 119433 (2021).
6) Oba, et al.: CIMAC 2023, Paper No.101.
7) Takasaki, et al.: CIMAC 2023, Paper No.103.

Recent Topics at IMO

— Outline of Discussion at IMO Committees —

External Affairs Department, Rule Development and ICT Division, ClassNK

1. INTRODUCTION

This article introduces recent topics discussed at International Maritime Organization (IMO). At the previous issue, a summary of the topics discussed at 78th Marine Environment Protection Committee (MEPC 78) held in June 2022 and 105th Maritime Safety Committee (MSC 105) held in April 2022 was provided.

This article provides a summary of the decisions taken at 79th Marine Environment Protection Committee (MEPC 79) held from 12 to 16 December 2022 and 106th Maritime Safety Committee (MSC 106) held from 2 to 11 November 2022 as below.

2. OUTCOMES OF MEPC 79

2.1 Greenhouse Gases (GHG) Emission Reduction Measures

Reduction of greenhouse gas (GHG) emissions to address global warming is a universal challenge, and the measures to reduce GHG emissions from international shipping have been deliberated at IMO. Such measures introduced at the IMO so far include the regulation of "Energy Efficiency Design/Existing Ship Index" (EEDI/EEXI), retaining of the "Ship Energy Efficiency Management Plan" (SEEMP) onboard, and rating by "Carbon Intensity Indicator" (CII).

Furthermore, taking the adoption of the Initial IMO Strategy on the reduction of GHG emissions from ships, which includes the emission reduction target and the candidate measures to reduce GHG emissions, the IMO continues to discuss on measures to reduce GHG emissions in order to decarbonize the international shipping.

2.1.1 Amendments to the Guidelines on the Method of Calculation of the Attained EEDI for New Ships

Taking the increasing demand for using ethane as a ship fuel, particularly for ethane carriers, 2022 Guidelines on the method of calculation of the attained EEDI for new ships were adopted to include the lower calorific value and conversion factor (CF) of ethane.

2.1.2 Amendments to the Guidelines on Survey and Certification of the EEDI

The calculation of EEDI requires the calculation of ship speed based on the speed trial results, by assuming that the weather is calm with no wind and no waves. The current Guidelines on survey and certification of the EEDI refers to ITTC Recommended Procedure 7.5-04-01-01.1 Speed and Power Trials 2017 (hereafter referred to as 2017 ITTC Procedure) or ISO 15016:2015 for determining ship speed taking into account the external effects (wind, current, waves, shallow water, displacement, water temperature and water density).

Since the revisions of ITTC Procedure are available, MEPC 79 adopted 2022 Guidelines to refer to the amended 2022 ITTC Procedure as well as 2017 ITTC Procedure.

2.1.3 EEDI Phase 4

Regulation 24.6 of MARPOL Annex VI keeps the IMO review the status of technological developments and, if proven necessary, amend the reduction rates etc. set out in the regulation. In accordance with the regulation, MEPC established the Correspondence Group to continue its work on the possible introduction of EEDI Phase 4.

Based on the final report of the Correspondence Group, MEPC 79 concluded that the introduction of EEDI Phase 4 should be carefully pursued at a future session, due to the fact that further investigations are required on regulations for both new propulsion technologies such as alternative fuels and wind energy that would affect application of EEDI Phase 4 and also additional regulatory scope taking into account the IMO Strategy on the reduction of GHG emissions from ships.

2.1.4 Carbon Intensity Indicator (CII)

CII is a rating mechanism for ships, which compares the attained CII, calculated based on the operational fuel consumption data collected from the IMO Data Collection System for fuel oil consumption of ships (DCS), with the CII reference lines.

MEPC 79 approved the following unified interpretations related to CII and DCS:

- If a ship is delivered in October or later, the rating based on the data between the delivery date and the end of that calendar year will not be counted for the determination of whether the ship should develop a Corrective Action Plan (i.e., a ship rated as D for three consecutive years or rated as E for one year).
- In case of a change of company, a new ship operational carbon intensity plan (SEEMP Part III) will be required to be submitted for the verification by the new company, where the year of change is the starting year of the three-year implementation plan.
- The Corrective Action Plan to achieve the required annual operational CII for a ship with an inferior rating (i.e., a ship rated as D for three consecutive years or rated as E for one year) should be developed to achieve the required CII for data collected in the second calendar year after the reporting year that resulted in such inferior rating.
- Data relating to boil-off gas (BOG) consumed onboard LNG-fueled ships or LNG carriers for propulsion or operation (including BOG burnt in a Gas Combustion Unit (GCU) for cargo tank pressure control or other operational purposes) is required to be collected and reported as fuel oil consumption as part of the IMO DCS.

2.1.5 Onboard Carbon Capture Systems

There have been initiatives to develop methods for reducing GHG emissions by segregating and capturing carbon dioxide (CO2) from exhaust gases onboard ships.

At this session, a proposal was made that the amount of CO2 captured by CO2 Capture Systems should be taken into consideration when calculating the attained EEDI/EEXI and CII. Due to the time constraints, MEPC 79 agreed that the discussion will be continued at the next session.

2.1.6 Revision of the Initial IMO Strategy on the Reduction of GHG Emissions from Ships

The Initial IMO Strategy on the reduction of GHG emissions from ships (hereafter referred to as the Initial IMO Strategy), adopted in 2018, envisages to improve transportation efficiency by at least 40% by 2030, pursuing efforts towards 70% by 2050, and also aims for the total annual emissions from international shipping reduced by at least 50% by 2050 compared to 2008. The IMO Strategy is subject to a review every five years.

Up until the last session, it was recognized that the aforementioned GHG reduction target should be improved and therefore agreed that the Initial IMO Strategy is subject to a review, aiming for adoption of the revision at MEPC 80 to be held in July 2023.

At this session, there were comments advising either zero GHG emission or net-zero GHG emission (practically zero by deducting the amount of GHG absorbed by forests from those emitted) and proposals such as to introduce a new target for GHG reduction by 2040. On the other hand, there were also comments advising that setting a new goal would necessitate a valid scientific background and therefore the GHG reduction goals in the current Initial IMO Strategy should be kept. In conclusion, MEPC 79 agreed to continue the revision process of the Initial IMO Strategy, aiming for adoption at MEPC 80.

2.1.7 Mid-term Measures for Reduction of GHG

The Initial IMO Strategy contains a list of measures such as market-based measures (MBM) etc. to achieve mid- and long-term GHG reduction goals. To proceed with the consideration of such measures, MEPC 76, held in 2021, developed the work plan shown as follows:

Phase I (2021-2022): Collation and initial consideration of proposals for measures
Phase II (2022-2023): Assessment and selection of measures to further develop
Phase III (2023): Development of measures for statutory requirements

At this session, there were a number of supports to the comments suggesting the adoption of GHG reduction measures that combine both regulatory and market-based measures, and therefore MEPC 79 agreed to the plan to conclude the work item in Phase II (assessment of measures) at MEPC 80. The mid-term measures proposed so far include the following:

Regulatory Measures

- GHG Fuel Standard (GFS)
  Each ship calculates GFS value, expressed in the mass of GHG emissions per unit of energy used (gCO2e/MJ). Reduction factor for GFS will be enhanced year by year.

Market-based Measures

- Feebate
  Ships using fossil fuels pay for the levy and ships using zero-emission fuels receive rebate.

・GHG Levy
Ships pay GHG levy for US$100 per tonne of marine fuel. The revenue will be funded to climate change mitigation and adaptation projects under UNFCCC, and subsidized to R&D projects for new technologies under IMO.
・International Maritime Sustainability Funding and Reward (IMSF&R)
Using CII mechanism, ships above upper benchmark level pay funding contributions and ships below lower benchmark level receive rewards.
・Funding and Reward (F&R)
Ships pay funding contributions according to the amount of CO2 emissions from ships and ships using eligible alternative fuels receive rewards.
・Emission Cap-and-Trade System (ECTS)
Based on the annual cap on GHG emissions, each ship is required to acquire and surrender allowances for GHG emissions by auctioning.

2.2 BWM Convention

2.2.1 Application of BWM Convention to Ships Operating at Ports with Challenging Water Quality

With regard to the use of ballast water treatment systems (BWMS), as there are ports with challenging water quality that make it difficult to operate BWMS continuously, there has been a proposal to allow that ballast water is taken without passing through BWMS in such ports, and employing ballast water exchange plus treatment (BWE + BWT) at areas where the treatment system can operate normally.

At this session, it was suggested that the criteria such as for the "challenging water quality" affecting continuous normal operation of the BWMS should be clearly defined. MEPC 79 agreed to continue the discussion at the next session.

2.2.2 Temporary Storage of Treated Sewage and Grey Water

The prohibition on the discharge of treated sewage and grey water at certain ports has led to temporary storage of treated sewage and grey water in ballast tanks.

At this session, it was endorsed that the BWM Convention did not preclude the temporary storage of grey water or treated sewage in ballast tanks and this storage should be permitted. Recognizing the need for developing specific procedures to prevent contamination of ballast tanks by temporary storage of sewage and greywater, MEPC 79 agreed to consider developing a guidance for such temporary storage at future sessions.

2.2.3 Commissioning Tests of BWMS

While commissioning tests of BWMS including analysis of treated ballast water have been required for those installed on or after 1 June 2022, MEPC 79 discussed on the interpretation on whether or not it is necessary to conduct commissioning tests in cases where an installed BWMS on board a ship undergoes an upgrade or change to a major component.

As a result, MEPC 79 approved a unified interpretation that if an installed BWMS on board a ship undergoes an upgrade or change to a major component, such BWMS shall be regarded as a newly installed BWMS, so a commissioning test shall be conducted accordingly.

2.2.4 Amendments to the Format of Ballast Water Record Book

It was noted that problems have arisen during PSC inspections due to different interpretations for recording the Ballast Water Record Book (BWRB) specified in Appendix II of the BWM Convention. The necessities for a revision of the BWRB format and a guidance on how to describe it have been under discussion.

MEPC 79 approved amendments to the BWRB format to be recorded in terms of Codes (letter) and Items (number), similar to the format of the Oil Record Book, with a view to adoption at MEPC 80.

2.3 Air Pollution

2.3.1 Unified Interpretation on Use of Synthetic Fuels

With the switch to alternative fuels under consideration from the perspective of GHG emission reduction, MEPC 78, held in June 2022, approved a uniform interpretation on the application of NOx emission limits to biofuels and a biofuel blend with fossil fuels. According to the unified interpretation, additional confirmation of NOx emission is not required, if the blend ratio of biofuel and fossil fuel is below 30% and if no changes to NOx critical components or setting/operating values are required in order to use biofuel or a biofuel blend.

At this session, revised Unified Interpretation was approved to treat synthetic fuels, produced from renewable sources similar

in composition to petroleum distillate fuels, which are expected to be used in the future, in the same way as biofuels in terms of NOx emission.

2.4 Amendments to Mandatory Instruments

2.4.1 Designation of Emission Control Area for SOx and PM

Amendments to MARPOL Annex VI to add the Mediterranean Sea as Emission Control Areas (ECAs) for SOx and PM were adopted. Requirements regarding SOx and PM emissions (Regulation 14 etc. of ANNEX VI) in the Mediterranean Sea Area as ECA will start being enforced on 1 May 2025.

2.4.2 Garbage Record Book

Amendments to MARPOL Annex V were adopted to expand the scope of Garbage Record Book, which has been required to be provided for vessels of 400 gross tons or more, to vessels of 100 gross tons or more. The amendments will enter into force on 1 May 2024.

2.4.3 Information to Be Included in Bunker Delivery Note (BDN)

Amendments to Appendix V of MARPOL Annex VI were adopted to include flashpoint as mandatory information in the BDN. The amendments will enter into force on 1 May 2024.

2.4.4 Information to Be Submitted under Data Collection Systems (IMO DCS)

With the introduction of CII regulations, amendments to Appendix IX of MARPOL Annex VI were adopted to add CII related information to reporting items from Flag/RO to IMO database under Data Collection System for fuel oil consumption of ships (IMO DCS). The amendments will enter into force on 1 May 2024.

3. OUTCOMES OF MSC 106

3.1 Adopted Mandatory Requirement

Mandatory requirement was adopted at MSC 106 as follows:

(1) Amendments to SOLAS Chapter II-2 for safety measures on use of fuel oil

Amendments to SOLAS Chapter II-2 to require providing with a declaration signed and certified by the oil fuel supplier's representative, that the oil fuel to be supplied is in conformity with paragraph SOLAS II-2 Reg.4.2.1 etc., and require that a bunker delivery note shall contain the flashpoint information, were adopted.

(2) The International Code of Safety for Ships Carrying Industrial Personnel (IP Code)

Newly developed IP Code and new SOLAS Chapter XV to make the Code mandatory were adopted. The Code applies to cargo ships and high-speed cargo craft, of 500 gross tonnage and upwards which carry more than 12 industrial personnel.

(3) Amendments to IGC Code

Amendments to add high manganese austenitic steel in Table 6.3 of IGC Code on plates, sections and forgings for cargo tanks, secondary barriers and process pressure vessels for design temperatures below -55°C and down to -165°C, were adopted.

(4) Amendments to IGF Code

Amendments to add high manganese austenitic steel in Table 7.3 of IGF Code on plates, sections and forgings for fuel tanks, secondary barriers and process pressure vessels for design temperatures below -55°C and down to -165°C, were adopted.

(5) Amendments to 2011 ESP Code

Amendments to 2011 ESP Code which mainly contain the following items were adopted.

1. The coating condition criteria of ballast tanks, excluding double-bottom tanks, of bulk carriers were strengthened from “POOR” to “less than GOOD”, which are used for the tank examination at annual intervals.
2. For void spaces bounding cargo holds of double-side skin bulk carriers exceeding 20 years of age and of 150m in length and upwards, it is required that the spaces in question should be examined at annual intervals where a hard protective coating is found to be in POOR condition.
3. It was clarified that oil tankers carrying oil in independent tanks which did not form part of the ship's hull were outside the scope of the ESP Code.
4. Timing of tank pressure testing for oil tankers at renewal survey was clarified.

(6) Amendments to IBC Code

Amendments to IBC Code were adopted, in order to allow submersion of some hinged watertight doors considered for stability criteria at any stage of flooding, as well as the amendments to IGC Code which have been adopted at MSC 104.

3.2 Approved Mandatory Requirements

The following mandatory requirements were approved at this session, and are expected to be considered for adoption at MSC 107 in June 2023. These amendments are also expected to enter into force on 1 January 2026 in accordance with ad hoc midterm amendment cycle for SOLAS.

(1) Amendments to LSA Code

Amendments to LSA Code to add new ventilation requirements applied to totally enclosed lifeboats, in conjunction with the amendments to the recommendation on testing of life-saving appliances (resolution MSC.81(70)) which newly stipulates the relevant operation tests, were approved.

On the other hand, any compelling need for ventilation requirements for partially enclosed lifeboats and liferafts would be continuously considered at the SSE Sub-Committee.

(2) Amendments to SOLAS Chapter II-2, etc. on the prohibition of perfluorooctane sulfonic acid (PFOS)

Amendments to SOLAS Chapter II-2, and the 1994 and 2000 HSC Codes to prohibit the use of fire-fighting foams containing PFOS, were approved.

On the other hand, the prohibition of other fire-fighting foam types in addition to PFOS, such as PFOA, would be considered at the SSE Sub-Committee.

(3) Amendments to SOLAS Chapter V and format of SE Certificate

Amendments to SOLAS Chapter V to require carriage of electronic inclinometers on container ships and bulk carriers of 3,000 gross tonnage and upwards were approved. Accordingly, format of SE Certificate was also amended to add new entry of “Container ship” in Particulars of ship.

3.3 Approval of Unified Interpretations (UIs), Guidelines and Guidance etc.

The following unified interpretations (UIs), guidelines and guidance etc. were approved during MSC 106.

(1) Unified interpretation of SOLAS Chapter II-2

The following unified interpretations of SOLAS Chapter II-2 were approved;

- Unified interpretation of 9.7.3.1.2 on fire insulation of ducts passing through “A” class divisions to clarify extent of the required fire insulation; and
- Unified interpretation of 9.7.3.2 on clearance of the duct penetration of the “B” class bulkheads was approved to clarify that no clearance should be allowed between the duct and the division.

(2) Amendments to the Guidelines for the approval of fixed dry chemical powder fire-extinguishing systems for the protection of ships carrying liquefied gases in bulk (MSC.1/Circ.1315)

Amendments to the Guidelines for the approval of fixed dry chemical powder fire-extinguishing systems for the protection of ships carrying liquefied gases in bulk (MSC.1/Circ.1315) were approved. The amendments specify the details of fire tests for dry chemical powder. In addition, the definition of dry powder is revised and the statement which is related to main components of dry powder in the definition is deleted. The amendments would be applied to the systems installed on or after 1 July 2023.

(3) Amendments to MSC.1/Circ.1374 on Information on prohibiting the use of asbestos on board ships

According to MSC.1/Circ.1374 on Information on prohibiting the use of asbestos on board ships, when asbestos containing material (ACM) is found to be installed on board ships in contravention of SOLAS Chapter II-1/3-5, it should be removed within three years. In order to make the provisions more practicable, amendments to MSC.1/Circ.1374 were approved to allow ACMs such as gaskets to be removed at an appropriate timing beyond three years at discretion of an Administration subject to the implementation of risk-based maintenance and monitoring.

3.4 Consideration of Requirements for Maritime Autonomous Surface Ships (MASS)

Taking into account recent investigation of automation surrounding a ship, it has been discussed at MSC on conventional requirements of safety and environmental protection relating to MASS.

At the previous session, the road map for developing goal-based MASS Code was endorsed, in which non-mandatory MASS guidelines will be developed in 2024 and mandatory goal-based MASS Code will be developed targeting entry into force in

2028.

At this session, development of non-mandatory MASS guidelines mainly on goal and functional requirements has been initiated, based on the report by the intersessional correspondence group and the meeting outcome arranged by the related working group.